Short-term prediction of local wind conditions

Landberg, Lars

Publication date:
1994

Document Version
Publisher's PDF, also known as Version of record

RISØ

Risø-R-702(EN)

Short-term Prediction of Local Wind Conditions

Lars Landberg

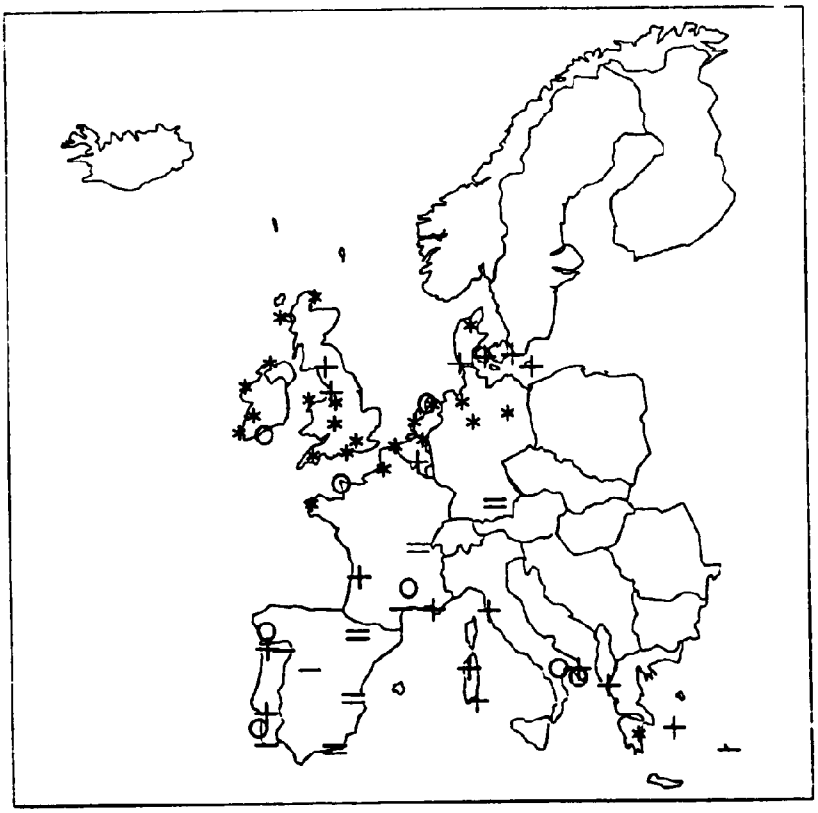

Risø National Laboratory, Roskilde, Denmark
March 1994

Short-term Prediction of Local Wind Conditions

Risø-R-702(EN)

Lars Landberg

Risø National Laboratory, Roskilde, Denmark
March 1994

Abstract This report describes the development and evaluation of different methods for predicting the wind locally. The look-ahead time of the forecasts ranges from 3 to 36 hours. The main model developed here is based on forecasts from a numerical weather prediction model. In this study HIRLAM (HIgh Resolution Limited Area Model) has been used. The HIRLAM forecasts are transformed to the surface using the geostrophic drag law and the logarithmic wind profile in their neutral versions. To take local effects into account, corrections output from WA^{S}P (Wind Atlas Analysis and Application Program) are used. The conclusion is that the model developed here performs significantly better than persistence. The model performs best when applied to sites in Northern Europe (having high wind speeds). When using MOS (Model Output Statistics) it is possible to improve the forecasts, mainly those that do not perform well.

This report is - with a few minor changes - a copy of my thesis submitted to the University of Copenhagen in partial fulfillment of the requirements for the PhD-degree.

ISBN 87-550-1916-1
ISSN 0106-2840

Grafisk Service · Risø · 1994

Contents

List of Figures

List of Tables

1 Introduction

The purpose of this study is to develop and evaluate methods to predict the wind speed, but also the direction, locally. The maximal look-ahead time (ie the maximal forecast range) is 36 hours. The predictions can be used in many different situations, eg on the site of a wind farm or in connection with chemical, radioactive and biological warning systems. Most attempts to solve this problem base themselves on statistical methods. This project will, however, use a *physical* model. Two 'tools' will be used:

- The High Resolution Limited Area weather prediction Model (HIRLAM) which was developed during the last few years as a joint effort between the meteorological institutes in Denmark, Finland, Iceland, Norway, Sweden and The Netherlands, see Machenhauer (1988).
- The siting model WA^{S}P which was developed at Risø National Laboratory in connection with the now completed European Wind Atlas project, see Troen and Petersen (1989) and Mortensen et al (1993).

The basic idea is that in order to make forecasts, a prognostic model is needed. This model must cover an area, which is so big, that within the maximal forecast range (+36 hours) the weather systems that are found when the model is initiated are not advected out of the area, and its modelling powers must be such that it can model meteorological events happening in the area within its prediction range. A model that fulfills these criteria for Europe is the HIRLAM model.

Because of the size of the HIRLAM model domain it is impossible now, and also in the nearer future, to obtain a resolution so fine that local effects, such as the speed-up on small hills, the shelter from obstacles, and the change in roughness lengths on a local scale (say tens to hundreds of metres) are modeled - if one wants to predict in real time. This is mainly limited by the available computer technology. Since the local effects are of crucial importance in calculating the wind locally, we introduce the WA^{S}P model, which takes exactly the effect of these phenomena into account. WA^{S}P is a *diagnostic* model, so it is necessary to use both models in order to make forecasts on a local scale.

The idea laid out here is thus building on state-of-the-art models, ie the best models presently available. Whether using this is good enough for the applications is another question, this study will try to answer.

The reason why this work is carried out here and now, is that in the World, but within the European Community, especially, it is foreseen that an increasing amount of electricity will be produced by wind energy. To be able to harness this energy, it is necessary to know, in advance, the expected power produced by the wind energy plants. This is done in order to save conventional fuel (oil, gas) more efficiently.

In Part I the basic equations will be derived, Part II covers the applied models, and in Part III the forecasting model will be developed. The evaluation will also be done in Part III.

Since quite a few models are presented and tested, an overview of all the models is given in Section 16.

Part I

Basic Equations

2 The geostrophic drag law

The geostrophic drag law is a result of a merging (or *matching*) of the wind in two different layers of the atmosphere: the surface layer and the free atmosphere (see Figure 1). This matching is necessary because the wind is geostrophic (ie derived from the pressure field only) in the free atmosphere, and the geostrophic wind does not fulfill the boundary conditions at the surface (the no-slip condition). The exact mathematical solution to this problem, which will be given in the next section, is based on the *singular perturbation method*, and is very elegantly given in Blackadar and Tennekes (1968). For a short non-rigorous derivation, see Tennekes and Lumley (1983), Chapter 5. In passing, it should be mentioned that the results obtained in the following, were first found in a somewhat different form by Rossby and Montgomery (1935) in a very thorough paper.

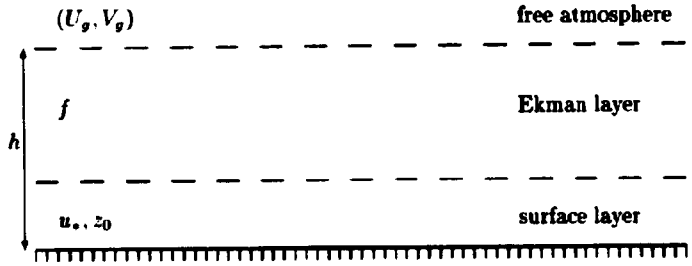

Figure 1. The planetary boundary layer (PBL) (or the atmospheric boundary layer (ABL)) of height h with its different layers, and some characteristic quantities having influence in each of the layers. Some name, what here is called the PBL, the Ekman layer, in that case the layer named the Ekman layer here, is called the outer *Ekman layer.*

2.1 The velocity-defect law

The equations of motion in the *free* atmosphere (ie the part of the atmosphere where the presence of the surface is not felt), express the balance between the Coriolis force and the pressure gradient force, called the geostrophic balance, and are given by, assuming that the flow is steady, horizontal, barotropic[1], adiabatic (no heat is exchanged with the surroundings), and homogeneous in horizontal planes:

$$-fV_g = -\frac{1}{\rho}\frac{\partial p}{\partial x} \tag{1}$$

and

$$fU_g = -\frac{1}{\rho}\frac{\partial p}{\partial y} \tag{2}$$

where $f = 2\Omega \sin\phi$ is the Coriolis parameter, Ω the angular velocity of the Earth, ϕ the latitude, U_g and V_g are the x- and y-components of the geostrophic wind, respectively, and p the pressure.

[1] A barotropic atmosphere is an atmosphere where the density is a function of pressure only, $\rho = \rho(p)$, as opposed to a baroclinic atmosphere where the density is a function of temperature, too. The implication of this being that the thermal wind equation gives that the geostrophic wind is *constant* with height.

Since the geostrophic wind does not meet the no-slip boundary condition at the surface (ie that the wind speed vanishes there) a transition layer must exist, where the wind adjusts to this condition. This layer is called the *Ekman* layer (cf Figure 1). The equations of motion in this layer are given by

$$-fV = -\frac{1}{\rho}\frac{\partial p}{\partial x} + \frac{d}{dz}(-\overline{uw}) \tag{3}$$

and

$$fU = -\frac{1}{\rho}\frac{\partial p}{\partial y} + \frac{d}{dz}(-\overline{vw}) \tag{4}$$

where U and V are the x- and y-component of the actual wind, and $\overline{uw}$ and $\overline{vw}$ are the correlation of the x- and y- component of the fluctuation of the horizontal wind with the vertical wind, respectively. These quantities are also called the Reynolds stresses. It is through the Reynolds stresses, that the presence of the surface is felt. Using the expression for the geostrophic wind, the equations can be rewritten as

$$-f(V - V_g) = \frac{d}{dz}(-\overline{uw}) \tag{5}$$

and

$$f(U - U_g) = \frac{d}{dz}(-\overline{vw}) \tag{6}$$

We assume that the coordinate-system is rotated in such a way that, at the surface, the stress vector has no y component, so that in the limit, $z \to 0$,

$$-\overline{uw} = u_*^2, \qquad \text{and,} \qquad -\overline{vw} = 0 \tag{7}$$

Generally, when flow in the *vicinity of a boundary* is considered, it is possible to derive a law, describing the behavior of the non-dimensionalised difference between the velocity (properly scaled) in the layer influenced by the boundary and the velocity in the uninfluenced layer as a function of the characteristic scales, this type of law is called a *velocity-defect law*, and has the form

$$\frac{(U - U_g)}{u_*} = F(\eta) \tag{8}$$

where η is a non-dimensional measure of the distance from the boundary, and u_* - in this case - is a characteristic velocity scale.

We proceed by trying to find the appropriate scales for the equations governing the flow in the atmosphere. For the velocities we assume that the friction velocity, u_*, is the only characteristic scale[2], this is of course not true for flows where heat transfer occurs, where other scales, such as $w_* = (g\beta Q_0 z_i)^{1/3}$, are in effect. The Reynolds stresses are of order u_*^2. As a scaling height, the height h of the Ekman layer is used. This quantity is considered as unknown and can be chosen freely. It is now possible to scale the equations in the following way:

$$-\frac{hf}{u_*}\frac{(V - V_g)}{u_*} = \frac{d}{dz/h}\left(\frac{-\overline{uw}}{u_*^2}\right) \tag{9}$$

and

$$\frac{hf}{u_*}\frac{(U - U_g)}{u_*} = \frac{d}{dz/h}\left(\frac{-\overline{vw}}{u_*^2}\right) \tag{10}$$

the height h is chosen to be

$$h = c\frac{u_*}{f} \tag{11}$$

[2]It can be shown (Blackadar and Tennekes, 1968) that the matching in the next section is possible, if the characteristic scale has the more general form: $W = u_*(u_*/fz)^K$, where K is a constant. The fact that $K = 0$ can be deduced from the observed form of the wind profile near the surface.

where c is a constant. Now it can be seen that Eqs. 9 and 10 can be written as a velocity defect law

$$\frac{U - U_g}{u_*} = F_u(zf/u_*) \tag{12}$$

and

$$\frac{V - V_g}{u_*} = F_v(zf/u_*) \tag{13}$$

Instead of using the geostrophic wind, the actual wind components at the top of the PBL can be used, see eg Byun (1991) and Clarke and Hess (1974).

2.2 The law of the wall

Generally, it is also possible to derive a non-dimensional relation for the same kind of flow as the one mentioned in the previous section, for the velocity in the flow in the *layer directly affected by the boundary*, this relation is called the *law of the wall*, and has the general form:

$$\frac{U}{u_*} = f(\alpha)$$

where α is a dimensionless distance parameter.

In the surface layer the proper height scale is *not* h, because now the flow is under influence of the presence of the rough surface. Rather, the height scale is the roughness length z_0, if the condition that $z_0 u_*/\nu \gg 1$ is fulfilled, where ν is the kinematic viscosity. ν/u_* is another combination of characteristic scales that has the dimension of a length. Now the nondimensional equations of motion in the boundary layer read

$$-\frac{z_0 f}{u_*^2}(V - V_g) = \frac{d}{dz/z_0}\left(\frac{-\overline{uw}}{u_*^2}\right) \tag{14}$$

and

$$\frac{z_0 f}{u_*^2}(U - U_g) = \frac{d}{dz/z_0}\left(\frac{-\overline{vw}}{u_*^2}\right) \tag{15}$$

Determining the order of the left-hand side of the equations, using atmospheric values, gives that it is small (of order 3×10^{-4}), so small that the left-hand side can be set equal to zero. This leads to the fact that the surface layer is a layer of *constant* stress, and thereby independent of the Coriolis parameter, f. To make the picture of the surface layer complete, it has to be noted that *at the surface* the frictional force is balanced solely by the pressure gradient force, see Arya (1985). The only independent non-dimensional parameter left is z/z_0. The law of the wall therefore reads, remembering that the coordinate system is rotated so that the y component of the stress at the surface is zero

$$\frac{U}{u_*} = f_u(z/z_0) \tag{16}$$

and

$$\frac{V}{u_*} = 0 \tag{17}$$

2.3 The matched equations

Matching the two laws derived in the previous sections is done by using the fact that there exists a layer where the equations describing the large-scale flow and the small-scale flow are valid *simultaneously* (see eg Blackadar and Tennekes, 1968). This layer, called the matched layer, is situated at the bottom of the Ekman layer, and at the top of the surface layer (cf. Figure 1). Its existence is based on Kaplun's extension theorem (Van Dyke, 1964).

The following notation is now introduced:

$$\zeta = \frac{z}{z_0}, \qquad \frac{z_0 f}{u_*} = \phi(Ro), \qquad \frac{zf}{u_*} = \zeta\phi$$

where $Ro = Gf/z_0$ is the Rossby number, and G the modulus of the geostrophic wind.

The two expressions for U/u_* are now matched, by inserting the equations for the law of the wall into the equations for the velocity defect law:

$$F_u(\zeta\phi) = f_u(\zeta) - \frac{U_g}{u_*}$$

Doing a partial differentiation with respect to the two independent variables, Ro and ζ, we get

$$\partial/\partial\zeta: \quad \phi F_u'(\zeta\phi) = f_u'(\zeta)$$

and

$$\partial/\partial Ro: \quad \zeta\frac{d\phi}{dRo}F_u'(\zeta\phi) = -\frac{d}{dRo}\left(\frac{U_g}{u_*}\right)$$

where prime indicates differentiation of the function with respect to its argument. Eliminating F_u', gives

$$\zeta f_u'(\zeta) = -\left(\frac{d\ln\phi}{dRo}\right)^{-1}\frac{d}{dRo}\left(\frac{U_g}{u_*}\right)$$

It can be seen from this equation that the left-hand side is only a function of ζ, and the right-hand side only of Ro. This implies that the two sides are constant. The constant is traditionally set equal to $1/\kappa$. If the left-hand side of the equation is integrated with respect to ζ from $\zeta_0 (= z_0/L)$ to ζ, and inserted in Eq. 16, and the differential equation on the right-hand side is solved, we get

$$\frac{U}{u_*} = \frac{1}{\kappa}\ln\left(\frac{z}{z_0}\right) + C \tag{18}$$

$$\frac{U_g}{u_*} = \frac{1}{\kappa}\ln\left(\frac{u_*}{fz_0}\right) - \frac{A}{\kappa} \tag{19}$$

The logarithmic profile is identified in Eq. 18 by setting $C = 0$. It therefore reads:

$$\frac{U}{u_*} = \frac{1}{\kappa}\ln\left(\frac{z}{z_0}\right) \tag{20}$$

where κ is the Von Kármán constant equal to 0.4 ± 0.01 (Högström, 1988).

Matching now the equations for the y-component of the wind, it is seen that since V vanishes at the surface, F_v must be equal to a constant:

$$\frac{V_g}{u_*} = -\frac{B}{\kappa} \tag{21}$$

It is now possible to derive an equation for the magnitude of the geostrophic wind, $G = \sqrt{U_g^2 + V_g^2}$, by combining Eqs. 19 and 21[3]:

$$\frac{G}{u_*} = \frac{1}{\kappa}\sqrt{\left[\ln\left(\frac{u_*}{fz_0}\right) - A\right]^2 + B^2} \tag{22}$$

[3]Note that there does not exist a convention for naming the constants A and B, here the convention of Blackadar and Tennekes (1968) is complied with.

this equation is called the *geostrophic drag law*. The angle, α, between G and the x-axis (pointing in the direction of the velocity at the surface) is given by

$$\tan\alpha = +\frac{V_g}{U_g} = \frac{-B}{\ln\left(\frac{u_*}{fz_0}\right) - A} \tag{23}$$

To resolve any directional ambiguity this angle is compared with the angle calculated by

$$\alpha = \sin^{-1}\left(\frac{V_g}{G}\right) = \frac{-B}{\sqrt{\left[\ln(\frac{u_*}{fz_0}) - A\right]^2 + B^2}}$$

Another way of writing the drag law, also found in the literature, is

$$\ln Ro - A = \sqrt{\left(\frac{\kappa G}{u_*}\right)^2 - B^2} - \ln\frac{u_*}{G} \tag{24}$$

and

$$\sin\alpha = \frac{-B}{\kappa}\frac{u_*}{G} \tag{25}$$

As can be seen form Eq 22 is it not possible to use the drag law at (or near) Equator, where $f = 0$. In WA^{S}P (described later) this is handled by setting all lattitudes, less than ± 5 degrees equal to plus or minus 5. Whether this can be justified in this study, has not been tested, since no stations near Equator were available.

The neutral value of A and B

A great deal of experiments have been carried out to determine the neutral values of the two constants, A and B, in the geostrophic drag law, see eg Clarke and Hess (1974) (the Wangara experiment) and Billard et al (1981) (the 'VOVES' experiment). A complete overview of these estimates up until 1988 is given by Zilitinkevich (1989), these values are plotted in Figure 2. In this figure the average values of these A's and B's (1.7 and 4.5, respectively) are also plotted. It is interesting to note that no single experiment finds these values. In another recent study by Troen and Petersen (1989) it is found that the best fit to the data from the stations in the European Wind Atlas is obtained with

$$A = 1.8 \quad \text{and} \quad B = 4.5$$

this point is also shown in the figure. It is this last set of values that will be used in the neutral model, see Part III, because the observations used to evaluate the model are taken from this set of stations and because the stations are representative of a wide range of landscapes, areas dominated by local-thermal effects etc.

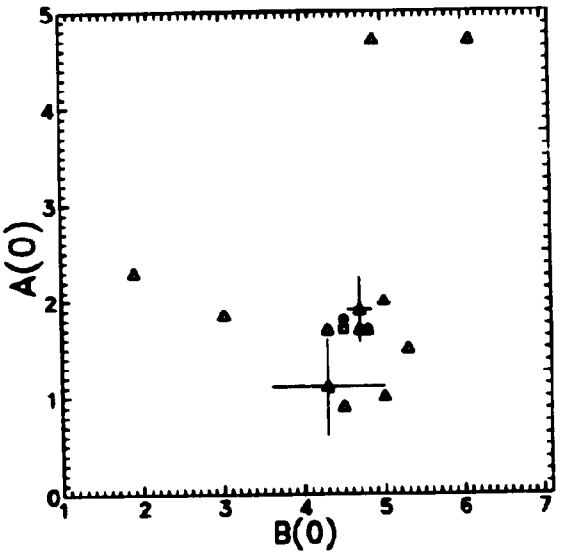

Figure 2. Different neutral values of A and B (△) from Zilitinkevich (1989). The mean value of these is marked by □. Furthermore, the value found by Troen and Petersen (1989) is shown (○). In two of the experiments, (Deacon, 1973, and Clarke and Hess, 1974), an estimate of the experimental scatter was also given, these are shown by the horizontal and vertical lines.

2.4 Theory for the stability dependence of A and B

The stability dependence of A and B have been derived by several using the matching technique, see eg Csanady (1972) and Zilitinkevich (1975). The following is derived along the lines in Long and Guffey (1977), since they have reported their derivation in some detail.

The stability dependence of the drag law is given by the variation of A and B with stability, as proposed by Kazanski and Monin (1960), in their *Rossby similarity theory*[4]. Another competing theory is the similarity theory proposed by Deardorff (1972), the major difference between this and the Rossby similarity theory is that in the latter, the height of the boundary layer, h, is considered as an independent variable. This latter line of thoughts is not followed here, because there is evidence based on measurements (see Clarke and Hess, 1974) that scaling the height by u_*/f is more relevant than by h. Furthermore, because of the layered structure and relatively coarse resolution of any (gridpoint-based) numerical model, it is difficult to get an accurate estimate of h. An objection to the Rossby similarity theory is that due to the action of the buoyancy source at the surface, and the thereby connected origin of an unstable stratified zone, it is very unlikely that the PBL will reach an equilibrium height in daytime unstable conditions (see eg Byun, 1991 and Zilitinkevich, 1989). Despite these arguments Arya (1975) compares A and B as functions of μ and $\mu_i = h/L$ and finds (in agreement with Clarke, 1970, and Billard et al, 1981) that there is no improvement in the correlation of empirical data, when using μ_i instead of μ. The equations therefore reads

$$\frac{U_g}{u_*} = \frac{1}{\kappa}\ln\left(\frac{u_*}{fz_0}\right) - \frac{A(\mu)}{\kappa} \tag{26}$$

$$\frac{V_g}{u_*} = -\frac{B(\mu)}{\kappa} \tag{27}$$

where the stability parameter is defined as $\mu = \kappa u_*/fL$; $L = u_*^3/\kappa \mid B_s \mid$ the Monin-Obukhov length[5], and B_s the near-surface value of the vertical buoyancy flux, defined as

$$B_s = \beta\frac{H_S}{c_p\rho} + 0.608\frac{gH_L}{L_c\rho} \tag{28}$$

where $\beta = g/\theta$ is the buoyancy parameter, H_S the sensible heat flux, c_p the heat capacity of air at constant preasure, ρ the density, g the gravitational acceleration, H_L the latent heat flux, and L_c the latent heat of condensation.

The atmosphere is now divided into 3 regions: $R_1 : z \sim z_0$, $R_2 : z \sim L$, and $R_3 : z \sim h$, where h is the height of the planetary boundary layer. The governing equation in region R_1 is the law of the wall, Eqs. 16 and 17. In region R_2 the equation is a velocity defect law similar to Eqs. 12 and 13, given by

$$\frac{U - \Delta U}{u_*} = \chi(\zeta), \qquad \frac{V}{u_*} = 0 \tag{29}$$

where $\Delta U = U(z = L)$ is the value of the mean wind at $z = L$ and $\zeta = z/L$. It is assumed that $z_0 \ll L \ll h$, thereby excluding the near-neutral case (where $L \gg h$).

Matching the equations in R_1 and R_2, ie using the principle laid out in the previous section, assuming that

$$\frac{\Delta U}{u_*} = m_1(\eta, \mu) \tag{30}$$

[4]For completeness it should be mentioned that the stability dependence of the temperature profiles is found to be dependent on a third function: C. Not to be confused with the constant C in the previous section.

[5]This definition renders L positive for both the stable and the unstable case.

where $\eta = z_0/L$, which is a quite general expression, gives the logarithmic profile for the mean wind, U, see Eq. 20. For ΔU, the following equation is found

$$\frac{\Delta U}{u_*} = \frac{1}{\kappa}\ln\eta + A_1 \tag{31}$$

where A_1 is a universal constant. As can be seen from this, $\Delta U/u_*$ does not explicitly depend on stability.

Differentiating the logarithmic profile with respect to z, gives

$$\frac{zU'}{u_*} = \frac{1}{\kappa} \tag{32}$$

In region R_3 the velocity defect law can generally be written

$$\frac{U - \Delta U}{u_*} = F\left(\frac{fz}{\kappa u_*}, \mu, \eta\right) \tag{33}$$

Since μ is very large and η very small, they can be neglected in F by doing a proper scaling of the velocity defect and the height. η (ie z_0) is not a scaling parameter in this case, but μ is. We therefore write

$$\frac{U - U_g}{u_*} = \mu^{n_1} F_u\left(\frac{fz}{\kappa u_* \mu^s}\right), \qquad \frac{V - V_g}{u_*} = \mu^{n_1} F_v\left(\frac{fz}{\kappa u_* \mu^s}\right) \tag{34}$$

where $h = \kappa u_* \mu^s / f$. The same exponent (n_1) on the multipliers of F_u and F_v have been used, because contrary to regions R_1 and R_2, the two components of the wind is expected to be of the same order of magnitude in R_3.

Generally the geostrophic wind can be written

$$\frac{U_g}{u_*} = p_1(\mu, \eta), \qquad \frac{V_g}{u_*} = p_2(\mu, \eta) \tag{35}$$

In region R_2 it can be seen from Eq. 29 that U' is not a function of z_0[6]. Therefore U' can be written as a function of ζ only:

$$U' = \frac{\kappa}{u_*^2} f(\zeta), \qquad V' = 0 \tag{36}$$

Integrating from $\zeta = 1$ to ζ using Eq. 31 we get

$$\frac{U}{u_*} = f_1(\zeta) - \frac{1}{\kappa}\ln\eta + A_1 \tag{37}$$

$$\frac{V}{u_*} = 0 \tag{38}$$

where

$$f_1(\zeta) = \int_1^\zeta f(\zeta)d\zeta$$

with $f_1(1) = 0$.

So far it has not mattered whether the atmosphere was stable or unstable, from now on, however, a distinction has to be made.

The unstable case

Using similarity arguments dating back to Prandtl (1932) and Priestly (1959), the function f_1 for an non-rotating, unstable atmosphere can be written

$$f_1(\zeta) = B_1(\zeta^{-1/3} - 1) \tag{39}$$

[6]Albeit U is dependent of z_0, because at $z = L$ it is equal to ΔU, given by Eq. 31.

where B_1 is a universal constant. Using this and matching regions R_2 and R_3, we get

$$\mu^{n_1} F_u\left(\frac{\zeta}{\mu^{s+1}}\right) = B_1(\zeta^{-1/3} - 1) - \frac{1}{\kappa}\ln\eta + A_1 - p_1(\mu,\eta) \tag{40}$$

$$\mu^{n_1} F_v\left(\frac{\zeta}{\mu^{s+1}}\right) = -p_2(\mu,\eta) \tag{41}$$

Differentiating these with respect to η, gives

$$\frac{\partial p_1}{\partial \eta} = -\frac{1}{\kappa\eta}, \qquad \frac{\partial p_2}{\partial \eta} = 0 \tag{42}$$

Integrating, assuming that $p_1(\mu,\eta)$ can be regarded as a combination of two functions, the one being dependent on η, and the other, γ_1, on μ, yields

$$p_1(\mu,\eta) = -\frac{1}{\kappa}\ln\eta + A_1 - B_1 + \gamma_1(\mu) \tag{43}$$

Hence the equations in the matched region are

$$\mu^{n_1} F_u\left(\frac{\zeta}{\mu^{s+1}}\right) = B_1\zeta^{-1/3} - \gamma_1(\mu) \tag{44}$$

$$\mu^{n_1} F_v\left(\frac{\zeta}{\mu^{s+1}}\right) = -p_2(\mu) \tag{45}$$

Eliminating F_u by cross-differentiation with respect to ζ and μ gives

$$n_1\left[B_1\zeta^{-1/3} - \gamma_1(\mu)\right] + \gamma_1'(\mu)\mu = -\frac{1}{3}(s+1)B_1\zeta^{-1/3} \tag{46}$$

Comparing terms dependent on ζ reveals that $n_1 = -\frac{1}{3}(s+1)$, and of μ that $\gamma_1 = D_1\mu^{-\frac{1}{3}(s+1)}$, where D_1 is an universal constant. Combining Eqs. 35 and 43 yields

$$\frac{U_g}{u_*} = \frac{1}{\kappa}\ln\left(\frac{L}{z_0}\right) + A_1 - B_1 + D_1\mu^{-\frac{1}{3}(s+1)} \tag{47}$$

Comparing this with Eq. 26, the following expression can be derived

$$A(\mu) = \ln\mu + \alpha_{1u} + \beta_{1u}\mu^{-\frac{1}{3}(s+1)} \tag{48}$$

where $\alpha_{1u} = \ln\kappa - \kappa(A_1 - B_1)$ and $\beta_{1u} = -\kappa D_1$. For the y-component it can be seen from Eq. 45 that F_v = constant $= -D_2$, where D_2 is a universal constant. Inserting this in Eq. 34 and comparing with Eq. 27 leads to

$$B(\mu) = \beta_{2u}\mu^{n_1} \tag{49}$$

where $\beta_{2u} = -\kappa D_2$.

To close the unstable case a determination of s is needed: The equation of motion can be written

$$\frac{d\tau_z}{dz} = -f(V - V_g) \tag{50}$$

where the kinematic momentum flux is given by $\tau_z = -\overline{u'w'}$. Integrating from $z=0$ to $z=h$, and using the fact that τ_z vanishes at h by definition, gives

$$-\tau_z(z=0) = -f\int_0^h (V - V_g)\,dz \tag{51}$$

Estimating the integral by using Eq. 34 it is found to be of order $u_*\mu^{n_1}h$, this yields

$$u_*^2 \sim f u_*\mu^{n_1} h \tag{52}$$

since $-\tau_z(z=0) = u_*^2$. Using that h is of order $u_*\mu^s/f$ gives

$$u_*^2 \sim u_*^2\mu^{n_1+s} \tag{53}$$

the conclusion of this being that $n_1 = -s$. Note, that this is not dependent on stability, and is therefore valid for both the stable and the unstable case.

For the unstable case (where $n_1 = -\frac{1}{3}(s+1)$) $n_1 = -\frac{1}{2}$ and $s = \frac{1}{2}$, and the stability dependent similarity functions can be written[7]

$$A(\mu) = \ln\mu + \alpha_{1u} + \beta_{1u}\mu^{-1/2} \tag{54}$$

$$B(\mu) = \beta_{2u}\mu^{-1/2} \tag{55}$$

The stable case

The derivation for the stable case proceeds much like that for the unstable case; the matching of R_1 and R_2 gives the logarithmic profile:

$$\frac{U}{u_*} = \frac{1}{\kappa}\ln\left(\frac{z}{z_0}\right) \tag{56}$$

and

$$\frac{\Delta U}{u_*} = -\frac{1}{\kappa}\ln\eta + E_1 \tag{57}$$

where E_1 is a universal constant. Using the theory of Obukhov (1946), that as z/L becomes large, U' becomes a constant, and therefore that U can be written as a constant times ζ, yields

$$\frac{U}{u_*} = -\frac{1}{\kappa}\ln\eta + E_1 + F_1(\zeta - 1) \tag{58}$$

with F_1 being a universal constant. Matching now regions R_2 and R_3 gives

$$\frac{U_g}{u_*} = -\frac{1}{\kappa}\ln\eta + E_1 - F_1 + H_1\mu^{s+1} \tag{59}$$

$$\frac{V_g}{u_*} = H_2\mu^{s+1} \tag{60}$$

where the exponent of $s+1$ comes about using the fact that $h/L \sim \mu^{s+1}$, and therefore that $n_1 = s+1$ for the stable case, H_1 and H_2 are universal constants, using that $n_1 = -s$, it can be seen that for the stable case $n_1 = \frac{1}{2}$ and $s = -\frac{1}{2}$. Comparing these equations to Eqs. 26 and 27, the similarity functions for the stable atmosphere reads

$$A(\mu) = \ln\mu + \alpha_{1s} + \beta_{1s}\mu^{1/2} \tag{61}$$

$$B(\mu) = \beta_{2s}\mu^{1/2} \tag{62}$$

where $\alpha_{1s} = -\ln\kappa - \kappa(E_1 - F_1)$, $\beta_{1s} = -\kappa H_1$, and $\beta_{2s} = -\kappa H_2$.

2.5 Empirical expressions for $A(\mu)$ and $B(\mu)$

Having the great scatter of the experimental values of A and B's neutral value in mind, we now proceed to obtain estimates of the stability dependence of these two coefficients. This is important since the atmosphere is very seldom in a neutral state, and the effect of stability on the flow, especially the direction, is strong. Here

$$\mu = \frac{\kappa u_*}{|f|\,L} \tag{63}$$

is used as a measure of stability, where $\kappa u_*/f$ is the boundary layer height, and $L = -u_*^3/\kappa B_s$ is the Monin-Obukhov length. Note that this is the standard definition

[7] Long and Gulley (1977) note that the use of actual atmospheric observations, where $U' \propto \zeta^{5/4}$, would lead to terms $\beta_{1u}\mu^{1/3}$ and $\beta_{2u}\mu^{1/3}$. They also note, however, that in comparison with atmospheric observations of A and B this is found to be a negligible effect.

of L, so now L is positive for stable conditions and negative for unstable, because B_s is positive, when the flux is directed upwards.

In order to determine the stability dependence of the A-, B-, (and C-) functions a number of experiments have been carried out, many of which can be found in the list of experiments to determine the neutral value of A and B. There are two 'classical' experiments: the WANGARA experiment near Hay, Australia (see Clarke et al, 1971, for details) analysed by Clarke and Hess (see eg Clarke and Hess, 1974), and the Great Plains experiment carried out near O'Neil, Nebraska (see Lettau and Davidson, 1957, for details) analysed by Zilitinkevich and Chalikov (1968). However, the two stability dependent functions found in these two papers differ significantly, originally explained by the large experimental scatter. This issue was taken up by Arya (1975) who completely reanalysed the two data sets, including a procedure to reject 'bad' runs, and he found that the scatter was significantly reduced. The functional dependence of A and B on stability found by Arya (1975) is given in Table 1 for the stable case, and in Table 2 for the unstable case. The functions are fitted to the WANGARA data, which are found to be taken in a more homogeneous terrain than the Great Plains data. Note again that the neutral values of $A(=1.01)$ and $B(=5.14)$ are different from the ones commonly used.

There have been a number of other attempts, theoretical as well as experimental, to determine $A(\mu)$ and $B(\mu)$, the results of which are shown in Table 1 for the stable atmosphere and in Table 2 for the unstable atmosphere.

Table 1. Different empirical evaluations of the A and B functions in Eqs. 26 and 27, for the stable *case.*

Arya (1975)	$A(\mu) = 1.01 - 0.105\mu - 9.9 \times 10^{-4}\mu^2 + 8.1 \times 10^{-7}\mu^3$
	$B(\mu) = 5.14 + 0.142\mu + 1.17 \times 10^{-3}\mu^2 + 3.3 \times 10^{-6}\mu^3$
Arya (1977)	$A(\mu) = 2.96 + \ln\mu^{1/2} - 1.52\mu^{1/2}$
	$B(\mu) = 1.1 + 1.82\mu^{1/2}$
Billard et al (1981)*	$A(\mu) = -0.024\mu - 1.67$
	$B(\mu) = 0.051\mu + 8.06$
Jensen et al (1984)	$A(\mu) = 1 - 1.58\mu^{1/2}$
	$B(\mu) = 5 + 1.58\mu^{1/2}$
Long and Guffey (1977)	$A(\mu) = \ln\mu + 23.3 - 5.28\mu^{1/2}$
	$B(\mu) = 2.55\mu^{1/2}$
Zilitinkevich (1975)‡	$A(\mu) = \ln\mu - 4\mu^{1/2}$
	$B(\mu) = 4\mu^{1/2}$
Zilitinkevich (1989)¶	$A(\mu) = \ln(1+0.88\mu^{1/2}) - 2.55\mu^{1/2} + 1.7$
	$B(\mu) = 1.76\mu^{1/2} + 4.5$

* linear regressional fit to data.

‡ Note, that the Zilitinkevich curves are from the O'Neil data set, before the correction by Arya (1975).

¶ Not shown in figures since only the dependence in the stable case is given.

Here two things are worthwhile taking notice of: firstly, that the functions are discontinuous in zero (neutral), and secondly, that again the neutral values are not equal to the ones normally chosen. Note, however, that in cases of near-neutral stability, the neutral version of the drag law should be used. A plot of the different A's and B's is shown in Figures 3 and 4.

As can be seen from both figures, the different functional expressions give somewhat different results. Since this is the case, and there exists no single commonly acknowledged profile, it has been found necessary to test all these different models, in order to find the one that will give the best results for the set of stations

Table 2. Different empirical evaluations of the A and B functions in Eqs. 26 and 27, for the unstable case.

Arya (1975)†	$A(\mu) = 1.01 - 0.105\mu - 9.9 \times 10^{-4}\mu^2 + 8.1 \times 10^{-7}\mu^3$
	$B(\mu) = 5.14 + 0.142\mu + 1.17 \times 10^{-3}\mu^2 + 3.3 \times 10^{-6}\mu^3$
Arya (1977)§	$A(\mu) = \ln \mid \mu \mid +0.58$
	$B(\mu) = 0.72 \exp(0.2\mu)$
Billard et al (1981)*	$A(\mu) = -0.07\mu + 1.08$
	$B(\mu) = -0.033\mu + 1.42$
Jensen et al (1984) ¶	$A(\mu) = 1 + \ln(1 - \kappa/\mu)$
	$B(\mu) = \frac{5-\kappa}{1-a\mu/\kappa} + \kappa\frac{u_*}{f}\left(\frac{1}{z_i} + \frac{1}{u_*/f}\right)\left(\frac{1}{h} + \frac{1}{u_*/f}\right)^{1/2}$
Long and Guffey (1977)	$A(\mu) = \ln \mid \mu \mid -1.47 + 11.7\mu^{-1/2}$
	$B(\mu) = 18.4 \mid \mu \mid^{-1/2}$
Zilitinkevich (1975)‡	$A(\mu) = \ln\frac{\mid\mu\mid}{\kappa} - 1$
	$B(\mu) = 10 \mid\mu\mid^{-1/2}$

† On the very unstable side (ie for $\mu < -50$) A approaches 3.69 and B 1.38.

§ Where the h in the paper has been approximated with $\kappa u_*/f$.

* linear regressional fit to data.

¶ $a = 1/25$.

‡ Note that the Zilitinkevich curves are from the O'Neil data set, before the correction by Arya (1975).

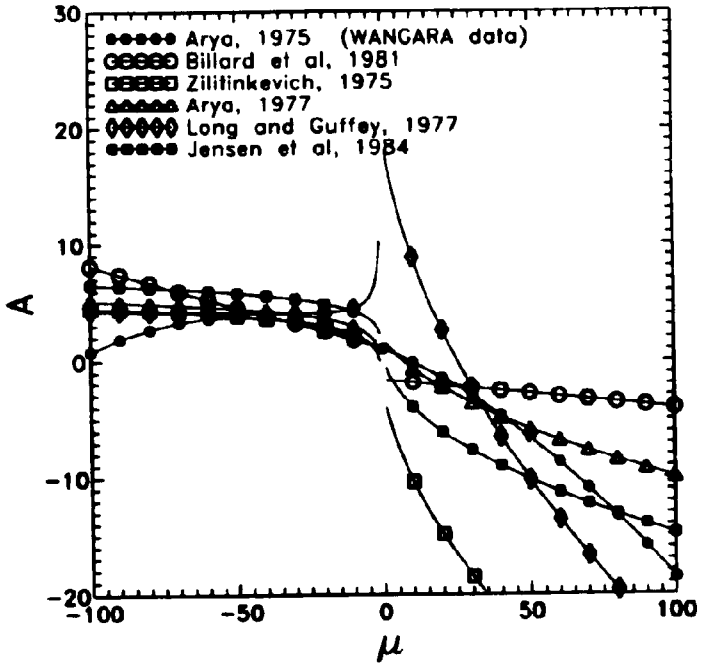

Figure 3. The functional dependence of A on stability, $\mu = \kappa u_*/\mid f \mid L$.

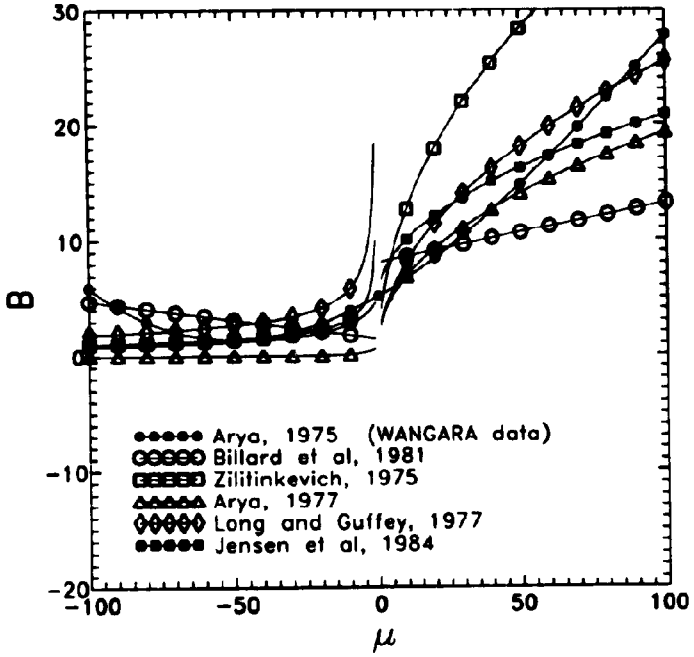

Figure 4. The functional dependence of B on stability, $\mu = \kappa u_* / |f| L$.

studied here. This will be done in Part III.

Influence of baroclinicity

Many researchers (see eg Yordanov and Wippermann, 1972) have suggested that the large scatter still present can be lessened by including baroclinicity dependence in the A and B functions, viz. $A = A(\mu, \mathbf{S})$, and $B = B(\mu, \mathbf{S})$, where

$$\mathbf{S} = (S_x, S_y) = \frac{\kappa^2}{f}\left(\frac{\partial u_g}{\partial z}, \frac{\partial v_g}{\partial z}\right) \tag{64}$$

represents the linear effect of baroclinicity. Billard et al (1981) tried to take this effect into account, and they conclude that it is not very likely that baroclinicity is an important parameter in Rossby similarity theory. They note also, however, that their conclusions are based on a rather limited set of data, and as a consequence of this that more experimental evidence is needed to sustain their statement. Clarke a[illegible] Hess (1974) assumed that A and B depend on baroclinicity in the following way:

$$A' = \frac{\partial A}{\partial \mu}\mu' + \frac{\partial A}{\partial S_x}S_x' + \frac{\partial A}{\partial S_y}S_y'$$

and

$$B' = \frac{\partial B}{\partial \mu}\mu' + \frac{\partial B}{\partial S_x}S_x' + \frac{\partial B}{\partial S_y}S_y'$$

The least-squares technique is used to determine the coefficients. Clarke and Hess (1974) emphasise that these values are tentative, because of measurement difficulties and the effect of unsteadiness in the atmosphere. They compare their values to the ones found by Wippermann (1972) and find considerable disagreement; they find qualitative agreement with Blackadar (1965) and Fiedler (1972). Because of

the weak dependence (maximum value of the coefficients is ≈ 0.2) and the disagreement found in the literature, the effect of baroclinicity will not be taken into account in this study.

2.6 Stability dependence of the velocity profile

Contrary to the A- and B-function there is better agreement concerning the stability dependence of the velocity profile. The most recent and reliable profiles are the ones given by Högström (1988). They have been found by using reported profiles from almost all known measurements, and modified to take dynamical flow distortion into account, since this is suspected to be the single major cause of the differences in the different profiles. The profiles are given by:

$$\frac{z}{u_*}\frac{\partial u}{\partial z} = \frac{1}{\kappa}\phi_m(\zeta) \tag{65}$$

where $\zeta = z/L$ is a non-dimensional measure of stability, and

$$\phi_m = \begin{cases} 1 + 4.8\zeta & \text{for } \zeta \geq 0 \\ (1 - 19.3\zeta)^{-0.5} & \text{for } \zeta < 0 \end{cases} \tag{66}$$

is the modified Dyer gradient (Dyer, 1974). Högström (1988) concludes that the expression for the stable case could as well be: $\phi_m = 1 + 6\zeta$, which is the modified Kansas profile. For neutral stratification ($\zeta = 0$), it can be seen that these expressions collapse to the logarithmic profile. Integrating Eq. 65 from $z = z_0$ (where $u = 0$) to z, we get the velocity profile as:

$$u(z) = \frac{u_*}{\kappa}\left[\ln\left(\frac{z}{z_0}\right) - \psi_m(\zeta) + \psi_m\left(\frac{z_0}{L}\right)\right] \tag{67}$$

where

$$\psi_m = \begin{cases} -\beta_m\zeta & \text{for } \zeta \geq 0 \\ 2\ln(1+x) + \ln(1+x^2) - 2\tan^{-1}(x) & \text{for } \zeta < 0 \end{cases} \tag{68}$$

and $\beta_m = 4.8$ and $x = (1 - 19.3\zeta)^{1/4}$.

These profiles will replace the logarithmic profile in the stability dependent versions of the neutral model, to be developed in the following.

Part II

The Applied Models

3 Introduction

In order to predict local winds up to 36 hours ahead, two things are needed:

1. A forecast model taking synoptic scale systems into account. To do this for Europe a model covering all of Europe and most of the Atlantic Ocean is needed. This is to ensure that systems that are likely to affect the site will be present in the initial analysis.
2. A model taking the local effects, such as the local topography, the local roughnesses and changes in roughness, and the shelter from nearby obstacles (such as houses, trees, etc), into account.

The reason why those two models can not be combined into one, generally, is that this would demand computer power and storage of data, far beyond the possibilities of today's technology.

The idea is then to do the forecast in two steps: First to calculate the general large-scale flow pattern, and then calculate the detailed flow pattern at the site only. To do this, two recently developed models are used. They are:

HIRLAM High Resolution Limited Area Model, developed by the meteorological institutes in Denmark, Finland, Iceland, Norway, Sweden, and The Netherlands (Machenhauer, 1988).

WAsP Wind Atlas Analysis and Application Program, developed by Risø National Laboratory (Mortensen et al, 1993).

In the following sections these two models will be described, with most of the weight on the theory behind WAsP. At the end of this Part a short summary of the theory behind neural networks will also be given, since these will be used in some of the prediction models.

4 WAsP

WAsP is a program to make wind atlases. A wind atlas is a generalised wind climate for an area. The idea behind the program is to take measurements from a specific site (eg a meteorological mast at an airport), calculate the sector-wise distribution of the wind (described by the two-parameter Weibull distribution, cf Weibull, 1951), and 'clean' this for the following effects, in the order stated:

1. Shelter from obstacles in the vicinity of the site.
2. Changes in the roughness of the surface.
3. Orography.

The corrected distribution is called a *wind atlas*, and it can be regarded as the generalised wind climate valid within an area surrounding the measurement site. The size of this area is dependent on the complexity of the terrain and the type of the dominating weather systems; in eg Denmark (flat terrain, dominated by the passage of low-pressure systems) it can be several thousands of km^2, but in mountainous areas and areas dominated by local thermally driven circulations (such as many areas around the Mediterranean), it can be down to only tens of km^2. Within this area it is possible to horizontally extrapolate the measured wind climate. This is done by taking the local description of the *new* site, and applying the aforementioned procedure to the atlas in *reverse* order. This gives the expected

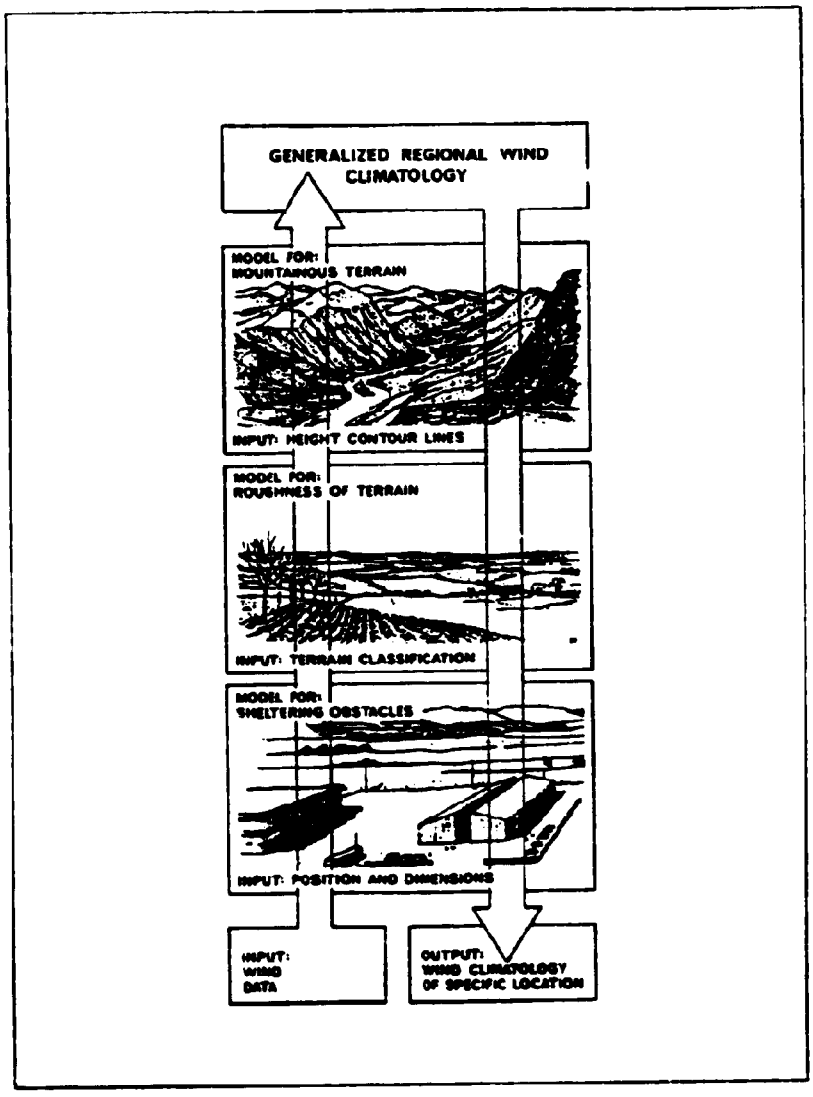

Figure 5. The basic idea of WA^{S}P and the European Wind Atlas. From Troen and Petersen (1989).

wind climate at the new site. The procedure, called the *wind atlas methodology*, is depicted in Figure 5.

Since WA^{S}P operates on wind speed distributions, and not, as is needed in this investigation, on time series, it is necessary to extract intermediate results from the models in WA^{S}P. This is done by using the dump option in WA^{S}P[8].

The WA^{S}P model consists of 3 main parts, modelling the aforementioned effects.

1 A model for flow in complex terrain

2 A model for taking roughness and roughness-changes into account

3 A model describing the influence of obstacles on the flow

[8] Technically speaking by setting parameter P_{63} in WASP.PAR equal to 3 and using the '-dump' command

Furthermore, the climatic variation of the stability is taken into account. The theory, which these 3 models are based upon, will be described in the following.

5 The model for flow in complex terrain

When the wind passes a topographical feature, such as a hill, an escarpment, or a valley, its magnitude and direction will undergo a change. In the case of a hill, the wind will accelerate at the top and decelerate at the foot; while part of the wind will be deflected. The fact that the wind is accelerated at a hill top, is used extensively in the siting of wind turbines. In a valley the wind is decelerated, and channeled in the direction of the valley. The flow over an escarpment is also accelerated at the top, and decelerated at the foot, however, no change in direction is found, because of the two-dimensional nature of the problem.

The fact that the flow separates after the passage of a hill/escarpment, steeper than a certain value, has a firm empirical background, see eg Finnigan (1988) and de Baas (1990); however, this effect is not modeled in the model described below. This is due to the fact that this model models potential flow only (ie based on equations dependent on a potential only), because it is meant to be simple in order to get a fast calculation of the right answer (in most cases). More complex models (as the K-ϵ model) are able to simulate the separation, see eg de Baas (1990).

The idea for modelling potential flow, presented here, was first laid out by Jackson and Hunt (1975) and has since then been used and refined by several: Mason and Sykes (1979), Mason and King (1985), Taylor et al (1983), and Walmsley et al (1986). The idea has also been used in the complex terrain model in the European Wind Atlas (Troen and Petersen, 1989).

In the Jackson and Hunt paper (Jackson and Hunt, 1975) the flow over a *two-dimensional* hump was considered. Their idea was that there existed two different flow regions: an *inner* region, where the flow is influenced by the hill, resulting in a flow perturbation increasing with height, caused by turbulent transports, and an *outer* region, where the basic flow is independent of height, and the perturbed flow is inviscid and decaying with height. The height separating these two flow regimes is of order $l_i = \mathcal{L}u_*/U$, where $\mathcal{L}$ is a characteristic horizontal length scale, U a characteristic flow speed, and u_* the friction velocity.

The derivation of the expressions in this model is described very clearly in Troen (1990). Starting from the governing equations for the *horizontal* flow in a neutral atmosphere a scale analysis (see eg Holton, 1979, Chap. 2) gives that these equations read:

$$\frac{dU}{dt} - fV = -\frac{1}{\rho}\frac{\partial p}{\partial x} \tag{69}$$

$$\frac{dV}{dt} + fU = -\frac{1}{\rho}\frac{\partial p}{\partial y} \tag{70}$$

$$\tag{71}$$

where U and V are the x- and y-component of the horizontal wind, respectively, f the Coriolis parameter, ρ the density, and p the pressure.

Writing now the equations of motion in their flux form, using the continuity equation and averaging (see eg Holton, 1979, Chap. 5), we get the following equations for the *mean* flow:

$$\frac{dU}{dt} - fV = -\frac{1}{\rho}\frac{\partial p}{\partial x} + \frac{1}{\rho}\frac{\partial \tau_x}{\partial z} \tag{72}$$

$$\frac{dV}{dt} + fU = -\frac{1}{\rho}\frac{\partial p}{\partial y} + \frac{1}{\rho}\frac{\partial \tau_y}{\partial z} \tag{73}$$

where all quantities are mean quantities, and $\tau = (\tau_x, \tau_y) = (-\rho\overline{u'w'}, -\rho\overline{v'w'})$, $\bar{x}$ denotes averaging of x, and $'$ the deviation from the mean caused by the turbulent eddies.

Assuming that the Coriolis terms (ie terms containing f) can be neglected, since we are very close to the surface where the frictional force is balanced by the pressure gradient, and assuming that the flow is stationary, the equations read

$$U\frac{\partial U}{\partial x} + V\frac{\partial U}{\partial y} + W\frac{\partial U}{\partial z} = -\frac{1}{\rho}\frac{\partial p}{\partial x} + \frac{1}{\rho}\frac{\partial \tau_x}{\partial z} \tag{74}$$

$$U\frac{\partial V}{\partial x} + V\frac{\partial V}{\partial y} + W\frac{\partial V}{\partial z} = -\frac{1}{\rho}\frac{\partial p}{\partial y} + \frac{1}{\rho}\frac{\partial \tau_y}{\partial z} \tag{75}$$

Assuming now that the effect of a hill on the flow can be described as a perturbation ($\mathrm{u} = (u, v, w)$) to the known horizontal mean flow ($\mathrm{U}_0 = (U_0(z), V_0(z), 0)$) (ie $U = U_0 + u$, $V = V_0 + v$, $W = w$) we get, where, for convenience, we only look at the x-component of the equation

$$(U_0 + u)\frac{\partial(U_0 + u)}{\partial x} + (V_0 + v)\frac{\partial(U_0 + u)}{\partial y} + w\frac{\partial(U_0 + u)}{\partial z} = -\frac{1}{\rho}\frac{\partial p}{\partial x} + \frac{1}{\rho}\frac{\partial \tau_x}{\partial z}$$

Expanding this, we get

$$U_0\frac{\partial U_0}{\partial x} + U_0\frac{\partial u}{\partial x} + u\frac{\partial U_0}{\partial x} + u\frac{\partial u}{\partial x} + V_0\frac{\partial U_0}{\partial y} + V_0\frac{\partial u}{\partial y} + v\frac{\partial U_0}{\partial y} + v\frac{\partial u}{\partial y} + w\frac{\partial U_0}{\partial z} + w\frac{\partial u}{\partial z}$$
$$= -\frac{1}{\rho}\frac{\partial p}{\partial x} + \frac{1}{\rho}\frac{\partial \tau_x}{\partial z}$$

Since $U_0 = U_0(z)$, all derivatives with respect to x and y are zero, and further assuming that products of perturbations are small ($= 0$), the equation becomes

$$U_0\frac{\partial u}{\partial x} + V_0\frac{\partial u}{\partial y} + w\frac{\partial U_0}{\partial z} = -\frac{1}{\rho}\frac{\partial p}{\partial x} + \frac{1}{\rho}\frac{\partial \tau_x}{\partial z}$$

Using K-theory, stating that

$$\tau = \rho u_*^2$$

and

$$\frac{\partial u}{\partial z} = \frac{u_*}{\kappa z}$$

which combined with the definition that

$$\tau = \rho K \partial u/\partial z$$

gives

$$K = u_* \kappa z$$

and neglecting vertical advection terms (ie terms of the form $w\frac{\partial}{\partial z}$), we finally get

$$U_0\frac{\partial u}{\partial x} + V_0\frac{\partial u}{\partial y} = -\frac{1}{\rho}\frac{\partial p}{\partial x} + K\frac{\partial^2 u}{\partial z^2} \tag{76}$$

If the same procedure is followed for the $y-$ and $z-$components, we get

$$U_0\frac{\partial v}{\partial x} + V_0\frac{\partial v}{\partial y} = -\frac{1}{\rho}\frac{\partial p}{\partial y} + K\frac{\partial^2 v}{\partial z^2} \tag{77}$$

and

$$U_0\frac{\partial w}{\partial x} + V_0\frac{\partial w}{\partial y} = -\frac{1}{\rho}\frac{\partial p}{\partial z} + K\frac{\partial^2 w}{\partial z^2} \tag{78}$$

The continuity equation becomes

$$\frac{\partial u}{\partial x} + \frac{\partial v}{\partial y} + \frac{\partial w}{\partial z} = 0 \tag{79}$$

since $\mathbf{U}_0 = (U_0(z), V_0(z), 0)$.

We have now 4 equations in four unknown perturbations: u, v, w, and p. The perturbations are now transformed into Fourier integrals in the two horizontal directions.

Applying this procedure to the terms and equations, gives the following set of equations for the wave number $\mathbf{k} = (k, l)$, where the phase-space perturbations, for convenience, are now written using the same notation as for the perturbations in physical space:

$$-ikU_0u - ilV_0u = ikp + K\frac{\partial^2 u}{\partial z^2} \tag{80}$$

$$-ikU_0v - ilV_0v = ilp + K\frac{\partial^2 v}{\partial z^2} \tag{81}$$

$$-ikU_0w - ilV_0w = -\frac{\partial p}{\partial z} + K\frac{\partial^2 w}{\partial z^2} \tag{82}$$

$$-iku - ilu + \frac{\partial w}{\partial z} = 0 \tag{83}$$

where p now is redefined as the pressure divided by the density, ρ.

The solutions to these equations are a sum of exponentials of the form: $\exp(\alpha_i z)$. This can be seen by inserting the expression in the equations. The α_i's can be determined from the following set of matrices

$$\begin{pmatrix} \Omega & 0 & 0 & -ik \\ 0 & \Omega & 0 & -il \\ 0 & 0 & \Omega & \alpha \\ -ik & -il & \alpha & 0 \end{pmatrix} \begin{pmatrix} u \\ v \\ w \\ p \end{pmatrix} = 0 \tag{84}$$

where $\Omega = -ikU_0 - ilV_0 - K\alpha^2$. This matrix has solutions if the determinant of the coefficient matrix is equal to zero:

$$(\alpha^2 - |\mathbf{k}|^2)\Omega^2 = 0 \tag{85}$$

This equation has two solutions

$$\alpha_1 = \pm |\mathbf{k}| \tag{86}$$

$$\alpha_2 = \sqrt{-i\frac{\mathbf{k}\cdot\mathbf{U}_0}{K}} \tag{87}$$

where the positive root in the α_1-solution is discounted, because it leads to non-physical exponential growth.

The two solutions, α_1 and α_2, represents two 'canonical' scales induced by the equations of motion: an outer scale, $L = -1/\alpha_1$ and an inner $\ell = 1/\alpha_2$.

If the outer scale is examined first, $\alpha = |\mathbf{k}|$ is inserted into the u-component of the equation of motion, giving

$$\Omega u = ikp \tag{88}$$

where

$$\Omega = -i\mathbf{k}\cdot\mathbf{U}_0(|\mathbf{k}|^{-1}) - K|\mathbf{k}|^2 \tag{89}$$

assuming that the relevant height is $z = |\mathbf{k}|^{-1}$, and therefore that the advection speed is the speed at that height. If furthermore, the expression for K is inserted, we get

$$\Omega = -i\mathbf{k}\cdot\mathbf{U}_0(|\mathbf{k}|^{-1}) - \kappa u_* |\mathbf{k}| \tag{90}$$

The two terms in Ω can now be evaluated

$$\frac{|\mathbf{k}\cdot\mathbf{U}_0(L)|}{u_*\kappa|\mathbf{k}|} = \frac{\ln(L/z_0)}{\kappa^2}|\cos\phi| \ll 1 \tag{91}$$

where $\cos\phi = \mathbf{U}_0 \cdot \mathbf{k} / |\mathbf{U}_0||\mathbf{k}|$. The inequality is valid if L (the outer scale) is much greater than z_0 (the roughness length), which is the same as saying that the horizontal scales in question have to be much larger than z_0. Furthermore, the wave number vector must not be perpendicular to the background wind - making $\cos\phi = 0$. The following analysis will show that the perturbation in this case is exactly zero. This means that for the outer scale, L, the diffusion term may be neglected.

The *inner* solution can be written, assuming this time that the height is equal to ℓ

$$\alpha_2 = \sqrt{-i\frac{\mathbf{k} \cdot \mathbf{U}_0(\ell)}{u_* \kappa \ell}} \tag{92}$$

It is now possible to establish a relation between the outer scale L, and the inner scale ℓ, viz.

$$\kappa^2 L = \ell \ln(\ell / z_0) \tag{93}$$

Looking back at the equations of motion, it is seen that since the inner scale is associated with $\Omega = 0$, the pressure (perturbation) must be equal to zero. Meaning that the pressure is determined solely by the outer solution.

The lower boundary condition for flow over complex terrain is that the terrain undulations induce a vertical flow, proportional to the slope of the terrain, see Figure 6. Since it is the pressure field that drives the flow, and only the outer flow has a non-zero pressure field, it is the outer scale that is the relevant scale, and thereby the outer velocity scale, $\mathbf{U}_0(L)$. The boundary condition can be written

$$\omega_0 = \mathbf{U}_0 \cdot \nabla h(x, y) = -i\mathbf{k} \cdot \mathbf{U}_0(L) h(\mathbf{k}) \tag{94}$$

where $h(x, y)$ is the altitude of the surface, and $h(\mathbf{k})$ is it's Fourier transform. From this equation it can be seen that if $\mathbf{k} \cdot \mathbf{U}_0 = 0$, the perturbation will be exactly zero.

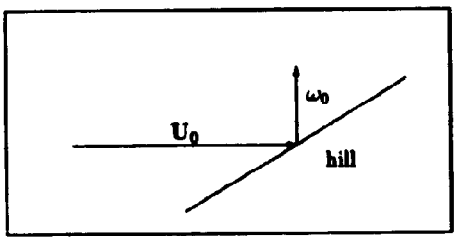

Figure 6. Illustration of the boundary condition induced on flow over complex terrain.

The solution for the pressure field is then given by

$$p(\mathbf{k}, z) = \frac{(\mathbf{k} \cdot \mathbf{U}_0(L))^2}{|\mathbf{k}|} h(\mathbf{k}) \exp(-z/L)$$

Following Mason and Sykes (1979) in solving for u and v, the pressure field is introduced in the original equations: (76) to (79). For the outer scale (ie $z \ll L$) the result for the horizontal velocity is

$$u(\mathbf{k}, z) = -\frac{\mathbf{k}}{|\mathbf{k}|} \frac{|\mathbf{U}_0(L)|}{|\mathbf{U}_0(z)|} \mathbf{k} \cdot \mathbf{U}_0(L) h(\mathbf{k}) \exp(-z/L) \tag{95}$$

For the inner scale the same procedure can be followed obtaining analytical solutions. A simpler solution is attained, however, in the BZ-model (Troen and Petersen, 1989) used in WA^{S}P. It assumes that Eq. 95 is valid down to $z = \ell$, and below this height the direction of the perturbation wind vector does not change significantly, and the relative speed change is constant.

5.1 Zooming grid

A special feature of the flow model in WA^{S}P is that it uses a zooming grid, ie a radial grid where the radial resolution decreases away from the center with a constant factor of 1.06. Using this grid has two advantages:

1. Near tne station the resolution is very high, typically around 1 metre
2. A large area can be covered

To use the zooming grid the equations need to be transformed into a polar coordinate system. In this coordinate system the velocity perturbation is related to a potential by:

$$\mathbf{u} = \nabla\chi$$

and the potential is, assuming that it vanishes at a given outer model radius, R, expressible as a sum with terms of the form

$$\chi_j = K_{nj} J_n\left(c_j^n \frac{r}{R}\right) \exp(in\phi) \exp\left(-c_j^n \frac{z}{R}\right)$$

where K_j^n are arbitrary coefficients, J_n the Bessel function of nth order, r radius, ϕ azimuth angle, z height, and c_j^n are the jth zero of J_n.

5.2 Verification of the flow model

As a result of the Workshop on Modelling of the Atmospheric Flow Field, held at ICTP, Trieste, Italy in May 1988, an article (Walmsley et al, 1990) was published, comparing four models (one of which being WA^{S}P) of surface boundary-layer flow with measurements made at Blashaval Hill, North Uist, Scotland. The experiment is described in Mason and King, 1985. In summary, the results of this test are that 1) the models are very alike in performance, and 2) that all of the models compare well with the measurements, both with respect to the speed at the top of the hill and the distribution of the wind. For WA^{S}P the largest error in the speed half way up the hill normalised with the speed at the foot, was 3%.

The analysis of the shape of the hill resulted in that *separation* of the flow could be expected in the wake of the hill. Since WA^{S}P (and the rest of the models) performed well, the separation – if it indeed occurred – had no effect on the flow at the measuring points.

6 Model for the effect of roughness changes

When the roughness of the terrain changes, say from water (smooth) to land (rough), the surface stress changes immediately (in this case it rises), this results in an upward convergence of momentum, leading to a deceleration of the air. Decelerating air causes a fall in the surface stress, which therefore falls toward its original value, a new equilibrium is reached with a surface stress higher than the original. When the air decelerates, the vertical wind shear in the layers above grows, causing an increase in turbulence intensity, and as a consequence the stress higher up increases, too, resulting in upward convergence of momentum, and so on.

If the situation is as in Figure 7, with the change of roughness along a line at right angles to the wind, the air can conceptually be divided into two layers: a layer where it has 'felt' the change, and a layer where it has not. An *internal boundary layer*, IBL, is said to have developed. The vertical speed with which this layer grows is, according to Miyake (1965), proportional to the friction velocity:

$$\frac{dh}{dx} = B\frac{u_*}{\bar{u}(h)} \tag{96}$$

where h is the height of the internal boundary layer, and B a constant.

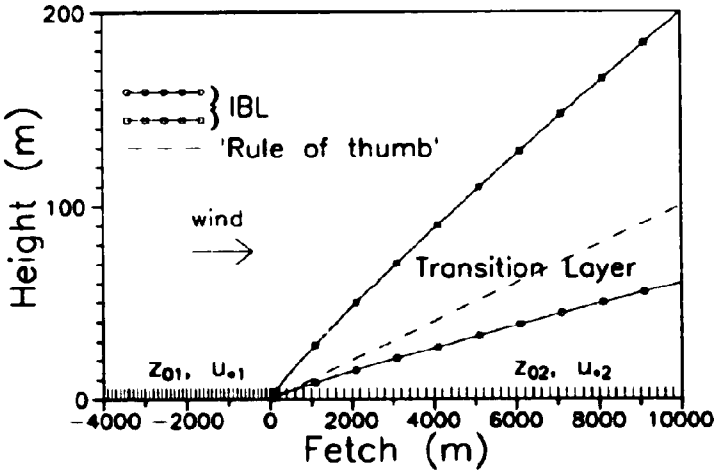

Figure 7. Illustration of the growth of an internal boundary layer, IBL. The line where the roughness of the surface changes is perpendicular to the wind. The dashed line refers to the rule of thumb saying that the IBL grows as 1:100.

If the stability of the boundary layer is assumed neutral, the logarithmic wind profile can be substituted for $\bar{u}(h)$ in Eq. 96. Integrating this, we get

$$\frac{h}{z_0}\left(\ln\frac{h}{z_0} - 1\right) = A\frac{x}{z_0} \tag{97}$$

where h is the height of the IBL at distance x from the change, and A a constant equal to 0.6 in Panofsky (1973). Later experiments gave a value of 0.9 (Larsen et al, 1982). The best fit of the equation is obtained, if z_0 is set equal to the roughness length of the rougher terrain.

It is now possible to find the surface friction velocity inside the IBL, u_{*2}. It is empirically found to be

$$\frac{u_{*2}}{u_{*1}} = \frac{\ln(h/z_{01})}{\ln(h/z_{02})} \tag{98}$$

where u_{*1} is the frictional velocity outside the IBL. This is equal to matching two neutral logarithmic profiles at the height h.

In one of the first papers on this subject (Panofsky, 1973) the resulting velocity profile was composed of two logarithmic profiles: one with the roughness length equal to the upstream roughness outside the IBL, and one equal to the downstream roughness length inside the IBL. Recent measurements (Sempreviva et al, 1990) and numerical simulations (Rao et al, 1974) have shown, however, that the perturbed wind profile is more likely to have the following form

$$u(z) = \begin{cases} \dfrac{u_{*1}}{\kappa} \ln\left(\dfrac{z}{z_{01}}\right) & \text{for } z \geq c_1 h \\ u'' + (u' - u'')\dfrac{\ln(z/c_2 h)}{\ln(c_1/c_2)} & \text{for } c_2 h \leq z \leq c_1 h \\ \dfrac{u_{*2}}{\kappa} \ln\left(\dfrac{z}{z_{02}}\right) & \text{for } z \leq c_2 h \end{cases} \tag{99}$$

where $u' = (u_{*1}/\kappa)\ln(c_1 h/z_{01})$ is the velocity at the boundary of the upper layer, $u'' = (u_{*2}/\kappa)\ln(c_2 h/z_{02})$ is the velocity at the boundary of the lower layer, $c_1 = 0.3$, and $c_2 = 0.09$.

In other words, the experiments show that the height of the layer influenced by the downwind roughness length is only $0.09h$. The layer influenced by the upwind roughness length penetrates down to $0.3h$. The velocity in between these two layers is found by interpolation.

If there is more than one roughness length change, Eq. 99 is used successively. There are, however, some limitations: roughness changes must not occur too close to each other, since the flow must have been in contact with the new surface for some time, for the flow to reach equilibrium and - as a consequence - for Eq. 99 to be valid. The following rule applies (Troen and Petersen, 1989): If x_n is the distance to the nth change in surface roughness, then the upstream roughness must be estimated as an average covering the area between the distance x_n and $2x_n$ in the azimuth sector considered.

The factor 2 is more or less arbitrary, and the rule may be deviated from in cases where clear roughness boundaries are found, eg at a coastline.

As mentioned in the beginning of this section the boundary layer reaches equilibrium with the new surface after some time, this is not incorporated in Eq. 99. To take the weakening influence with distance into account, a weighting factor is included. The idea is that the roughness change looses importance as x/D, where D is the equilibrium distance. Typically this distance is taken to be 10 km. So instead of considering a change from z_{0n} to z_{0n+1} at a distance x_n, the value

$$\ln(z_{0n}) + \exp\left(-\frac{x_n}{D}\right)\ln\left(\frac{z_{0n+1}}{z_{0n}}\right) \tag{100}$$

substitutes $\ln(z_{0n+1})$.

7 Shelter from obstacles

When an undisturbed flow meets an obstacle (eg a house or a shelter belt) the flow is disturbed by the presence of the obstacle. The main effect is that downstream (in the wake) of the obstacle *lee* is generated. This effect has been used by many (eg agriculturalists, architects), but has not been studied in great scientific detail, until just a few decades ago. The picture that has emerged is that for 2-dimensional objects the flow (ie the stream-lines) is lifted above the object. In front and behind of the object exists a separation zone in which the flow is confined. Further downstream a turbulent wake is generated. The flow near the object is highly dependent on the shape of the object, whereas the flow in the wake fulfills a general theory. In the 3-dimensional case the picture is more or less the same, with the important difference that vortices are generated at the edges of the object, and that the separation zone is not a cavity, so mixing close to the object is driven by convection. A sketch of the 3-dimensional flow is shown in Figure 8. As the porosity (ie the ratio of the open area to the total area) increases this recirculation eddy is weakened, and it disappears when the porosity gets above 0.3.

In the following sections the theory, measurements, and the application in WASP will be described.

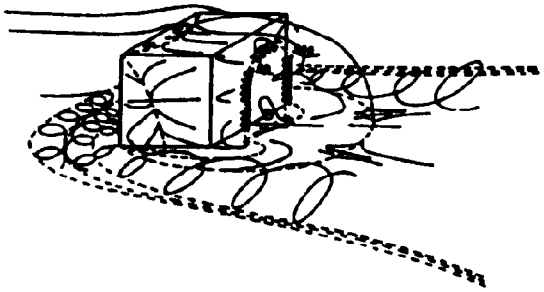

Figure 8. A sketch of the flow around a 3-dimensional obstacle in a turbulent boundary layer, from Hunt et al (1978).

7.1 Theory

The cornerstone in the theoretical work regarding two-dimensional wakes in *turbulent* flows is the work by Counihan et al (1974)[9]. This work has its basis in the theory for wakes in *laminar* flows by Hunt (1971). It assumes that the flow around the obstacle is as depicted in Figure 9.

Furthermore the following assumptions are made:

- If k, h and δ are the heights of the roughness elements in the incident boundary layer, of the obstacle, and of the boundary layer, respectively, then

  $$k \ll h \ll \delta$$

  Moreover the shape of the obstacle must be such as to cause a well-defined turbulent separation bubble in its lee.

- At some distance (greater than the length of the wake, X, but not so great that the structure of the boundary layer changes) downstream, the mean velocity returns to its value in the undisturbed layer.

[9] Actually, Counihan did the experiment, and Hunt and Jackson the theoretical work.

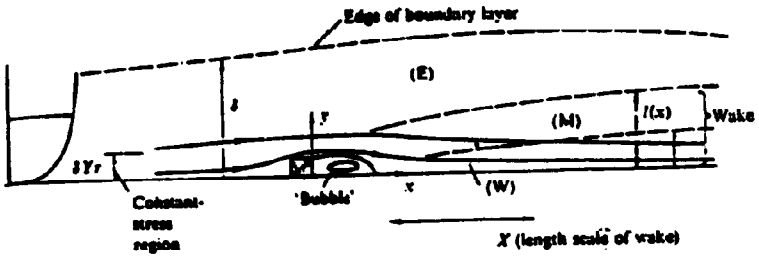

Figure 9. The flow around an obstacle in a turbulent boundary layer, from Counihan et al (1974).

- The velocity profile in the upstream boundary layer can be described by a power law:

  $$U(z) = U_\infty[(z - z_1)/\delta]^n$$

  where U_∞ is the wind speed outside the boundary layer, and z_1 the zero displacement. However, very close to the roughness elements (ie when $z \approx k$) the logarithmic profile

  $$U(z) = \frac{u_*}{\kappa} \ln\left(\frac{z - z_1}{z_0}\right)$$

  must apply. κ (=0.4) is the von Kármán constant, u_* the friction velocity, and z_0 the roughness length.

- and finally, that the flow can be divided into 3 regions, marked *E*, *M*, and *W* for External, Mixing, and Wall region, on the sketch. Each region has its own physical interpretation.

The region of interest here is the *M* region. This is because a general model is wanted and the flow close to an obstacle (less than 10 h away) is very dependent on the actual shape of the obstacle, see eg Taylor (1988) and Peterka et al (1985) for an overview.

In the *M* region the perturbation stress τ has to be related to the perturbation mean velocities. This relation is found by scaling consideration and is assumed to be

$$\tau_{xz} = \rho 2\nu_0(z = h)\partial u/\partial z$$

where $\nu_0(z = h) = T_{xz}/(dU/dz)$, and T_{xz} the mean stress in the undisturbed boundary layer. This assumption is based on reasoning by Bradshaw (1971) and Townsend (1972) concerning the eddy viscosity.

These assumptions lead to that the equation of motion can be written

$$U_\infty\left(\frac{z^n}{\delta}\right)\frac{\partial u}{\partial x} + U_\infty n\left(\frac{z^{n-1}}{\delta}\right)\frac{v}{\delta} = -\frac{1}{\rho}\frac{\partial p}{\partial x} + 2\nu_0(h)\frac{\partial^2 u}{\partial z^2} \tag{101}$$

with the displacement height z_1 omitted, which is of no consequence because the *M* region is so far from the surface that $z \gg z_1$.

The following solution to this equation is proposed:

$$\frac{u}{U(h)} = \frac{\hat{u}}{x^m}\frac{df}{d\eta} \tag{102}$$

$$\frac{v}{U(h)} = \frac{\hat{u}}{x^{m+1}}\left[mf - \frac{x}{l}\frac{dl}{dx}(f - \eta f')\right]\left(\frac{l}{h - z_1}\right) \tag{103}$$

$$\frac{p}{\rho U^2(h)} = \frac{\hat{u}p_0}{x^m}\left(\frac{l}{h - z_1}\right)^n \tag{104}$$

where $\bar{x} = x/(h - z_1)$ and $\eta = z/l(\bar{x})$. It can be seen that these equations describe a self-preserving flow, ie a flow in which (citing Townsend, 1956) "motions at different sections differ only in velocity and length scales, and are dynamically similar in those aspects of motion controlling mean velocity and Reynolds stress".

After elaborating quite a bit on this, the following solution for the velocity deficit in the M region is found

$$\frac{u}{U(h)} = -\frac{\tilde{C}/I(n)}{K(h-z_1)^2U^2(h)}\left(\frac{h-z_1}{x}\right)\frac{d}{d\eta}\left[\eta^2\,{}_1F_1\left(\frac{2-n}{2+n}, \frac{n+4}{2+n}, \frac{-\eta^{n+2}}{(n+2)^2}\right)\right] \quad (105)$$

where

$$I(n) = \frac{(1+n)(2+n)^{(4+n)/(2+n)}}{1+2n}\frac{\Gamma\left(\frac{4+n}{2+n}\right)\Gamma\left(\frac{1-n}{2+n}\right)}{\Gamma\left(\frac{2-n}{2+n}\right)}$$

having a typical value of 7.08 for $n = 0$, and 7.95 for $n = 0.2$, $\tilde{C}$ is a constant given by

$$-\int_0^\infty zU(z)\tilde{u}dz$$

which is only valid if the wall region is ignored; this can be shown to cause only a small error. ${}_1F_1$ is the confluent hypergeometric function, defined in Abramowitz and Stegun (1964). This solution for the velocity deficit is the basis for most theoretical and empirical work done in wake theory.

Note that Eq. 105 implies that the efficiency of the shelter belt, $s = -u/U(h)$, is proportional to $(x/h)^{-1}$. Another result from the theoretical model is that the perturbation shear stress in the M-region, $-(\tau_{xz})_{z=0}$, is proportional to $(x/h)^{-3/2}$. A plot of the velocity deficit in the M region versus the height η is shown in Figure 10.

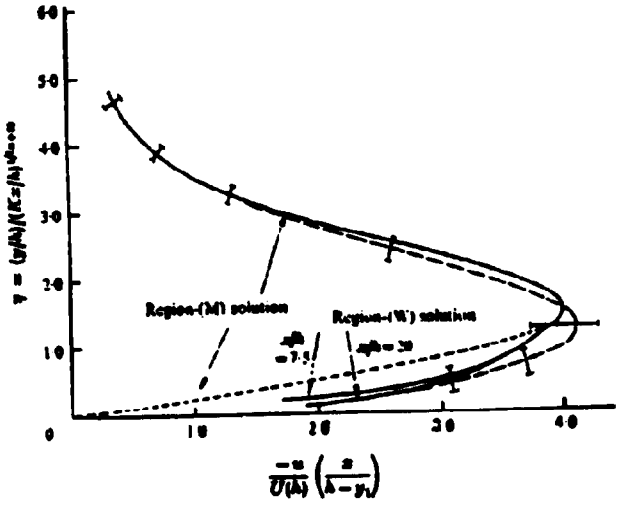

Figure 10. The velocity deficit plotted versus height, from Counihan et al (1974).

Porosity

The porosity, P, of an obstacle is the ratio of the open area to the total area, a solid wall therefore has a porosity of 0. It is an important quantity, both in

wind-tunnel experiments (where it is easily controlled, by for instance holes in the plates), and in full-scale ditto. Here the problem is that it is difficult to assess the porosity exactly: there will always be a certain amount of subjectivity in the determination. A more objective method has been tried by Lindholm et al (1988). They used photos of the wind breaks taken at 4 m, and processed these images with a computer-based image analysis system, to determine the proportion of the background. They found that only "2-dimensional" gaps were registered, rendering the optical porosity smaller than the real porosity.

As a general guideline the following table for the porosity of windbreaks can be used (Troen and Petersen, 1989):

Apperance	Porosity, P
Solid	0
Very dense	≤ 0.35
Dense	0.35-0.50
Open	≥ 0.50

The effect of the porosity of an obstacle on the velocity deficit, is that it is decreased by multiplication with the factor $(1 - P)$.

7.2 Measurements

Most of the research regarding shelter has been done experimentally. In the following, results from a few experiments will be presented. They are divided into experiments carried out in wind-tunnels and full-scale.

Wind-tunnel experiments

When conducting experiments in the wind-tunnel it is critical that the flow fulfills a similarity constraint; namely that the ratio of the height of the fence to the roughness length is the same as in full-scale experiments.

Counihan et al (1974) also conducted experiments in connection with the theoretical derivation, referenced above. The experiments were carried out in a wind-tunnel at C.E.R.L. (Central Electric Research Laboratories), for details see Counihan (1969). The power-law and the logarithmic law fitting the measurements best, with the logarithmic law being marginally better, were found to be

$$\frac{U(z)}{U_\infty} = 0.965(z/\delta - 0.02)^{0.128} \tag{106}$$

$$\frac{U(z)}{U_\infty} = 0.125 \ln\left(\frac{z/\delta - 0.01}{0.0003}\right) \tag{107}$$

Comparing the measurements with theory they found that the self-preservation hypothesis, for velocity deficit and shear stress, seemed to be fulfilled, since the scatter of the data showed no indicative systematic deviation, the value of n being $\frac{1}{8}$. Moreover, they found that the theoretically derived expressions, for velocity deficit and shear stress, were in good accordance with the measurements. They also found that the maximum value of $u(z)$ falls off as x^{-1}.

Perera (1981) did wind tunnel measurements of a simulated rural atmospheric boundary layer with solid and porous (up to $P = 0.5$) fences immersed in it. They tried different forms of holes in the fence, and found that for the same porosity, the form of the holes had no influence. Furthermore, and more important, they found

an empirical formula for the velocity deficit in the constant-stress layer using the self-preserving formula by Counihan et al (1974):

$$\tilde{u} = 9.75(1 - P)\eta \exp(-0.67\eta^{1.5}) \tag{108}$$

where $\tilde{u} = -[\delta\overline{u}(z)/\overline{u}_R(h)] \cdot \Sigma$ is the normalised velocity deficit, $\delta\overline{u}(z)$ the velocity deficit defined as the difference between the reference velocity (measured in the absence of the fence), $\overline{u}_R(h)$, and the actual measured velocity, P is the porosity, and

$$\eta = \frac{z}{h-d}(K\Sigma)^{-1/(n+2)}$$

where n is the exponent of the approach velocity profile, normally taken to be between 0.125 and 0.14 (conventional), h the height of the fence (obstacle), d the zero displacement length, $\Sigma = x/(h-d)$, and

$$K = \frac{2\kappa^2}{\ln((h-d)/z_0)}$$

Perera (1981) also gave an empirical formula for the shear stress perturbations.

A plot of Eq. 108 can be seen in Figure 11.

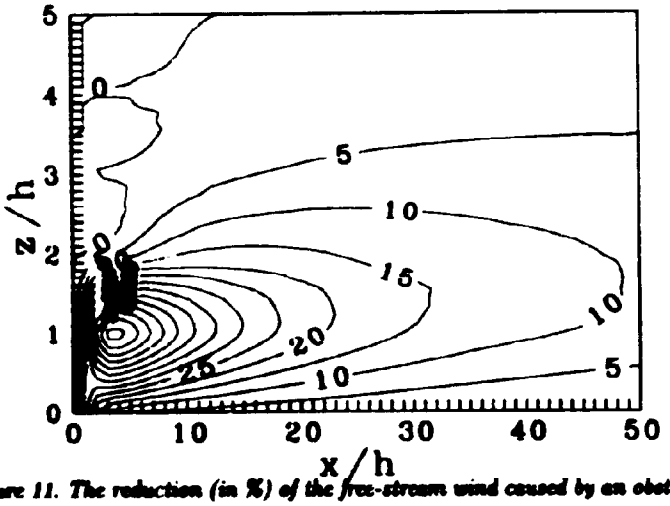

Figure 11. The reduction (in %) of the free-stream wind caused by an obstacle with height h, cf Eq. 108. Along the x-axis is plotted the horizontal distance from the obstacle normalised by h, and along the y-axis the height above ground level, also normalised by h.

Full-scale experiments

Bradley and Mulhearn (1983) carried out measurements in Bungendore, New South Wales, on a 1.2 m high fence having a 50 % porosity. The ratio of h/z_0 was about 600 ($z_0 = 2$ mm). Only measurements when the atmosphere was neutral (here defined as a Monin-Obukhov length within the range [100 m, −20 m][10]), were used. They found that the non-dimensionalising (self-preserving) scheme of Counihan et al (1974) collapsed the data reasonable well in the outer part of

[10]The asymmetry is due to the fact that the wake behaviour is more sensitive to slightly stable than to unstable conditions.

the flow. They found that $\Delta u/u_h|_{max}$ is proportional to $(x/h)^{-1}$. However, they found that the Reynolds stress perturbation data did not agree with the $(x/h)^{-1}$ decay found by Castro (1979) and Perera (1981), but more along the lines of the theoretical prediction ($(x/h)^{-3/2}$, Counihan et al, 1974) with an even more rapid decay.

In another experiment, Nord (1991) did in situ full-scale measurements at 4 different locations in southern Sweden. Only horizontal profiles were considered, the measurements were taken at 2 m. Both single and multiple rows of trees were chosen. The porosity was determined by two methods: the aforementioned photographic method by Lindholm et al (1988) and in a wind tunnel, where the measured profiles were reconstructed by changing the porosity. An interesting fact appeared, namely that it was necessary to have different porosities in the lower part, than in the upper part of the shelter belt The results were not compared quantitatively to other measurements, but some interesting findings were done. Firstly, they found that the reduction of the wind in the summer in the lee of the shelter belt was dependent on the incoming wind speed: the higher the wind the higher the porosity (ie the less dense). This was more pronounced for a thin single row of trees than for dense multiple rows. This can be explained by the presence of the leaves. Another finding was that this effect was dependent on stability, in the sense that under unstable conditions the influence was less than under neutral conditions.

7.3 WA^{S}P

In WA^{S}P the empirical formula by Perera (1981) is used, but some modifications had to be applied because the formula was derived for a 2-D obstacle and obstacles are generally considered 3-dimensional in WA^{S}P. First of all, were situations in the near wake (ie never closer than 5 obstacle heights and in the first one half obstacle height, not closer than 10 heights) not taken into account, since the flow here is entirely dependent on the actual shape of the obstacle To take the finite extension of the obstacle into account, a reduction of the shelter because of lateral mixing at the edges was taken into account. Furthermore, the fact that several objects could generate shelter from the same direction (when viewed from the site) was treated by adding the shelter from the individual obstacles.

8 HIRLAM

All forecasting of the wind in this work, based on physical models, will be done by HIRLAM (HIgh Resolution Limited Area Model). The development of this model was started in 1985 as a joint project between the meteorological institutes in Denmark, Finland, Iceland, Norway, Sweden and The Netherlands. The main objective was to develop an operational high resolution data-assimilation and forecast model system to be utilised for short-range forecasting, see Machenhauer (1988).

HIRLAM is primarily based on ECMWF's (European Center for Medium-range Weather Forecasts) operational analysing system[11] and grid point model. HIRLAM has been operational in Denmark since autumn 1990.

8.1 The equations

The basic equations in HIRLAM are the primitive equations, which have the following form in the (x, y, σ) coordinate system:
Momentum equation:

$$\frac{d\mathbf{V}}{dt} + f\mathbf{k} \times \mathbf{V} = -\nabla\Phi + \frac{\sigma}{p_s}\nabla p_s \frac{\partial\Phi}{\partial\sigma}$$

Continuity equation:

$$\nabla \cdot (p_s\mathbf{V}) + p_s\frac{\partial\dot{\sigma}}{\partial\sigma} + \frac{\partial p_s}{\partial t} = 0$$

Hydrostatic approximation:

$$\frac{\partial\Phi}{\partial p} + \alpha = 0$$

Thermodynamic energy equation:

$$\frac{\partial\theta}{\partial t} + \mathbf{V}\cdot\nabla\theta + \dot{\sigma}\frac{\partial\theta}{\partial\sigma} = \frac{\theta}{c_p}\frac{ds}{dt}$$

where $\sigma \equiv p/p_s$, p the pressure, $p_s(x, y, t)$ the surface pressure, $\mathbf{V}$ the horizontal wind, f the Coriolis parameter, $\mathbf{k}$ the vertical unit vector, Φ the geopotential, $\theta = (p_0/p)^{R/c_p}(p\alpha/R)$ the potential temperature with p_0 being equal to 1000 hPa (normally) and $\alpha = 1/\rho$. Here the total derivative is defined as

$$\frac{d}{dt} = \frac{\partial}{\partial t} + \mathbf{V}\cdot\nabla + \dot{\sigma}\frac{\partial}{\partial\sigma}$$

The advantage of the σ coordinate system over the isobaric is that the problem with the lower boundary condition is solved by having a nondimensionalised vertical coordinate. The boundary condition now reads

$$\dot{\sigma} = 0 \quad \text{at} \quad \sigma = 0, 1$$

In order to close the system, a last equation is needed, it combines the boundary conditions with the continuity equation, and it reads

$$\frac{\partial p_s}{\partial t} = -\int_0^1 \nabla\cdot(p_s\mathbf{V})d\sigma$$

The vertical grid in HIRLAM is actually a σ/pressure hybrid coordinate system, so the equations used in the model differ somewhat from the ones here stated.

[11] This system was used until the spectral version of the operational model was implemented.

8.2 The model

The time schedule for HIRLAM is shown in Figure 12, the model used in this project is GR-HIRLAM (GR for Greenland), which has the bigger of the two model domains shown in Figure 13. This model is used for duty work for Greenland, and is run twice a day at 00Z and 12Z. The reason why the model based on observations from 00Z is not run until 4:30Z is that observations (made at 00Z) for areas critical for the forecast for Greenland are not received till this time. The reason that GR-HIRLAM is used is that forecasts are wanted out to 36 hours, and therefore it is important to have as great an area as possible, in order to catch systems advected into the area.

The horizontal grid consists of 162×136 grid points with a mesh width of 0.51° (approx. 57 km), and it is rotated so that the pole is at 180° E, 25° N, which means that the grid is almost equidistant over Europe. The vertical grid has 16 levels. The time step is 6 min (5 min in the winter time), and the physical tendencies are computed every third time step.

As boundary values are used the newest available ECMWF forecasts with 6 hour intervals. To get values in between the ECMWF forecasts linear interpolation is used.

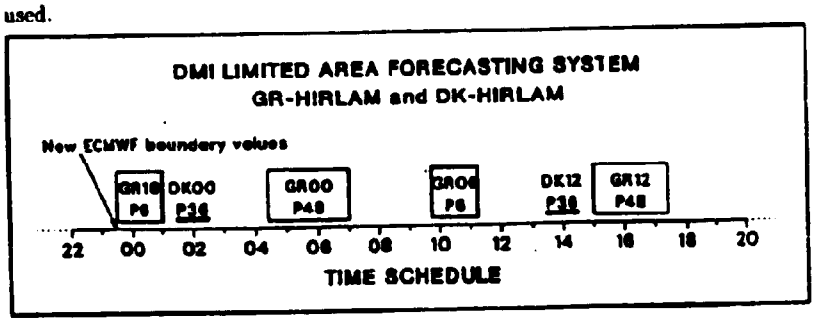

Figure 12. The time schedule for the HIRLAM model.

8.3 Accuracy of HIRLAM

Many aspects of HIRLAM's prediction abilities have been evaluated by several (Joelsen (1990), Autsen (1991) and Hall (1987)). A recent survey of, among others, the 10 metre wind has been given in Machenhauer et al (1991), where the 10 m forecast of HIRLAM was compared to that of UK Limited Area Model (grid resolution in the comparison: 1.25 degrees). It is found that the biases, the mean absolute error, and the RMS error were generally of smaller or equal size as those of the UKLAM.

8.4 New version of HIRLAM

Recently a new version of HIRLAM, HIRLAM 2, has been developed at the Danish Meteorological Institute, see Sass and Sørensen (1992). This model has an improved resolution: 194×163 grid points (resulting in a mesh width of 0.42 deg or approx. 47 km) and 31 vertical levels. The time step is reduced to 4 min. The aforementioned values are valid for GRV-HIRLAM.

It is expected that using this new version will improve the forecasts given in the following, in the same manner, but not to the same extent, as the higher resolution UK MESO model used in Section 15.3.

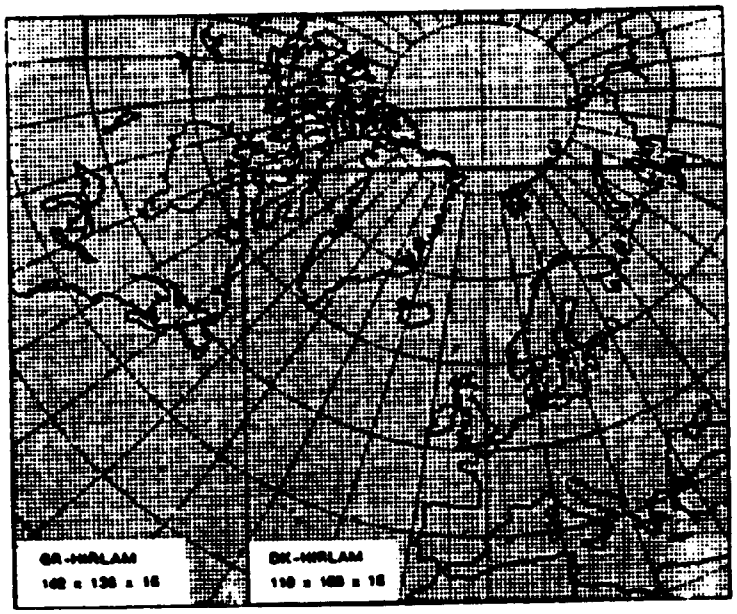

Figure 13. The domain of the HIRLAM model.

9 Neural networks

A neural network is a (large) number of simple computational units (called *formal or model neurons*) massively connected. The idea behind neural networks is based on how the brain was thought to work in the fifties and early sixties. Neural networks have been described in several publications, see eg Rumelhart et al (1986). For publications describing applications of neural networks to time series, see eg Lapedes and Farber (1987) and Landberg (1992).

9.1 The formal neuron

A formal neuron can have a number of inputs and *one* output. The output can be (and normally is) transferred to several other neurons. A sketch of a model neuron is shown in Figure 14.

The resulting input, net_i, to the ith neuron is given by

$$net_i = \sum_j W_{ij} O_j - T_i$$

where W_{ij} is the weight applied to the output from neuron j, O_j, and T_i is the threshold of the ith neuron.

The output from the ith neuron, O_i, is given by

$$O_i = f_i(net_i)$$

where f_i is a function specific to the ith neuron, called the *activation function*. Normally two different functions are used: a linear function for the input and output neurons[12]

$$f_i(x) = x$$

and a sigmoid[13] for the hidden neurons, given by

$$f(x) = 0.5(1 + \tanh x)$$

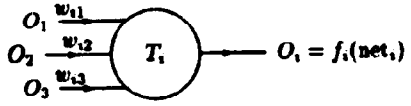

Figure 14. A sketch of the ith formal neuron. This neuron has 3 inputs: the output from neuron 1, O_1, from neuron 2, O_2, and from neuron 3, O_3. Each of these inputs is weighted with an individual weight, w_{i1}, w_{i2}, w_{i3}, respectively. The output from this neuron, O_i, is here given by $f_i(\text{net}_i = \sum_{j=1}^{3} w_{ij} O_j - T_i)$.

9.2 The neural network

When a number of neurons are connected, a neural network is formed. A neural network is characterised by the following

- The architecture
- The signal propagation
- The training algorithm

[13] For a definition of input, hidden, and output neurons, see later.
[12] Sigmoid means shaped like an S.

The architecture The *architecture* of a neural network determines which neurons are connected to which. For networks solving problems in connection with time series a *layered* network is normally used. A layered network is a network where the neurons form layers connected with each other, the neurons in a layer are not inter-connected, see Figure 15. The layer where the time series is being presented to the network is called the *input layer*, and the layer from which the output from the network comes is called the *output layer*. Any layer which is not an input nor an output layer is called a *hidden layer*. A layered network is identified according to the following syntax:

$$(\#input, \#hidden\ layer\ 1, \ldots, \#hidden\ layer\ N-1, \#output)$$

where $\#input$ is the number of neurons in the input layer, $\#hidden\ layer\ k$ the number of neurons in the kth hidden layer, and $\#output$ the number of neurons in the output layer. A (1,5,1) network would therefore be a three layered network, with 1 neuron in the input layer, one hidden layer with 5 neurons, and 1 output neuron, cf Figure 15.

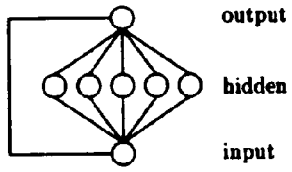

Figure 15. A (1,5,1) neural network with a direct connection from the input layer to the output layer. See text for details.

The signal propagation There are two possible ways that the signal can traverse from the input layer to the output layer: either it can go directly from layer to layer, or it can return to a layer it has already been sent out from. The first case is called *feed-forward*, and the second *recursion*. A feed-forward layered neural network is also called a *perceptron*, and it is networks constructed in this way that will be used in the following.

The training algorithm One of the characteristic features of neural networks is that they, in order to perform any task, must be trained. This can be done in several ways, the one utilised here is the *delta rule* or steepest descent method. The idea is to minimise the error that the neural network makes when presented to a known pattern. This is done by minimising the total error given by

$$E_{tot} = \sum_p E_p$$

where the error made by the network when presented for the pth input/output-pair is given by

$$E_p = \sum_i (O_i^{(p)} - \mathrm{targ}_i^{(p)})^2$$

where $O_i^{(p)}$ is the *actual* output from the ith output neuron and $\mathrm{targ}_i^{(p)}$ is the *wanted* output from this output neuron.

The minimisation algorithm states that a minimum of any quadratic function, $S(x_1, x_2, \ldots, x_n)$, can be found by moving one step in the opposite direction of the gradient, so the new position in phase-space, $x_i^{(t+1)}$, is given by

$$x_i^{(t+1)} = x_i^{(t)} - \epsilon \frac{\partial S}{\partial x_i}$$

where ϵ is a small positive number.

In the case of neural networks the quadratic function is the total error, E_{tot}, which is a function of the weights, W_{ij}, and the thresholds, T_i. Finding the derivative of E_{tot} with respect to W_{ij} and T_i, gives that the weights and thresholds one step closer to a minimum are given by (see eg Landberg, 1992)

$$W_{ij}^{t+1} = W_{ij}^{t} + \Delta W_{ij}$$

and

$$T_i^{t+1} = T_i^{t} + \Delta T_i$$

where

$$\Delta W_{ij} = \epsilon_W \left(-\frac{\partial E_{tot}}{\partial W_{ij}} \right) = \epsilon_W \sum_p \delta_i^{(p)} O_j^{(p)}$$

and

$$\Delta T_i = \epsilon_T \left(-\frac{\partial E_{tot}}{\partial T_i} \right) = -\epsilon_T \sum_p \delta_i^{(p)}$$

where

$$\delta_i^{(p)} = -2(O_i^{(p)} - \mathrm{targ}_i^{(p)}) f_i'(\mathrm{net}_i^{(p)}),$$

if the ith neuron is in the output layer, and

$$\delta_i^{(p)} = f_i'(\mathrm{net}_i^{(p)}) \sum_{j \in M_{l+1}} \delta_j^{(p)} V_{ji},$$

if the ith neuron is not in the output layer. For a definition sketch see Figure 16.

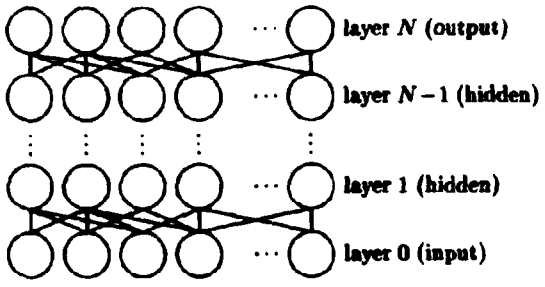

Figure 16. A generalised neural network with $N+1$ layers. Layer 0 is the input layer, and layer N the output layer. Only a few of the connections are shown.

The minimising method used here (the steepest descent) has some problems in connection with it. Firstly, the method finds the *nearest* minimum, this is not necessarily the wanted global minimum. To avoid that the training of the neural network is being trapped in a presumed local minimum, a method has been developed. When a situation occurs where the error seems to converge (this can mean two things: the global minimum has been reached, in which case the weights

and thresholds have been stored, or that a local minimum is encountered), the weights and thresholds are stored, and a big (10 times the present) step is taken, this should take the error out of the local minimum. The error is said to converge when it has not changed significantly during a certain period (normally 50 presentations). The iteration is then continued from the new position. The big step normally leads the system to a position with a higher error, and the system will oscillate for some time before a new minimum is reached. In order to keep the system stable, the time after which the algorithm allows another big jump is made longer and longer. Normally it is not a big problem with local minima, and the method proposed here seems to take care of the problem when it occurs.

Another problem with steepest descent is that the convergence is slow. A method for speeding up the convergence is therefore utilised here. The method is as follows: every time a step is taken and the error decreases, ϵ is multiplied[14] with 1.05. This larger value sometimes increases the error, in which case ϵ is divided by 1.10. After a number of iteration (normally 500) ϵ is not allowed to change, since it is assumed that the system is converging, and only finer and finer steps are needed. A plot of a training session using this method is shown in Figure 17.

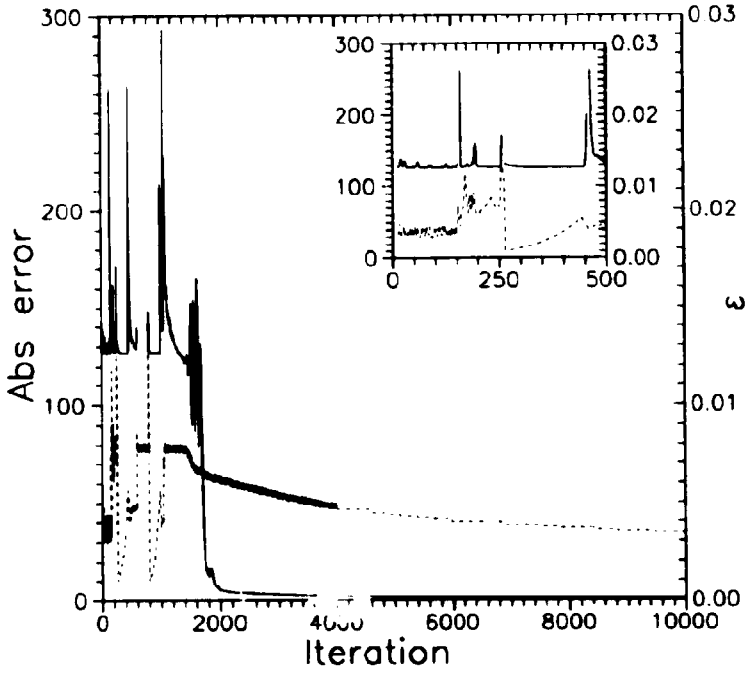

Figure 17. An example of the error (solid line) and ϵ (dashed line) plotted versus the number of iterations for a complete training session of a neural network trained on the Fiegenbaum series (ie $x_{i+1} = 4x_i(1-x_i)$). The left y-axis refers to the error and the right to ϵ. The peaks in the error are where the error is about to diverge (explode), as seen this is detected by the training algorithm and ϵ is decreased. The insert shows the first 500 iterations in more detail.

[14] In the traditional steepest descent ϵ is constant.

Part III

Prediction of Local Wind Conditions

10 Introduction

In this part models for forecasting local wind conditions will be developed and evaluated. They are all based on the theory laid out in the preceding sections. It must be kept in mind that the goal is that any of the models must be able to run on a PC, so that they can be used practically anywhere (as eg by the operator of even a small power plant). The time spent doing the calculations must also be small, to be of any practical use. In order to determine the quality of one model as opposed to another, a framework for evaluating model results is constructed.

Trying to predict the wind locally is not a new thing, especially with the advancement of NWP (Numerical Weather Prediction) models. Using HIRLAM (also used in this study) Machenhauer et al (1991) predicted – among others – the wind speed at two stations (Copenhagen and Paris) using the 10 m wind from the model. They found high correlations (>0.8) between the observed and predicted wind speeds at the two stations, for the +24 hour forecast. Forecasting of the wind with relation to wind energy has also be done by Watson and Halliday (Landberg et al, 1993) using a linear regression model, regressing on the wind speed, wind direction, time of day, rainfall output from the UK Met. Office mesoscale model. Another method, similar to the one presented here, was used by Palutikof et al (1986) to predict the wind for a selection of stations in the UK. Finally, a study by Söder (1988) was carried out to assess the influence of using forecasts of the wind energy produced power in Sweden.

This part begins with a section on evaluation. Since several models will be proposed it is necessary to develop a common framework for measuring the quality (ie how well they predict the observed values) of the models. To that end, observations from 50 (originally 60) stations scattered all over Europe have been obtained. Three measures have been chosen in the quantitative evaluation: the mean of the error, the absolute value of the mean error, and the root-mean-squared (rms) error. There is a certain overlap between the rms error and the absolute value of the error.

Thereafter 3 models will be described and evaluated. The first is a model building in essence on the neutral geostrophic drag law, the second is a model based on the stability dependent drag law. The third is a model using either neural networks or a linear relation for MOS (Model Output Statistics) on the neutral model. Furthermore, the neural networks and the linear model will be used to do forecasts, having knowledge only of the timeseries itself. Finally, a conclusion will be given, including a proposed model to do short-term prediction of local wind conditions.

11 Evaluation of the models

In this section the framework, within which the different models will be evaluated, are presented. In order to make the evaluation as representative as possible, a number of stations scattered all over Europe have been selected, situated at different geographical locations. The stations can be grouped as follows:

- coastal/non-coastal,
- mountainous/non-mountainous,
- in areas where local thermally driven winds (anabatic/katabatic) prevail.

The selected stations are shown in Figure 18 and listed in Table 3; a more detailed listing can be found in Appendix A. As can be seen, stations from all the countries in the EEC are present. The stations are all stations analysed in the European Wind Atlas (Troen and Petersen, 1989). A complication is that one of the stations (Exeter) has been moved during the period, this station will therefore be dealt with separately in Section 12.2.

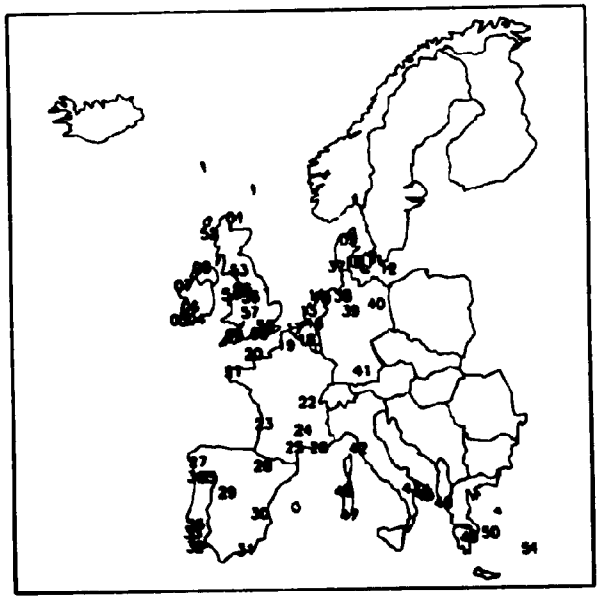

Figure 18. Map showing the location of the selected stations. The numbers refer to the numbers used in this study. See Table 3 for names.

The observations cover the period from December 1st, 1990 to November 31st, 1991. The meteorological observations of speed and direction are taken every 3 hours (given as a 10 minute average) and are reported to the GTS-network (Global Trunk System). Most of the stations comply with WMO standards and report at 10 m agl.; for exceptions, see Appendix A.

The data flow in this study, during the year when data was collected, was as follows: the Danish Meteorological Institute gets the observations from the GTS-network, the data are collected here and sent on – together with the output from HIRLAM – to Risø National Laboratory every month. For a sketch of the data flow, see Figure 19.

Table 3. The selected stations, the numbers in parentheses are the numbers assigned to the stations in this study, a more detailed description can be found in Appendix A. Stations marked with an asterisk (*) are stations that were originally selected, but later rejected because of lack of data.

Belgium	Middelkerke(17)	Florennes(18)	
Denmark	Beldringe(10)	Kastrup(11)	Rønne(12)
	Ålborg(9)		
France	Brest(21)	Cherbourg(20)*	Abbeville(19)
	Bordeaux(23)	Istre(26)	Carcassonne(25)
	Lyon(22)	Mont Aigoual(24)*	
Germany	List/Sylt(37)	Bremen(38)	Hannover(39)
	München(41)	Berlin(40)	
Great Britain	Benbecula(52)	Birmingham(57)	Blackpool(55)
	Bournemouth(60)	Eskdalemuir(53)	Exeter(59)
	London(58)	Manchester(56)	Valley(54)
	Wick(1)		
Greece	Naxos(50)	Rodos(51)	Kerkyra(48)
	Athina(49)		
Ireland	Belmullet(7)	Valentia(5)	Shannon(6)
	Roches Point(4)*	Malin Head(8)	
Italy	Brindisi(44)	Pisa(42)	Cagliari(47)
	Alghero(46)	Gioia del Colle(43)*	Lecca Galatina(45)*
The Netherlands	Schipol(13)	Eindhoven(16)	Eelde(15)
	Terchelling(14)*		
Portugal	Bragança(35)	Lisboa(36)	Sagres(32)
	Viano do Castelo(34)	Sines(33)*	
Spain	Albacete(30)	Almería(31)	Zaragoza(28)
	Sant. de Compos.(27)*	Salamanca(29)	

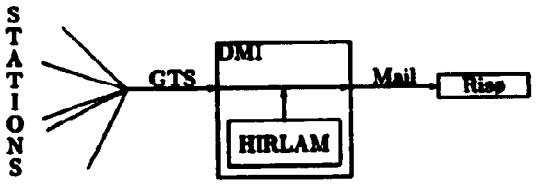

Figure 19. The data flow from the meteorological stations to the Danish Meteorological Institute via the GTS-network, and from DMI to Risø National Laboratory by mail.

When assessing the accuracy of the different models it must be borne in mind that the data are reported to the GTS-network with a resolution of 1 knot (≈0.5 m/s) only, cf Figure 20. This means that even a perfect forecast of the real wind may have an absolute error of 0.25×1 knot (=0.13 m/s) and a rms error of $1/(2\cdot\sqrt{3})$ (=0.15 m/s). These numbers are calculated assuming that the distribution is stepwise uniform, see Appendix D. The direction is given with a resolution of 10 degrees.

An analysis of the station data quality, Q, defined here as the ratio of the number of available measurements to the total number of possible measurements for a given station in per cent, has been carried out to assess how frequent the

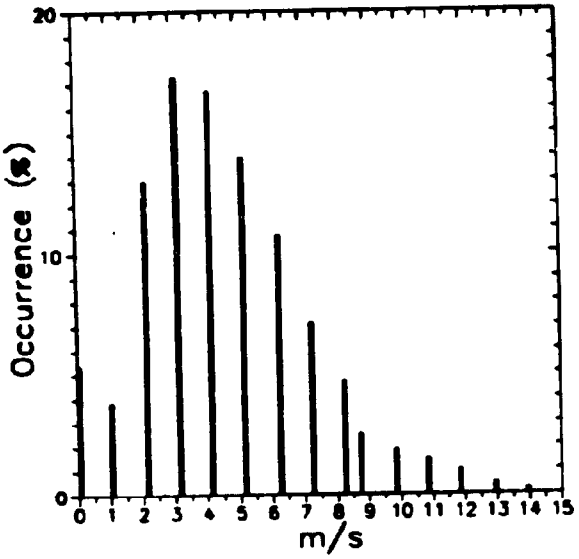

Figure 20. Plot of the distribution of the observed values of station 19 (Abbeville) for the entire period. The binning is 0.1 m/s.

different stations report to the GTS-network. This analysis (shown in Figure 21) has lead to the rejection of some of the stations because of lack of data (Q below 36%, corresponding to approximately 1000 data points). These stations are marked with an asterisk (*) in Table 3.

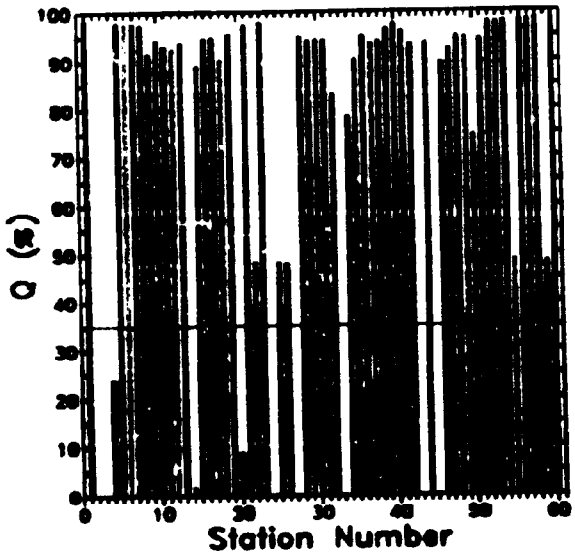

Figure 21. The data quality, Q, of each station for the entire period. Q is defined as the ratio of the number of available measurements to the total number of possible measurements for a given station for the period in question, in per cent.

11.1 Evaluation parameters

To evaluate the quality of the different models, they were run for each of the above-mentioned stations for one year ranging from December 1st 1990 to November 30th 1991, and the forecasts were compared with the observations, using the following quantities as a measurement of the quality:

- The mean value of the error for the sth station,

$$e_s = \frac{1}{N}\sum_{i=1}^{N} e^{(i)} \tag{109}$$

  where N is the number of forecasts (typically around 720 per station per look-ahead time), $e^{(i)} = x^{(i)}_{\text{model}} - x^{(i)}_{\text{obs}}$ the error of the ith presentation, $x^{(i)}_{\text{model}}$ the ith forecast made by the model, and $x^{(i)}_{\text{obs}}$ the corresponding observation.

- The mean value of the absolute error for the sth station,

$$|e_s| = \frac{1}{N}\sum_{i=1}^{N} |e^{(i)}| \tag{110}$$

  where $|e^{(i)}|$ is the absolute value of $e^{(i)}$.

- The root-mean-squared (rms) error of the forecast for the sth station,

$$\text{RMSE}_s = \sqrt{\frac{1}{N-1}\sum_{i=1}^{N}(x^{(i)}_{\text{model}} - x^{(i)}_{\text{obs}})^2} \tag{111}$$

- The standard deviation of the error for the sth station,

$$\sigma_{e_s} = \sqrt{\frac{1}{N-1}\sum_{i=1}^{N}(e^{(i)} - e_s)^2}$$

For the more general evaluation of the different models a number of compound quantities are also defined:

- The average mean error for all stations,

$$\langle e_s \rangle = \frac{1}{S}\sum_{s=1}^{S} e_s$$

  where $\langle\rangle$ indicates averaging over all stations, and S the number of stations (≈ 50).

- The standard deviation of the mean error for each station with respect to the mean error,

$$\sigma_{e_s} = \sqrt{\frac{1}{S-1}\sum_{i=1}^{S}(e_s - \langle e_s \rangle)^2}$$

- The average over all stations of the root-mean-squared error for each station,

$$\langle \text{RMSE}_s \rangle = \frac{1}{S}\sum_{s=1}^{S} \text{RMSE}_s$$

Other parameters are also typically used to evaluate predictions of wind speed and direction (eg the vector error), but since we are dealing solely with wind predictions for wind turbines, which turn themselves into the wind, the above-mentioned parameters (all focusing on the speed) have been chosen.

In wind energy meteorology, the wind is often weighted by a typical power-curve for a wind turbine (ie a curve giving the power output from a turbine as a function of the wind speed). This means that wind speeds below a certain threshold, the *cut-in* speed, will not be taken into account, because the turbine will not be rotating. Speeds above the *cut-out* speed will also be rejected, because the turbine is stopped to avoid structural failures. In between these two speeds, the wind energy is converted into power, according to the power-curve of the turbine. An example of a power-curve is give in Figure 22. This method has not been used in this study. An example of its use on the forecasts generated in this study, can be found in Landberg and Ingham (1992).

A more elaborate evaluation of the performance of the forecasts from this study can be found in Landberg et al (1993), where the forecasts have been used as input to the Reading University/Rutherford Appleton Laboratory National Grid Model, which is a model modelling the English and Welsh electric grid. This model has been run with different degrees of penetration of wind energy (up to 40 per cent).

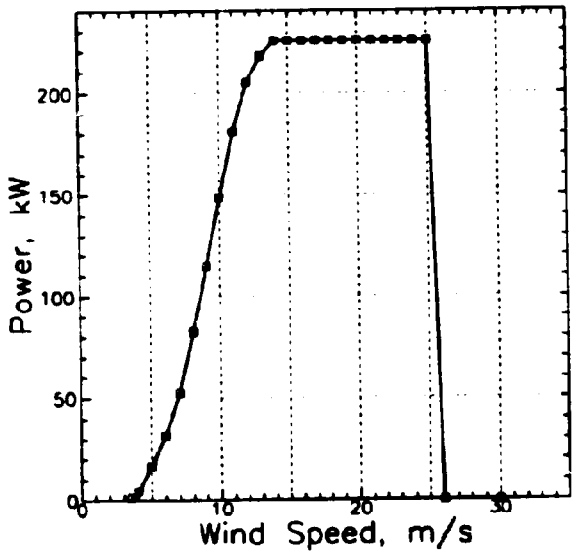

Figure 22. A power-curve for a typical 225 kW wind turbine (Vestas V27). The cut-in wind speed is 3 m/s, and the cut-out speed is 25 m/s.

The error in direction is not directly assessed, but since the correct prediction of the wind is tightly linked to the direction (because the corrections in WAsP are direction dependent) it is evaluated through the evaluation of the speed. To get an idea of the error in the forecasted direction, scatter plots of forecasted versus observed direction will be used.

The correlation coefficient has also been looked into; it was found, however, that it was not able to distinguish well between good and bad predictions.

11.2 Persistence

In order to establish a reference model, the *persistence model* has been chosen. The persistence model is the worst enemy of any forecast model in meteorology (and in many other fields, too!). It has the advantage of being simple (very simple), and that it quite often gives good results. The model is as follows:

$$u_{t+\ell} = u_t \tag{112}$$

$$\theta_{t+\ell} = \theta_t \tag{113}$$

This equation can easily be stated in words: the quantity one wants to forecast is the same ℓ hours ahead as it is now. The reason why this is a good approximation to flow in the atmosphere, is that the atmosphere can be considered quasi-stationary, ie changing very slowly. A characteristic time scale in the atmosphere is f^{-1}, where f is the Coriolis parameter. Using 10^{-4} s^{-1} for f gives that this scale is approximately 3 hours.

In this study the persistence model will be used as a frame of reference, because if the developed models are not better than persistence, they can not be considered as modelling the actual process, and certainly not be recommended for forecasting. Another reason is that most predictions for scheduling purposes presently are using this model.

In the statistical evaluation following, the mean error of the persistence model will typically be very small; this can easily be explained, since it follows from the definition of the error that:

$$e_{persist} = \frac{1}{N-\ell}\left(\sum_{i=1}^{\ell} x_i - \sum_{i=N-\ell+1}^{N} x_i\right)$$

where ℓ is the look-ahead time and x_i the ith value of the timeseries. As can be seen from this expression, the mean error depends only on the 'head' and 'tail' of the time series, so is the series of a certain extent, ie N large, $\ell \ll N$, and the head of the series is of the same magnitude as the tail, the mean error will be very small. The rms error, on the other hand, can get quite big: when ℓ is so large that the series can be considered un(auto)correlated the persistence model's standard deviation of the error, becomes equal to the standard deviation of the timeseries times $\sqrt{2}$.

As an example of the abilities of the persistence model, the persistence forecast for Wick (station 1) is shown in Figure 23. As can be seen from this figure the rms error is quite small for the first 6 hours, it then rises to a certain level and stays there. For all the stations there seems to be a small dip at 24 hours, this is also seen in the figure. A possible explanation of this is that the atmosphere to a very high degree is periodic (with respect to stability, wind etc), with a 24 hour period (driven by the solar heating). It is more interesting to compare the abilities of the models developed in the following to the abilities of the persistence model, this will be done in several places in the following.

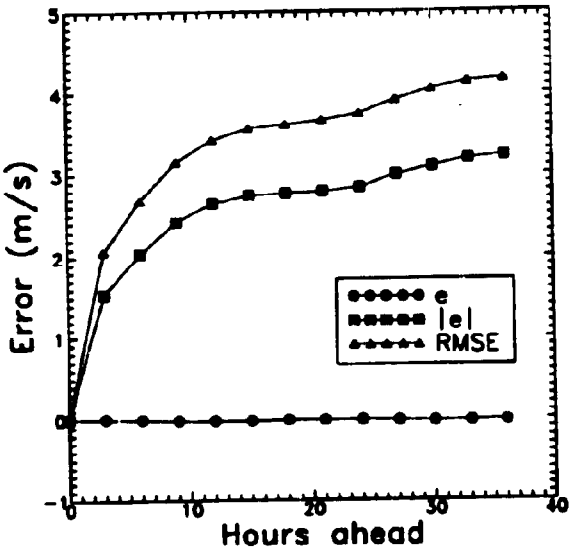

Figure 23. The mean error, e, mean absolute error, | e |, and rms error, RMSE, (all in m/s) versus forecast length in hours for the persistence model for Wick (station 1) for the entire period (December 1990 to November 1991). See figure for legend.

12 Input to the models

In the following the input to the different models used to predict the wind locally will be described. The *input* to these models, are the *output* from HIRLAM and WA^{8}P.

12.1 Output from HIRLAM

All models using meteorological forecasts use the output from HIRLAM. In order to have the possibility of trying out different models, as eg stability dependent models, or models using different winds (geostrophic/non-geostrophic), the following quantities have originally been selected:
At the surface:

- The surface temperature over land, T_s^{land}
- The surface temperature over water, T_s^{water}
- The sensible heat flux over land, H_s^{land}
- The sensible heat flux over water, H_s^{water}
- The latent heat flux over land, H_l^{land}
- The latent heat flux over water, H_l^{water}
- The x- and y-components of the geostrophic wind, $U_g^{(0)}$

In the model levels at 30, 137, 359, 729, 1266, 1979 m above the surface in the HIRLAM grid:

- The x- and y-components of the actual HIRLAM wind, $U_h^{(i)}$
- The x- and y-components of the geostrophic wind, $U_g^{(i)}$
- The potential temperature, θ
- The pressure, p
- The humidity, Q
- The vertical wind, w

For each station all of the above quantities are extracted in the four surrounding grid-points, and then interpolated to the location of the station, using bi-linear interpolation (cf Figure 24).

Conversion of the HIRLAM data

Since the physical quantities of HIRLAM are reported following normal mathematical conventions for vectors (ie the direction of the vectors are in the direction they *point*, angles are defined so that 0 degrees is due east and increasing counterclockwise) and the observations are reported using the meteorological conventions (ie the direction of the vector is from where it is *coming*, having 0 degrees due north and angels increasing clockwise) it is necessary to transform from the one system to the other. This is done in the following way:

In the HIRLAM coordinate system we have the x- and y-components of the wind, (U,V), these are converted into polar coordinates by:

$$r = \sqrt{U^2 + V^2} \tag{114}$$

$$\theta = \tan^{-1}\left(\frac{V}{U}\right) \tag{115}$$

Converting this set of equations into polar coordinates in the *meteorological* coordinate system, we get

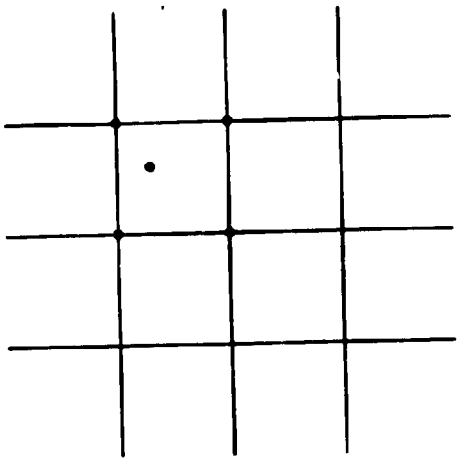

Figure 24. The grid with a station (solid circle) and the 4 nearest grid points (circles) used to interpolate the physical quantities at the stations. The interpolation is done by bi-linear interpolation.

$$r_{\text{met}} = r \tag{116}$$

$$\theta_{\text{met}} = 90 - \theta + 180 \tag{117}$$

where +90 and the minus on θ are to convert to the new coordinate system, and +180 is to comply with the meteorological definition of the direction, ie the direction from which the wind comes. This leads to, that the x- and y-components of the wind in the meteorological system, $(U_{\text{met}}, V_{\text{met}})$, are given by

$$\begin{aligned} U_{\text{met}} &= r_{\text{met}} \cos(\theta_{\text{met}}) \\ &= r \cos(90 - \theta + 180) \\ &= -r \sin(\theta) \\ &= -V \end{aligned} \tag{118}$$

and

$$\begin{aligned} V_{\text{met}} &= r_{\text{met}} \sin(\theta_{\text{met}}) \\ &= r \sin(90 - \theta + 180) \\ &= -r \cos(\theta) \\ &= -U \end{aligned} \tag{119}$$

respectively.

12.2 Output from WA^{S}P

The WA^{S}P model is run for each of the 50 stations to make a correction matrix for the local effects at the site. Note that this is not the normal way of using the program, since no horizontal extrapolation is made, only a calculation of the different local effects at the site. To perform these calculations a description of the following is needed for each station:

- The dimensions (height, width, depth, and porosity) and positions of close-by obstacles.
- The roughness rose, ie the sector-wise distribution of the roughness, of the site.
- The orography of the surrounding terrain, in the form of a digitised map.

All the information concerning the stations is taken from the work done in preparing the European Wind Atlas (Troen and Petersen, 1989). For each of the stations a file containing the effect of the aforementioned information (as calculated by WA^{S}P) plus a 'meso-scale' roughness (calculated using the formula in Eq. 100) in twelve 30-degree sectors has been generated, the matrices are listed in Appendix B. Note, that an implicit assumption, is that the free-stream wind is blowing in a flat terrain, with no obstacles, and a uniform roughness.

The only station that has been analysed in this study is station 59 (first Exeter), since this station has been moved during the selected period. The analysis of the new site, *RAF Dunkeswell*, will be described in the following.

WA^{S}P analysis of RAF Dunkeswell

In the following the station will be analysed along the lines laid out in the European Wind Atlas. Such an analysis includes: an overview description of the site, and description of the orography, roughness and obstacles.

To carry out this analysis, the site has been visited and photographed and 1:50 000 and 1:25 000 scale maps have been studied and digitised.

Description The meteorological station at RAF Dunkeswell (WMO code 3840) is situated at position: 3° 14′ W and 50° 52′ N (UTM: 312 782 mE, (6)107 496 mN), the height above mean sea level is 250 m. The mast is 10 m high and is equipped with a cup anemometer and a wind vane both at 10 m agl. The station started operating on of June 1st, 1991, and took over from Exeter (WMO code 3839), which ended operation on the May 31st, 1991. The station is at an airfield on a plateau, and is surrounded by quite a few low buildings.

Orography The orography of the station's surrounding terrain has been digitised using the following maps: Landranger 181 (Ordnance Survey): Minehead & Brendon Hills area, scale 1:50 000, Landranger 192 (Ordnance Survey): Exeter, Sidmouth & surrounding area, scale 1:50 000, Pathfinder 1296 (Ordnance Survey): Honiton & Collompton, scale 1:25 000. The digitised map is shown in Figure 25. It is made in such a way that the resolution close to the site is maximal (ie height increments of 5 m), further away from the site the resolution is decreased to 10 m, furthest away, it is decreased even further to 25 m. This is in compliance with the idea behind the zooming grid in the orographic model of WA^{S}P, see Section 5.1. A 3-dimensional plot of this map is shown in Figure 26.

Roughness From studying the terrain and the maps mentioned in the previous paragraph, the following roughness classes in the surrounding area have been identified:

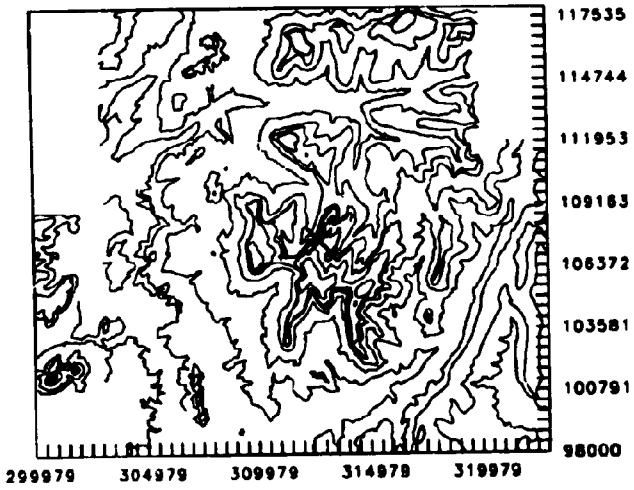

Figure 25. The digitised orography of RAF Dunkeswell. The mast is at (312782,107496), marked with a cross.

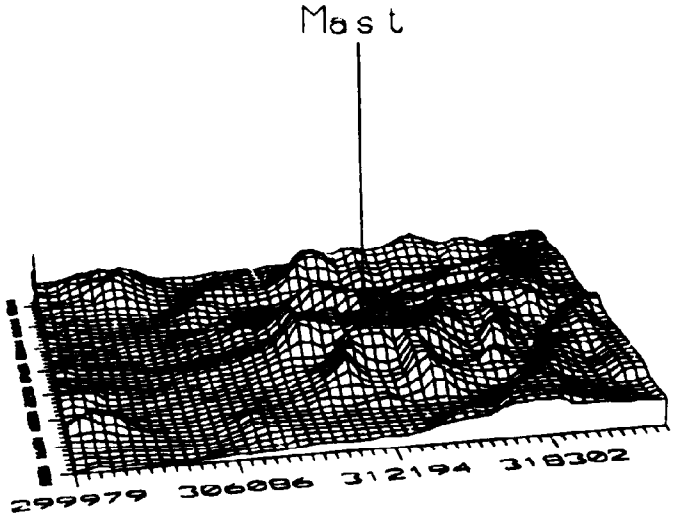

Figure 26. The 3-dimensional plot of the digitised orography of RAF Dunkeswell. The vertical exaggeration is 10.

0	Water (roughness length: 0.0 m)
Ia	Farmland (roughness length: 0.1 m)
IIIa	Villages (roughness length: 0.5 m)
IIIb	Small villages (roughness length: 0.4 m)
IIIc	Plantation, non-coniferous (roughness length: 0.3 m)
IIId	Plantation, coniferous (roughness length: 0.4 m)
IIIe	Plantation, mixture of IIIc and IIId (roughness length: 0.3 m)

Note that in WASP water is given the roughness length 0 m. This is for WASP to be able to treat stability over water (which is different from over land) correctly.

A plot of the digitised roughness map is shown in Figure 27 and the resulting roughness rose of the mast is shown in Table 4. As can be seen from this, the basic landscape type is farmland, only slightly perturbed by the presence of the woods and villages.

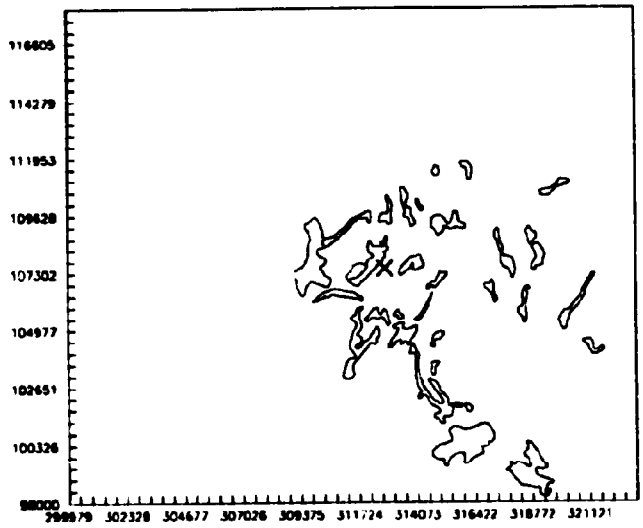

Figure 27. The map showing the different identified roughness areas of the surroundings of RAF Dunkeswell. The mast is located at the cross.

Table 4. The roughness rose, ie the sector-wise distribution of the roughness length, of RAF Dunkeswell, derived - by WAsP- from the map shown in Figure 27. $z_0^{(i)}$ *is the aerodynamic roughness length (in m) after the ith roughness change and* $d^{(i)}$ *the distance (in m) to the ith roughness change.*

sector	$z_0^{(0)}$	$d^{(1)}$	$z_0^{(1)}$
0	0.1060		
30	0.1036		
60	0.1046		
90	0.1077		
120	0.1016		
150	0.1140	20920	0.0000
180	0.1063	20350	0.0000
210	0.1052		
240	0.1094		
270	0.1877	3461	0.1001
300	0.2634	886	0.1057
330	0.2396	1049	0.1016

Obstacles From photos taken on-site and maps of the area, the obstacles (in this case only houses) listed in Table 5 and shown in Figure 28 have been identified. The dimension (height, width, and depth) have been determined from the on-site photos.

Table 5. The obstacles at RAF Dunkeswell. α_1 and α_2 are the angles of the two closest corners of the obstacle (in degrees from north), r_1 and r_2 are the distances to the aforementioned corners (in m), h is the height of the obstacle (in m), d the depth (in m), and P the porosity (0 means solid).

	α_1	r_1	α_2	r_2	h	d	P
1	83	25	97	25	3	15	0.00
2	113	100	123	100	5	9	0.00
3	146	147	148	147	5	10	0.00
4	157	261	163	261	6	6	0.00
5	164	112	166	112	3	2	0.00
6	23	281	30	281	5	15	0.00
7	50	360	58	360	8	20	0.00
8	6	385	19	398	6	8	0.00
9	124	126	126	124	6	8	0.00

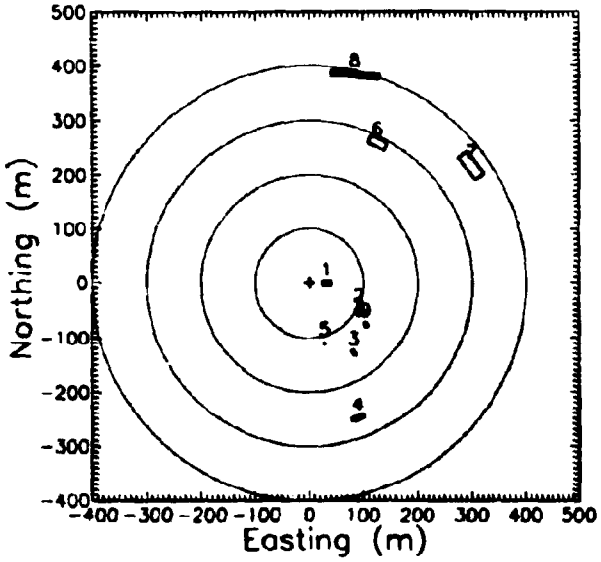

Figure 28. Plot of the obstacles identified at RAF Dunkeswell. The mast is situated at (0,0).

Result file The resulting correction matrix, to be used in this study, is listed in Table 6. As can be seen from this, the local corrections with respect to obstacles as well as roughness are quite small. The orography – on the other hand – does have some influence (an increase of the undisturbed wind of, at the most, 20% and a turning of the wind of 7 degrees).

Table 6. The correction matrix used in the models based on the geostrophic drag law. z_0 is the roughness used in this law, and is an averaged ('meso-scale') roughness. For each local effect, the percentage of over/under-speed (0 means that the local effect in question has no influence on the free-stream wind) and the turning (positive clock-wise) are given. All correction are given per sector (to be found in the column marked 'Dir').

Dir	Obstacles		Roughness		Orography		z_0
0	−1.126	0.000	0.000	0.000	−0.198	−5.868	0.1060
30	−1.702	0.000	0.000	0.000	−4.855	−1.008	0.1036
60	−2.102	0.000	0.000	0.000	−2.960	4.612	0.1045
90	−0.792	0.000	0.000	0.000	7.658	6.276	0.1077
120	−6.417	0.000	0.000	0.000	20.801	1.331	0.1016
150	−2.275	0.000	-7.980	0.000	12.092	−5.341	0.0521
180	−0.546	0.000	-8.121	0.000	−0.198	−5.868	0.0468
210	0.000	0.000	0.000	0.000	−4.855	−1.008	0.1052
240	0.000	0.000	0.000	0.000	−2.960	4.612	0.1094
270	0.000	0.000	−4.752	0.000	7.658	6.276	0.1203
300	0.000	0.000	−7.561	0.000	20.801	1.331	0.1142
330	0.000	0.000	−7.058	0.000	12.092	−5.341	0.1106

Forecasting RAF Dunkeswell

In this section, a brief discussion of using the HIRLAM forecasts given for *Exeter* together with the local corrections for RAF Dunkeswell, evaluated on the data from RAF Dunkeswell, will be given. The distance between the two masts is approx 20 km. Since only forecasts of the large-scale flow from the *old* site are available, it is expected that this separation will result in quite large errors on the forecasts. Studying Table 7 this is seen to be the case, since the HIRLAM/WA^{S}P model at no time performs better than the persistence model.

These results give an idea of the sensitivity of HIRLAM, because there is seen a marked difference between the forecast at Exeter (where the HIRLAM forecast and the WA^{S}P matrix are valid), see Appendix C, and then using the same forecast only 20 km away, bearing in mind that the resolution of HIRLAM is 51 km. We can conclude that the bi-linear interpolation (as compared to eg just taking the nearest grid point) is needed for the forecasts to be as accurate as possible.

Table 7. The result of predicting RAF Dunkeswell using HIRLAM forecasts for Exeter and the WAsP matrix for RAF Dunkeswell ('HIRLAM/WAsP') compared to the persistence forecast ('Persistence'). The period evaluated is from June 1991 to November 1991. The column labeled '+F' is the forecasting time (in hours), 'e' is the mean of the error, '|e|' is the mean of the absolute error, and the column labeled 'RMSE' is the rms error of the forecast. The entries marked 'N/A' denote that the +0 hour persistence forecast is not defined.

	HIRLAM/WAsP			Persistence		
+F	e	|e|	RMSE	e	|e|	RMSE
0	−0.489	2.063	2.697	N/A	N/A	N/A
3	−0.146	2.137	3.015	−0.004	1.030	1.443
6	0.020	2.118	2.756	0.001	1.384	1.855
9	0.169	2.095	2.748	−0.001	1.601	2.127
12	−0.178	2.153	2.871	−0.000	1.753	2.282
15	−0.087	2.151	2.812	0.003	1.796	2.362
18	0.085	2.155	2.786	−0.001	1.794	2.396
21	0.172	2.100	2.638	−0.003	1.770	2.369
24	−0.169	2.252	2.934	−0.010	1.795	2.380
27	−0.113	2.180	2.763	−0.014	1.889	2.454
30	0.099	2.236	2.811	−0.018	2.012	2.575
33	0.187	2.129	2.658	−0.019	2.117	2.680
36	−0.172	2.188	2.861	−0.017	2.122	2.700

13 The neutral model

In this section, the analysis leading to the development of the forecasting model will be described. The model is based on the geostrophic drag law and the logarithmic wind profile in their neutral form. This model will form the basis of the models developed later on.

13.1 First-guess model

The general method of predicting the local wind, ie the wind where the local effect of the shelter from obstacles, the change in the roughness of the surface, and of the orography are taken into account, when knowing the meteorological conditions at *another* place, is depicted in Figure 5. This method has been developed by Troen and Petersen (1989) for use in the European Wind Atlas. Here the method was used to make a *horizontal* extrapolation of the wind climate from a measuring site to a site of interest, where no mensurements existed. In this project the tentative idea is to apply this method to the HIRLAM forecast, ie clean the forecast for the effect of the low resolution orography and roughness descriptions, and then insert a high-resolution map of both the orography and the roughness, covering the area around the site of interest. This is depicted in Figure 29. The difference between this method and the Wind Atlas Methodology is that we are not doing a horizontal extrapolation here, but a correction of the wind at the site. The individual steps are analysed in detail in the following.

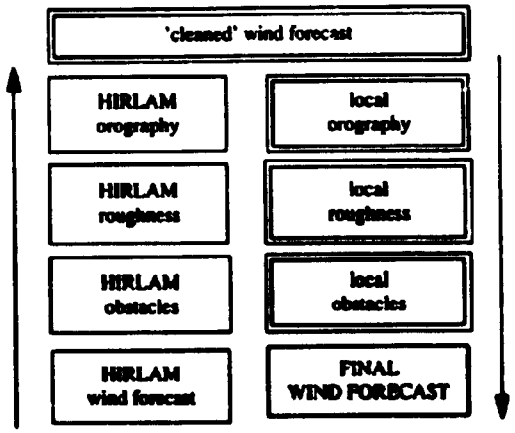

Figure 29. Flow diagram of the first-guess method used to predict local wind conditions from a HIRLAM forecast.

Analysis of the orography in the HIRLAM-model

By calculating the local effect at the site of the orography in the HIRLAM-model by using the flow model from WAPP, it is found that even in the most mountainous areas in Europe, as eg the station Mont Aigoual (height 1565 m a.s.l.) in the Massif Central in France, the HIRLAM orography is so coarsely resolved that the slope even here, is of order 1:190 only, giving a correction from WAPP of max. 0.8 %. Looking at Europe as a whole, the worst cases are the Alps, where on Mt. Blanc

the acceleration due to the terrain is 2.6 % at the most, and in the Pyrenees, where the effect at Maladetta is 2.4 % at the most. The two summits are at the steepest points in the two mountain ranges, and it is very unlikely that a meteorological mast, and even more so a wind turbine, will be placed there. This means that the box labeled "HIRLAM orography" in Figure 29 can be removed in this study[15]. This does not mean that the orography has no effect in the HIRLAM model, on the contrary: on the large scale it has cardinal effect, which is one of the reasons why a high-resolution model can make better forecasts than a low resolution model. It is only when it comes to scales of the order of 10's of kilometres that the resolution of HIRLAM is not sufficient.

Analysis of the roughness in the HIRLAM-model

In the framework build so far, the generation of internal boundary layers by changes in roughness, has to be considered. However, since the generation and growth of these layers is not modeled in HIRLAM - because of the locality of such an effect - it would be wrong to correct the wind from HIRLAM for this effect. Another aspect of this, is that the roughnesses in HIRLAM are given in grid-points, and not as lines denoting the change in the actual roughness, any number of changes in roughness can therefore be generated, just by increasing the resolution of the contours drawn. This means that the box labeled "HIRLAM roughness" in Figure 29 has to be deleted.

Analysis of shelter from obstacles in the HIRLAM-model

Because of the relative low resolution in HIRLAM, it is without meaning to include shelter from obstacles, since this effect is on a - by far - too small scale, and since no obstacles of any kind are modelled in HIRLAM. Hence, the box in Figure 29 labeled "HIRLAM-obstacles" must also be left out.

13.2 The resulting neutral model

The conclusions drawn from the analysis of the HIRLAM model in the previous section, lead to the development of a new model for the prediction of local wind conditions, where the input to the model is a 'raw' HIRLAM wind, meaning that the forecast is started from the box at the top of Figure 29.

To be sure not to introduce any unwanted boundary-layer effect from the HIRLAM boundary-layer model, a wind from outside the surface layer must be chosen and then transformed down to the surface, before using the local corrections. This means that the obvious choice of the HIRLAM 10 m wind is ruled out. Another reason for not using the HIRLAM 10 m wind is that this wind is optimised for off-shore conditions, and all the stations in this study are land-based.

The transformation of the wind from outside the boundary layer to the surface is done using the geostrophic drag law,

$$\frac{G}{u_*} = \frac{1}{\kappa}\sqrt{\left[\ln\left(\frac{u_*}{f z_0}\right) - A\right]^2 + B^2} \qquad (120)$$

see Section 2 for further details. One of the assumptions done while deriving the geostrophic drag law was that the atmosphere is barotropic. This is very seldom the case, so the geostrophic wind is expected to change with height, in both magnitude and direction. The first objective in developing the model is therefore

[15] In the HIRLAM-model the subgrid variation of the orography is included in the roughness length, resulting in rather large values of these, but also in smaller gradients of the orography.

to decide the height from which the wind should be taken. Besides, since the vertical coordinate system in HIRLAM is of the sigma-pressure hybrid type, ie with pressure surfaces (defined differently with height) as the horizontal layers, leading to difficulties in calculating the geostrophic wind, it must also be resolved whether it is the geostrophic wind or the actual wind from the model, that is the best approximation to the theoretical geostrophic wind, G, used in the drag law. Note, that in the expression for the geostrophic wind, there is no height dependence, so there is a freedom of choice, at least a priori.

Having found the proper wind from HIRLAM, the model will be as follows (cf Figure 30): Taking the forecasted wind from HIRLAM that represents the best approximation to the theoretical geostrophic wind, and entering this wind into the drag law to calculate u_*. When u_* has been found, the free-stream wind, U, at the site of interest is calculated using the logarithmic wind profile:

$$\frac{U}{u_*} = \frac{1}{\kappa} \ln\left(\frac{z}{z_0}\right) \tag{121}$$

Finally the free-stream wind is corrected for the effects of the local topography, as found by WA^{S}P. The resulting wind is the local wind.

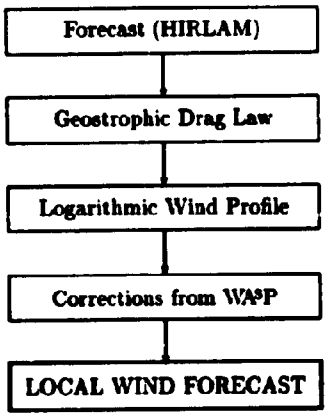

Figure 30. A simple sketch of the resulting model.

The model

In this section the model will be described in some detail, a flow-chart is shown in Figure 31.

The first step is to get the forecasted large-scale wind representing the geostrophic wind, in this work this is done by reading a file containing HIRLAM forecasts for all forecast times for all stations. In an operational model for a single station the forecast should be either typed in from a eg fax, or electronically obtained by a direct link to the computer running the large-scale forecasting model. Note that the only outside information needed is the $x-$ and $y-$component of the forecasted large-scale wind, at each forecast step. In the present model where we are doing a 36 hour forecast in steps of 3 hours, only 12 vectors (= 24 numbers) are needed.

The rest of the calculations are done locally on the PC. Since the large-scale model is run twice a day, a total of 48 numbers are needed a day.

To get the rest of the variables in the geostrophic drag law (ie z_0 and f) for the station in question, the WA^{S}P-matrix generated as described in Section 12.2 is read to get the roughness. The latitude of the station is read from another file containing this information. This step is only necessary here because several stations are dealt with simultaneously, in the case of a forecast for an individual station these parameters would appear as constants in the program.

All the variables in the geostrophic drag law have now been determined, and it is possible to calculate the friction velocity, u_*. u_* is not given implicitly in the geostrophic drag law, hence it is not possible to solve the drag law analytically, therefore a numerical iterative method, based on a combination of the Newton-Raphson method and bisection is used, see Press et al (1986). Since z_0 (and the rest of the quantities in the WA^{S}P-matrix) is given in the 12 sectors, a function using linear interpolation is used to provide values for any direction. To start the iteration a guess for u_* is needed, here a value of 0.3 m/s is used. Furthermore, a guess of the direction at the surface is needed to get a value of z_0, the rule of thumb saying that this value is equal to the direction of the geostrophic wind less 25° is used. The iteration can now be started, typically, u_* is found after a few (< 10) iterations. It is stopped, when the difference between the geostrophic wind calculated using u_* and the geostrophic wind from the large-scale model is less than $\pm 10^{-3}$ m/s. Because of the variation of the roughness with direction, it has appeared necessary to check, whether the direction of the geostrophic wind calculated using the u_* from the iteration, is actually equal to the direction of the wind from the large-scale model. If this is the case the correct value of u_* has been found, if not the iteration is continued.

Assuming neutral conditions, it is now possible to calculate the free-stream wind at the site by using the logarithmic wind profile. To introduce the local effects of the site the file holding the WA^{S}P matrix is read and the corrections are applied to the free-stream wind. We have now got the predicted local wind at the site.

Having the forecasted large-scale wind, the program runs for a few seconds per forecast time per station on a 386-PC, ie the whole 36-hour forecast in 3 hours steps is done in less than half a minute.

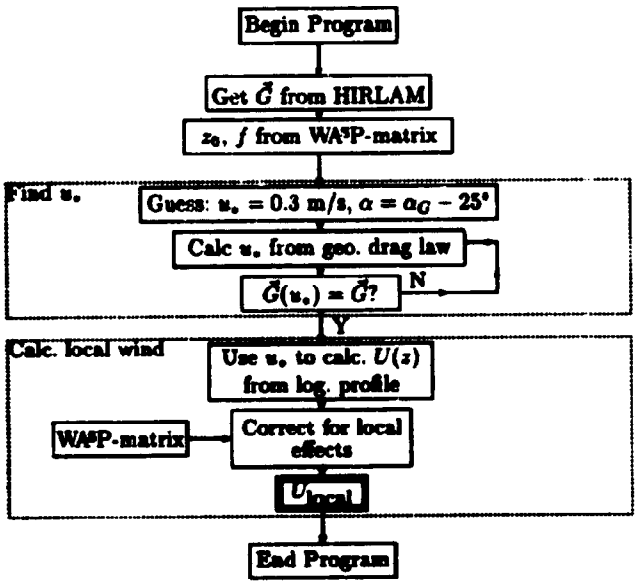

Figure 31. A sketch of the resulting model used to predict the wind locally from a HIRLAM forecast.

Finding the right wind

Since the type of the HIRLAM wind (ie geostrophic or actual) and height of the level from which it is taken, are still undetermined, the first part of this analysis will be to find the wind that approximates the theoretical geostrophic wind best. This is to be understood in the sense that it is the wind that results in the smallest mean error and rms error, when inserted as G in the geostrophic drag law and then used in the model for all the selected stations. This is done by focusing on two months: one representing summer conditions (June 1991) and one winter conditions (December 1990). The reason for looking in detail at two months, is to be sure to capture any "drift" in HIRLAM forced by the changing seasons. Furthermore, these two months do also represent a month (June) where the model is performing well compared to persistence, and one where the model is performing not so well (December). For each case the two different types of winds from each level are used as an approximation to the theoretical geostrophic wind, the model is applied to all the stations and the results evaluated. Finally, the resulting forecasts of all these 'physical' winds are compared to each other and with the persistence model. The model is run for all forecast times, ie from +3 to +36 hours with increments of 3 hours.

The parameters used in this first coarse evaluation are the mean of the mean error for all stations, $\langle e_s \rangle$, the standard deviation (taken over all stations) of the mean error σ_{e_s}, and the mean of the rms error for all stations $\langle \text{RMSE} \rangle$, for a definition see Section 11.1. All these parameters give a rough idea of the general performance of the models, since they average over all the stations. Later in this section, a more detailed analysis will be carried out, when most of the different candidate winds have been ruled out. The results of running the model with the different candidate winds, are shown in Figure 32 and 33.

Theoretical considerations indicate that the geostrophic wind at the surface is the best candidate, since it is here that the frictional force is balanced by the pressure gradient. Looking at Figure 32 and 33 it is seen, however, that this is far from the case here: the worst results are obtained by using the model geostrophic wind at the surface. Generally it can be seen that any geostrophic wind, no matter the height, is not a good approximation. This implies that actual model winds from HIRLAM must be used. Looking at the figures, it can be seen that the results of using the model winds at the different heights are very similar. Therefore, a more detailed analysis has to be carried out. Before continuing, it must be borne in mind that this has the consequence that the model is not very sensitive to from which level the wind is taken.

In this analysis the different actual model winds at the different heights (at 30, 137, 359, 729, 1266, 1979 m), have been used to make forecasts for half a year (March 1991 to August 1991) for all forecast times (from +3 to +36h in steps of 3 hours) for each station. For each station the error, e_s, defined in Eq. 109, the absolute error, $|e_s|$, defined in Eq. 110, and the rms error, RMSE_s, Eq. 111 has been calculated and every time the forecast based on the wind at a certain height gave the best result (ie the smallest values), the model got one point. The result of this analysis is shown in Table 8. As can be seen from this, there is a close run between the model using the actual HIRLAM wind from the level at 137 m and the one using the wind from the 359 m level.

To see which of these two produces the most accurate forecast for the entire period and to study the individual forecast times in more detail, the two models have been compared for the entire year, for each forecast time in turn. To check that the conclusions drawn in the study of the half year period are valid for the entire year, the forecasts based on the actual HIRLAM wind at 729 m are also included. The results of this analysis are shown in Table 9. It can clearly be seen

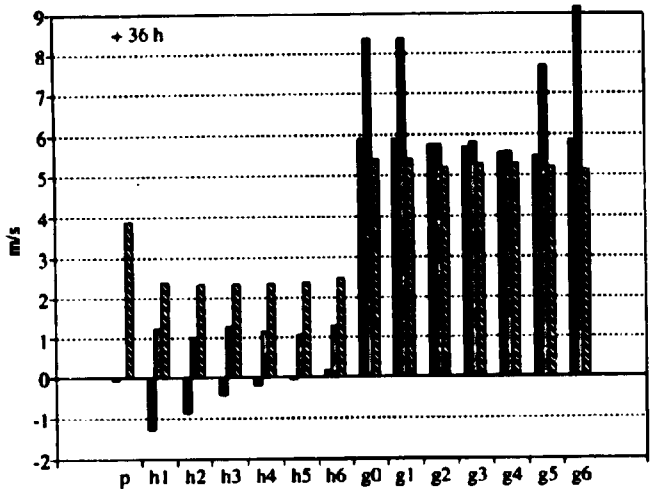

Figure 32. The 36 hour predictions for June 1991 (the summer case) using the neutral HIRLAM/WASP-model with actual model winds (h1-h6) and geostrophic winds (g0-g6) from the HIRLAM model. Level 0 is at the surface, 1 is at 30 m , 2 at 137 m, 3 at 359 m, 4 at 729 m, 5 at 1266 m and level 6 at 1979 m agl. The predictions are compared to persistence (p). The first column (in each group of 3) in connection with each model is the mean value of the mean error averaged over all stations, the second is the standard deviation of the mean error taken over all stations, and the third the mean of the rms error for the individual stations. Bars extending outside the horizontal boundaries signifies that the values they represent are outside the extreme values of the y-axis.

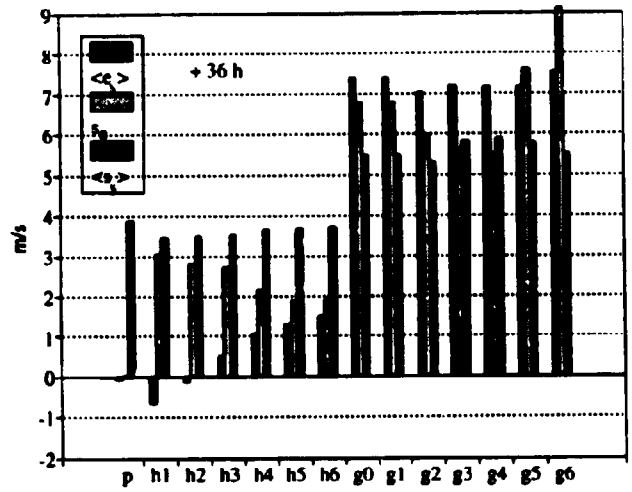

Figure 33. The 36 hour predictions for December 1990 (the winter case), see text at Figure 32 for explanation.

Table 8. The score of the prediction models based on the different actual HIRLAM winds. One point is given if the model using the wind from the level in question, for a certain station and all forecast times gives the most accurate forecast. A total of 50 stations have been used. The height of the level is given in column 2. e_s is the error, $|e_s|$ the absolute error, and RMSE$_s$ *the rms error of the forecast.*

Level	Height(m)	e_s	$\|e_s\|$	$RMSE_s$	Total
1	30	4	3	3	10
2	137	9	18	14	41
3	359	13	17	20	50
4	729	9	6	5	20
5	1266	7	5	7	19
6	1979	8	1	1	10

from this table *that the model based on the actual HIRLAM wind at the 137 m level (level 2), is the one that produces the most accurate (with respect to all the tested parameters) forecasts.* It is actually even more pronounced for the 1 year period than for the 1/2 year period. Studying the individual forecast times, it can also be seen here that the selected model performs best.

Table 9. The result of comparing the two best models, ie the models using the actual HIRLAM wind at 137 m (level 2, first row in each table) and 359 m (level 3, second row), respectively. For reference, the forecast using the 729 m (level 4, third row) wind is also included. The three sub-tables contain the results of the e_s, $|e_s|$, and RMSE$_s$ *analysis, respectively. The scoring scheme is as in Table 8.*

e_s	0	3	6	9	12	15	18	21	24	27	30	33	36	Total
2	12	16	27	27	15	19	26	29	19	20	29	30	18	287
3	18	19	12	15	20	19	12	11	17	19	10	10	18	200
4	20	15	11	8	15	12	12	10	14	11	11	10	14	163
$\|e_s\|$	0	3	6	9	12	15	18	21	24	27	30	33	36	Total
2	10	22	29	31	20	27	29	33	23	29	31	36	26	346
3	25	16	9	12	17	13	11	11	15	13	9	8	12	171
4	15	12	12	7	13	10	10	6	12	8	10	6	12	133
RMSE$_s$	0	3	6	9	12	15	18	21	24	27	30	33	36	Total
2	9	21	27	26	21	25	29	33	23	29	30	33	25	331
3	25	15	12	16	14	14	12	10	14	10	9	10	12	173
4	16	14	11	8	15	11	9	7	13	11	11	7	13	146

Others have reached results along the same lines: Clarke and Hess (1974) used the actual wind in $z = 0.15u_*/f$ which is approximately 450 m for typical values, this level is the level with the strongest winds, and where the wind is geostrophic on the average under neutral conditions. If the atmosphere is highly stable the wind is super-geostrophic, and in the highly unstable case the wind will be sub-geostrophic. In another study (Zilitinkevich and Chalikov, 1968) the actual wind at a fixed height (approximately 1 km) was used as G in the geostrophic drag law.

13.3 Results

The model selected and developed in the preceding section is now run for all stations in the period from December 1st, 1990 to November 30th, 1991, giving one year's worth of data. The selected model will be called the 'neutral HIRLAM/WA^{S}P model' or just the 'HIRLAM/WA^{S}P model', and abbreviated 'H/W'. In the following the results are presented.

One of the tasks this work set out to undertake, was to see whether it was possible to make forecasts that performed better than persistence. Having this in mind, we have defined a *'good' station*, as a station where the forecasts produced by the model are better than persistence after 6 hours, and a *'bad'*[16] *station* as a station where persistence is doing better than the model for all look-ahead times. The reason for the 6 hour lower limit is that *none* of the stations perform better than persistence until from somewhere between 3 and 6 hours. Looking at all the stations, it has been found that 80 % can be labeled as 'good' for the +18 hour forecast. For shorter range forecasts, this percentage is reduced and for longer increased. The +36 hour forecast yields 88 % and the +3 h 0 %. The performance as a function of look-ahead time of a 'good' and a 'bad' station can be seen in Figures 34 and 35. For stations where the neutral model is performing better, the absolute mean error and the rms error are around 60 to 80 % of the persistence model's for the +18 h forecasts, cf Figure 36.

Returning to Figures 34 and 35, two interesting features are seen:

1. The rms error and the mean error of the HIRLAM/WA^{S}P model are constant for the 'good' as well as for the 'bad' station. This is seen generally for all the 50 selected stations. This is quite difficult to explain, since it would be expected that it would be harder and harder to predict rightly as the look-ahead time increases; this is found to be the case for the persistence model. One possible explanation could be that only the level of the wind speed is predicted rightly and not the variation. If this was to be the case, the rms error of the prediction should more or less be equal to the standard deviation of the observations themselves. This is seen not to be the case. As an example consider the forecast for Birmingham (Figure 34) where the rms error of the HIRLAM/WA^{S}P model is approximately 1.8 m/s and 2.2 m/s for the time series itself, which is a difference of 18 per cent, furthermore, is it seen from Figure 58 that models with higher resolution have smaller rms errors.
   Another explanation is that the area covered by HIRLAM (which is including the Atlantic Ocean) is so big that within a 36 hour period, generally most of the large-scale weather systems affecting any site in Europe are present in the initial analysis, with the result that major developments within the 36 hour time-frame are know equally well, and therefore predicted equally well. This is of course assuming that the physical model keeps the atmosphere on 'the right track' during the integration. This is confirmed by Figure 58, where it is seen that the UK MESO model (covering a significantly smaller area) does show the expected behaviour of a constant and then increasing rms error with time, even within the 18 hour range. The reason for the variability in the first 6-9 hours is probably due to the error induced by the initialisation of the fields in HIRLAM.
   There is no doubt, though, that the limited variability of atmospheric wind speeds (ie from 0 to typically around 15 m/s) is putting an upper limit on the rms error of any physical model, working reasonable well.

2. The mean error of the persistence model is always close to zero. This is explained in Section 11.2.

[16] or not so good

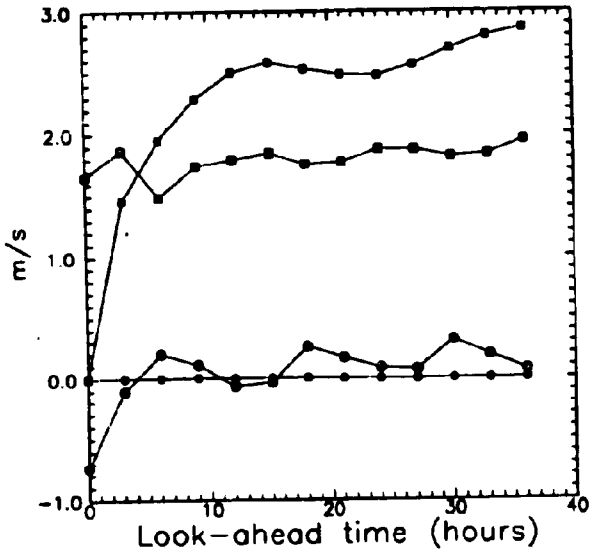

Figure 34. The mean error (in m/s, denoted by circles) and rms error (in m/s, denoted by squares) of the HIRLAM/WASP-model (open symbols) compared to persistence (solid symbols) for Birmingham (station 57, a 'good' station) for the entire period (December 1990 to November 1991). The look-ahead time (in hours) is along the x-axis.

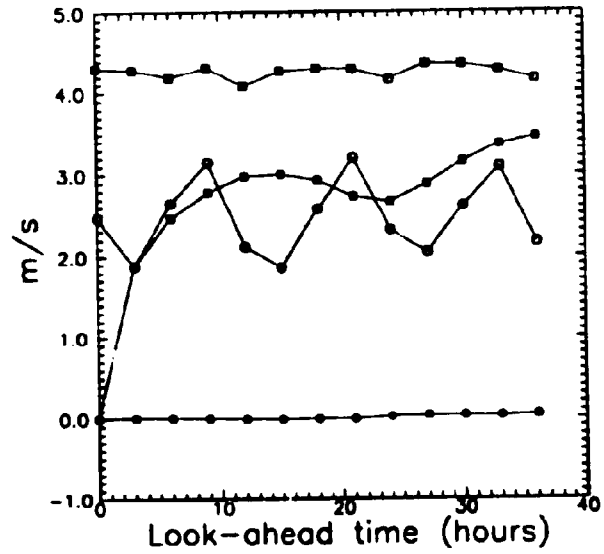

Figure 35. As in Figure 34 but for Salamanca (stat. 29) which is a 'bad' station.

In Figure 37 the selected stations have been labeled according to their performance relative to the persistence model. As can be seen from this figure, the majority of the good predictions are found for stations located in Northern Europe, this is very much in line with the experience gathered from using the WASP program, since the flow at these locations is mainly governed by the large-scale atmospheric flow, ie a non-locally generated flow. As we get nearer to the Mediter-

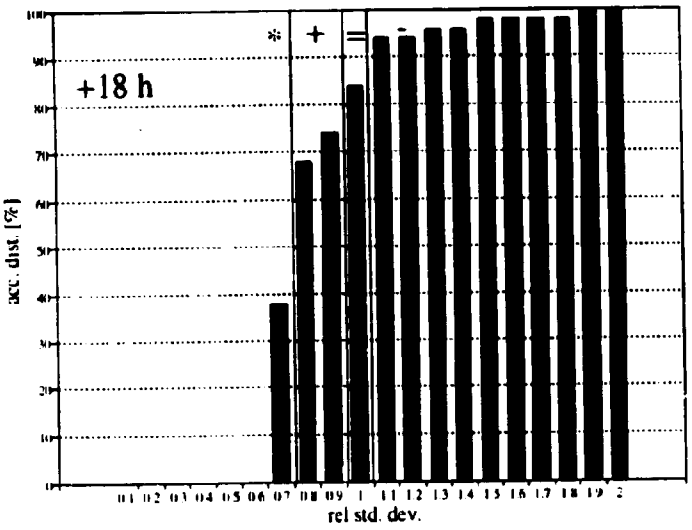

Figure 36 The accumulated distribution of the relative rms error (ie the rms error of the HIRLAM/WASP model relative to that of the persistence model) for all stations for the +18 hour forecast. The classification (, +, =, and −) applied in Figure 37 is shown at the top of the figure.*

ranean Sea, we experience that the quality of the forecasts decreases, but note that even here does the model generally outperform persistence. Note also, as is shown in Section 14, that using MOS improves the quality of the predictions for the 'bad' stations. The improvement is such that these stations, after MOS has been applied to the H/W-forecast, can be labeled 'good'.

Since the produced amount of data is quite big (12 sets of predictions (+3,..., +36h) for 50 stations for one year), we have chosen to look in some detail at two stations: Birmingham (station 57) representing the 'good' stations and Salamanca (station 29) the 'bad'. Note, that only 20 % of the stations have been classified as 'bad', but it is quite illustrative to see why the forecast failed. For a more complete reading refer to Appendix C, where the three error measures are listed for all stations for the +3, +18, and +36 hour forecasts for the HIRLAM/WASP model as well as for the persistence model.

In Figures 38 and 39 the scatter-plot of the observed versus the forecasted wind speed for the 'good' respectively the 'bad' station are shown. As can be seen from these, the scatter from the 'bad' station is quite a bit more pronounced than for the 'good'. Studying now Figures 41 and 39 a major part of the explanation of why the WASP-method - which is dependent on directional corrections - fails, is found: it has not been possible for HIRLAM to forecast the right direction for the bad station, and as a result the correction from the WASP-matrix are of no use. Looking at the plot it seems as if there is a 180 degrees off-set of the data. As will be seen in the next section, it is actually better not to use the matrix in this case. The poorness of the forecast is probably due to the fact that at the bad station, local thermally driven wind regimes prevail. The direction for the good station is predicted quite well.

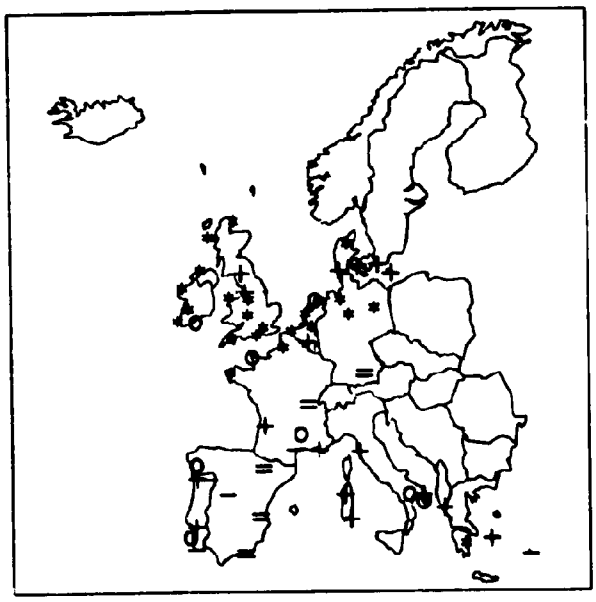

Figure 37. The performance of the neutral HIRLAM/WAPP model seen relative to the persistence model for all the selected stations. An ∘ indicates that the absolute error and the rms error of the model are less than 0.7 times that of the persistence model for the +18 and +36 hour forecast, a + that they lie in between 0.7 and 1.0, = that they are equal, and − that the persistence model performed better. Stations marked with ∘ are stations originally selected but rejected because of lack of data (typically they reported only twice a day to the GTS-network).

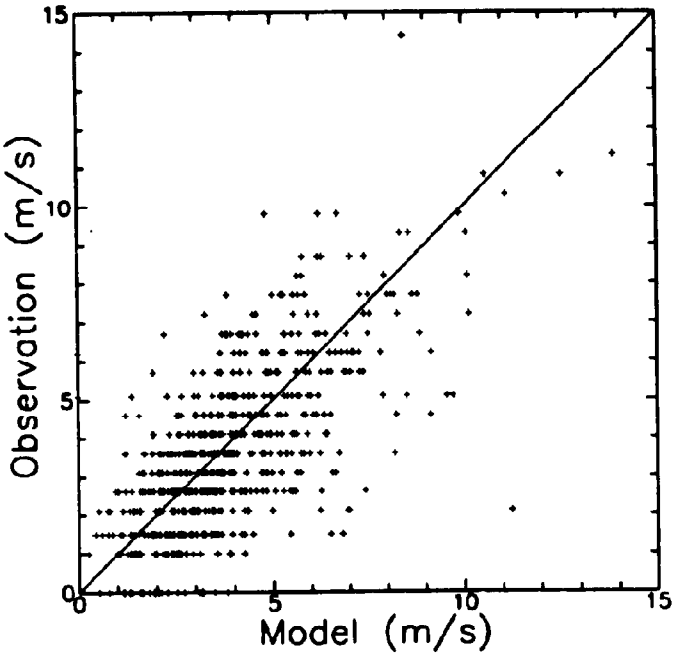

Figure 38. A scatter-plot of the forecasted wind speed versus the observed, for the +18h forecast for the 'good' station (Birmingham, station 57) for the entire period. The existence of the horizontal lines in the plot is due to the resolution of the observations (which is 1 knot).

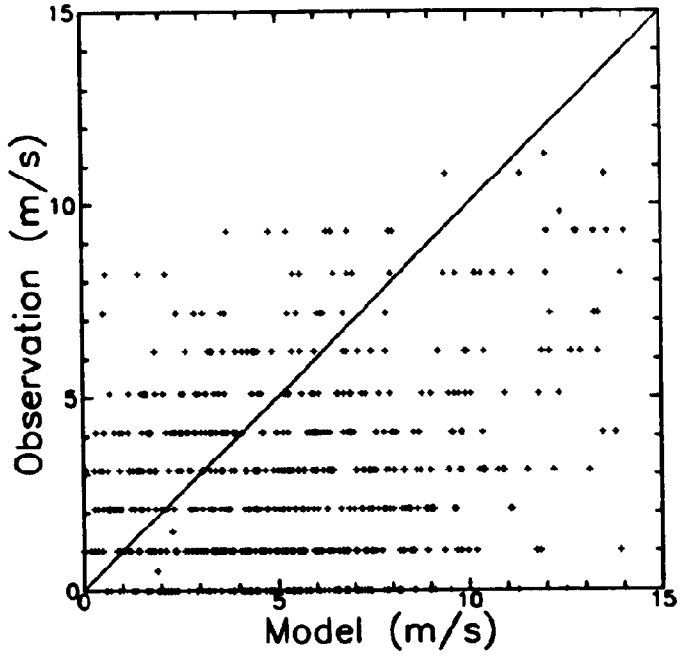

Figure 39. A scatter-plot of the forecasted wind speed versus the observed for the 'bad' station (Salamanca, station 29). Note that the scale is the same as in Figure 38.

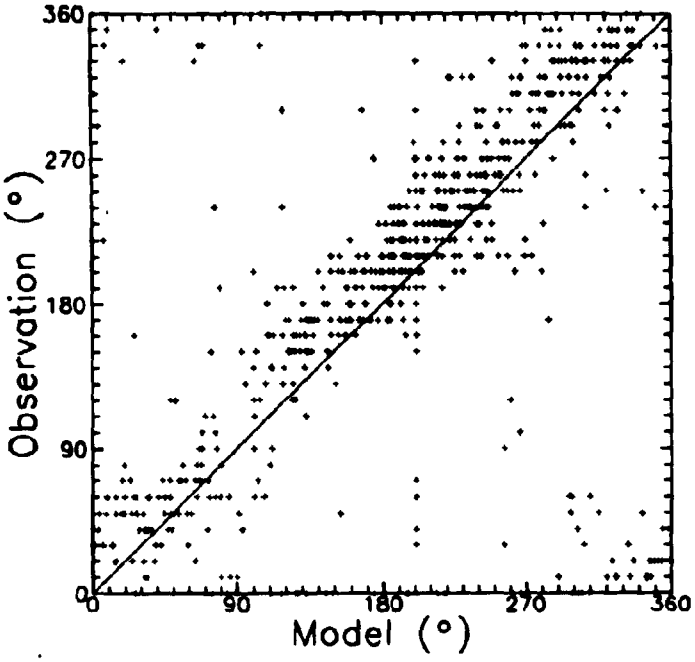

Figure 40. A scatter-plot of the forecasted wind direction versus the observed for the 'good' station (Birmingham, station 57).

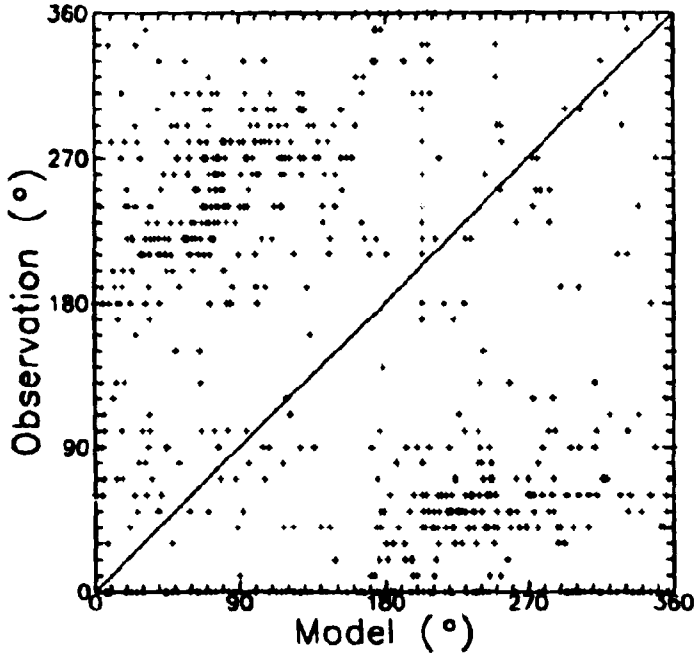

Figure 41. A scatter-plot of the forecasted wind direction versus the observed for the 'bad' station (Salamanca, station 29).

It is also useful to see the distribution of the forecasted versus the observed wind, since in many applications a wind climate is represented solely by its (Weibull) distribution. The distributions are shown in Figures 42 and 43. Comparing the distribution of the forecasted wind to the observed, a quite interesting feature leaps to the eye: the expected distribution for the 'good' station is actually predicted better (ie more smoothly and accurately) by the forecast than by the observations, cf Figure 42. This fact calls for some explanation; experience has shown that most observations of the wind speed can be represented by the 2-parameter Weibull distribution (Weibull, 1951), but as can be seen from the figure there seems to be patches of missing data in the observations (eg 3, 10 and 17 knots), these patches are not present in the forecast, for which reason the distribution appears more smooth. Here is also found another explanation of why the 'bad' stations are not well predicted when using the mean error and the rms error as the measure. It is obvious that measurements within the entire interval spanned should be present when looking at 1 year's worth of data. So quite some doubt can be raised concerning the quality of some the measurements.

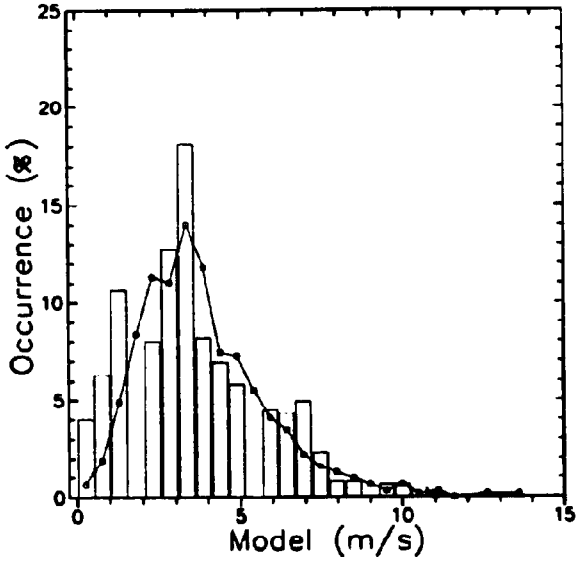

Figure 42. The distribution of the forecasted wind speed (lines) versus the observed for Birmingham (station 57, a 'good' station) (bars). The look-ahead time is +18h and the predictions are taken for the entire 1 year period. The bin width is 1 knot.

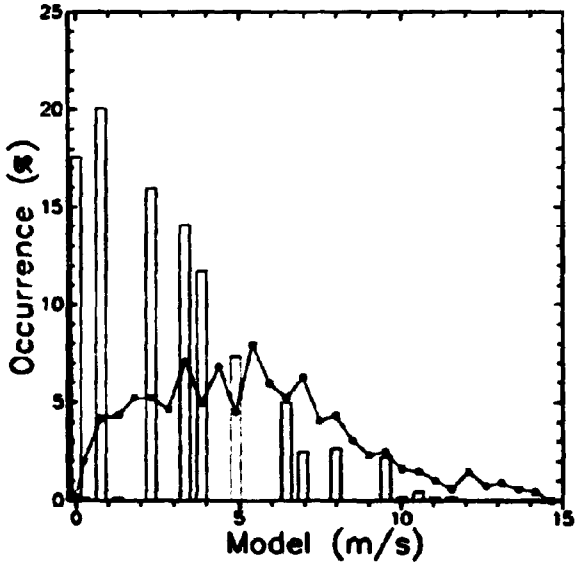

Figure 43. The distribution of the forecasted wind speed (lines) versus the observed (bars) for the +18 h forecast for Salamanca (station 29, 'bad').

Finally, the distribution of the error is looked into. This is important to know, otherwise it is not possible to assign any meaning to the rms error, see Figure 44 and 45. As can be seen from these two figures the distribution of the error can, to a good approximation, be labeled Gaussian. The displacement (away from zero) of the distribution seen in Figure 45, is of course due to the large error of the prediction for the 'bad' station.

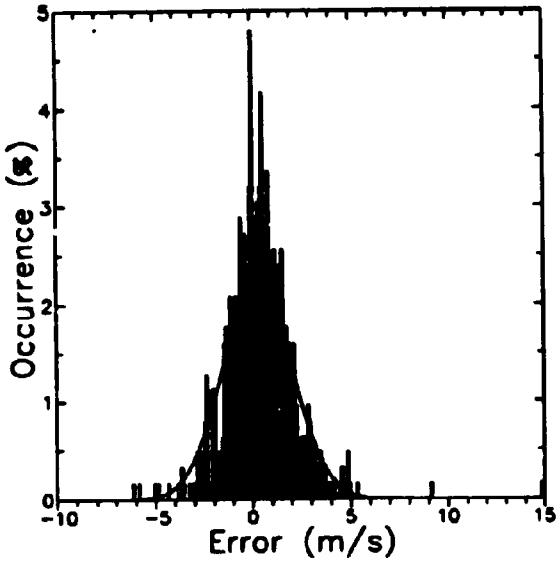

Figure 44. The distribution of the error (model – observed), compared to the Gaussian curve having the mean and variance of the distribution, for the +18h forecast for Birmingham (station 57, a 'good' station). The bin-width is 0.1 m/s.

The dependence of the error on the time of year has also been looked into, as it could be expected that seasons dominated by storms/strong winds would be easier to predict than seasons with low winds, cf Section 14.2. This has been found not to be the case at all. The only month different from the others was September, and this was due to the fact that there was *one* day where all HIRLAM forecasts were bad.

The dependence of the error on time of day has not been looked into, since it is not possible to make a fair comparison, because the prediction model (HIRLAM) is only run twice a day, resulting in that only two times of day have the same look-ahead time a day. What can be said is that, judging from eg Figure 34, there does not seem to be any significant variability, since the mean and rms error are constant.

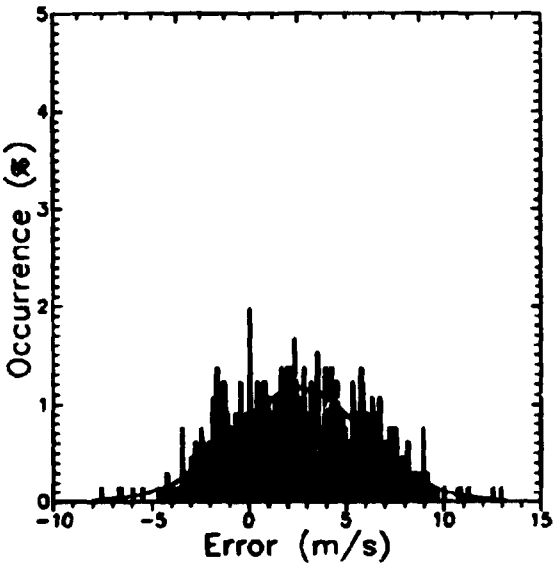

Figure 45. The distribution of the error (model – observed), compared to the Gaussian curve having the mean and variance of the distribution, for the +18h forecast for Salamanca (station 89, 'bad'). The bin-width is 0.1 m/s.

14 Model output statistics

When applying a physical model to real situations, errors will inevitably occur. These errors can have different causes. The *model* can have some inherent errors, because the physical model does not exactly match reality. In the case of the neutral HIRLAM/WA^{S}P model, the defects of the model are that it is neutral, which means that the stability dependent effects are not taken into account, and that the spatial resolution is low. Furthermore, the model assumes that the atmosphere is barotropic, which it generally is not. This constraint is partially circumvented by the fact that the wind used as the geostrophic wind, is in fact the real wind (of a baroclinic model). The conditions at the *site* may have been changed since the WA^{S}P analysis of the station was carried out, this is not at all uncommon: the mast may have been moved (this was found for station 59 (first Exeter and then Dunkeswell)) and the surroundings of the mast may have been changed, typically new buildings build or demolished. Finally, the analysis can initially be erroneous. In this study it is likely that it is the spatial resolution of HIRLAM that most contributes to the error.

The *data* can also be incorrect, either because the instrument is not calibrated properly, or because the instrument simply is old. Remember here, that part of the variance of the error is caused by the inexactitude (as compared to present day measuring capabilities) of the reported observations, see Section 11, since the observations are reported in integer knots compared to accuracies of 0.1 m/s.

Another important cause of error related to the model, is that there is a 'gap' in between the scopes of HIRLAM and WA^{S}P, since HIRLAM covers atmospheric phenomena on scales from the semi-planetaric down to scales of the order of 100's of kilometres. WA^{S}P, on the other hand, covers phenomena related solely to the stationary flow on scales of the order of 1000 m down to 1 m. So atmospheric phenomena on the meso-scale, such as local thermally driven circulations (sea-breezes, anabatic and katabatic winds), are not modeled by any of the models.

To see if it is possible to correct some (or all) of these errors, the output from the physical model is corrected using *MOS (Model Output Statistics)*, which is basically putting the output from the physical model through a non-physical (statistical) post-processor, see Figure 46. Normally this procedure is used to predict parameters not forecasted directly by the model, as eg the minimum temperature at a specific location. See Glahn and Lowry (1972) for an introduction to traditional MOS. Two different types of MOS are used here: a 0th order linear model that corrects only systematic under/over-prediction and scaling on a sector-by-sector basis, and a neural network with different combinations of the output from the physical model and measurements as input.

To test the effect of these two MOS approaches, 6 stations (out of originally 50) have been selected: 3 'good' stations where the neutral model performed well[17]: stations 19, 56, 57, and 3 'bad' where the neutral model did not perform well[18]: stations 29, 35, 41. The parameters of the MOS systems are optimised using data from December 1990 to May 1991 (the first half of the period) and they are tested on the data from June 1991 to November 1991 (the last half of the period).

Before the presentation of the two MOS systems two aspects of the forecasting problem will be analysed: What is the effect of not using the local corrections (ie not using the WA^{S}P matrix)? and what is the inherent variation of the observed wind speeds?

[17] Meaning that the model forecast rms errors were better than 0.7 times the persistence errors for the +18 and +36 hour forecast.

[18] Meaning that the model forecast rms errors were greater than the persistence errors.

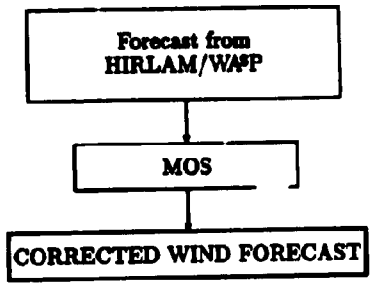

Figure 46. The idea of correcting a forecast based on a physical model with a statistical post-processor (MOS). In this project the MOS system is either linear regression or neural networks.

14.1 Sensitivity to the local corrections

To see whether the inclusion of the local corrections from WA^{s}P actually improves the forecast in transforming the HIRLAM forecast down to the surface layer, it has been tried to run the neutral model without applying the local corrections (ie without the WA^{s}P matrix) on the 6 selected stations. Not using the local corrections can be expressed in "WA^{s}P language" as that the stations are considered as not being influenced by obstacles and orography, and having a homogeneous roughness length in all directions of 0.03 m. The results can be seen in Table 20 in Appendix C, an example is shown in Figure 47. It appears from the figure and the table that the local corrections improve the forecasts for the 'good' stations; mainly by reducing the mean error. For the 'bad' ones the local corrections sometimes increases the mean error and sometimes the rms error. It can be seen that some stations (eg station 29) can not be 'saved' (ie the value of the evaluation parameters of the model brought under those of the persistence model) by either method.

The reason why the 'bad' stations are predicted worse when using WA^{s}P is due to the fact that the direction is predicted wrongly by HIRLAM (cf Figure 41), and that, as a consequence, the correction for the local effects are taken from a wrong sector. As an example, consider a mast located at a lake side: if the free-stream wind is actually coming from land but is predicted as coming from the lake, the resulting local wind will be much too high.

14.2 Statistical properties of the observed data

To get a better idea of the errors given in the following sections, a list of the statistical properties of each of the 6 selected stations is given in Table 10. As can be seen from this table the 'bad' stations have quite low mean wind speeds, and the standard deviations (from the mean) are of the same magnitude as the mean value. The 'good' stations – on the other hand – have higher means and the standard deviation is of a smaller magnitude than the mean. This is a general feature: 'good' stations have means higher than the standard deviation, and 'bad' lower or equal. As a rule one would place wind turbines at sites with high winds. In these cases the neutral HIRLAM/WA^{s}P model is seen to perform well.

14.3 0th order system

The 0th order MOS model used here takes output from the HIRLAM/WA^{S}P model and calculates the linear relationship between it and the observation. This is done sector by sector for the twelve 30 degree sectors:

$$u_{obs} = a(\theta_i) + b(\theta_i) u_{H/W}(\theta_i) \tag{122}$$

where u_{obs} is the observed wind, $u_{H/W}$ the forecasted wind form the HIRLAM/-WA^{S}P model coming from the direction sector θ_i, and $a(\theta_i)$ and $b(\theta_i)$ are the regression coefficients of the twelve 30 degree sectors. The relationship is established using data from the first half year (ie from December 1990 to May 1991) and tested on data from the last half year. The result is shown in Table 12 for the +3, +18 and +36 hours forecast. There is no quantitative difference between these three look-ahead times and the ones not shown. As can been seen there is an improvement when using this method: 'good' stations are as a rule left untouched, with a slight bias toward an improvement, and the performance of the predictions for the 'bad' stations is without exception improved. The 'bad' stations are actually improved to such an extent that after having applied MOS they can all be classified as 'good'.

It is likely that this method – in the limit – will perform better or as well as an optimal WA^{S}P analysis, particularly since the data are binned in directional bins. The reason is that looking at the two methods as black-boxes they both have (if we consider speed only) one scale-factor per sector. Actually, the linear method has the theoretical possibility of being better since this method also has an off-set, ie 2 parameters.

14.4 Neural networks

Neural networks will now be used as the model for predicting the wind locally. A neural network is a network of heavily connected simple computational units and it is characterised by its number of input, hidden and output neurons (for a more detailed description of neural networks see Section 9). A network is also characterised by the type of input and output, here the measured wind is used as input and the networks are trained to give a prediction (of eg the wind 18 hours ahead) as output.

To select the best neural network for the desired task, involves quite a bit of trial-and-error, since no rules of thumb exist concerning the optimal number of neurons and the number of layers in the network. The straightforward rule, that the more neurons, the better the result, is *not* valid. However, in a study similar to this (with respect to some points) Landberg (1992) found that simple neural networks (as eg the (1,5,1) net, for a definition of this syntax, see Table 11) gave satisfactory results, compared to persistence as well as to more complex networks (as eg (5,10,10,1)).

The search for the optimal network is therefore carried out among the networks listed in Table 11. Studying the errors that these networks cause, an unexpected feature is seen: the only thing that governs the performance of the network is the number of *input* units, ie a (1,1) network gives the same error and rms error as a (1,8,8,1) network. This means that all the neural network can learn about the relation between the forecast generated by the model and the observations, can be described by *very* few weights and thresholds. In the case of the (1,1) network, only one weight and one threshold is involved, ie a linear relation between the output of the forecasting model and the observations. This is actually what has been investigated in the previous section. Note also that the rule stating that more neurons do not necessarily lead to higher accuracy is confirmed.

The interesting result of the runs is that the neural network MOS system *improves* the forecasts for the 'bad' stations and leaves the forecasts of the 'good' stations more or less untouched. For the 'bad' stations, the forecasts are not only improved relative to the neutral model but also relative to persistence; actually, the forecast is, after MOS has been applied, now a 'good' forecast. Two examples of this are given in Figures 48 and 49. Figure 48 shows the 36 hour forecast for Birmingham (station 57, a 'good' station), it can be seen that the HIRLAM/WA^{9}P model is performing very much like the neural networks, especially if the smaller mean error is also considered. In Figure 49 the 36 hours forecast of Salamanca (station 29, a 'bad' station) is shown, it can be seen that all neural networks perform better than the persistence model, contrary to the HIRLAM/WA^{9}P model, and thereby converting the 'bad' station to a 'good' station.

Another way of training the neural network MOS - aimed directly at wind energy use - is to apply the power-curve (Figure 22) to the predictions and the observations before training. This would put more emphasis on the interval between the cut-in and cut-out wind speeds. This procedure has not been tried here.

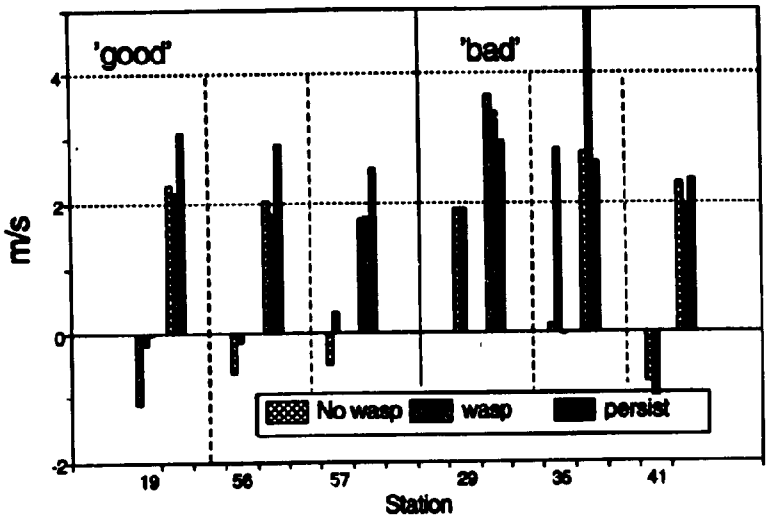

Figure 47. A comparison between using the full neutral HIRLAM/WA^{S}P model and using the model without the WA^{S}P corrections for the 6 selected stations For each station 6 bars are displayed in groups of 3: the first three are the mean error (in m/s) of the model without WA^{S}P corrections ('No wasp'), the full neutral HIRLAM/WA^{S}P model ('wasp') and persistence ('persist'), respectively; the last three bars for each station are the rms error (in m/s) for the 3 different models. The comparison is made for the +18h forecast for data from the last half of the period (June 1991 to November 1991.)

Table 10. A list of different statistical properties of the observations from the 6 selected stations. The first column is the name and station number, the second the mean of the wind speed (in m/s), the third the standard deviation (in m/s), and the fourth the number of observations.

Station	Mean	Std. dev.	No. obs.
Abbeville (19)	4.57	2.62	2779
Salamanca (29)	2.96	2.48	2747
Bragança (35)	2.81	2.32	2631
München (41)	3.01	2.01	2830
Manchester (56)	4.11	2.70	2863
Birmingham (57)	3.76	2.20	2863

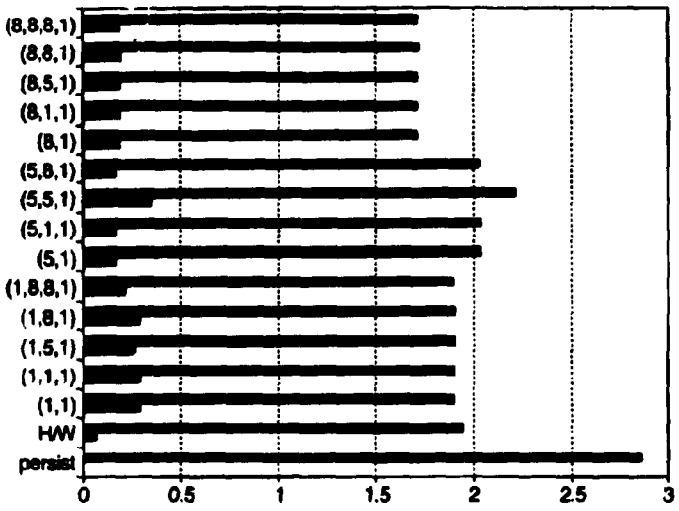

Figure 48. The performance (mean error (the lower bar of the two bars per model) and rms error, both in m/s) of the 14 tested neural networks compared to the HIRLAM/WA^{9}P model ('H/W') and persistence ('persist') for Birmingham (station 57) for the 36 hour forecast.

Table 11. The different neural networks used in the trail-and-error approach of finding the network that improves the forecast by the neutral model the most. The network architecture is read as follows: the first number in the parentheses is the number of neurons in the input layer, the last is the number of neurons in the output layer, and the numbers in between are the number of neurons in the hidden layers (eg (5,8,1) is a 3-layer network with 5 input units, one hidden layer with 8 units and 1 output unit).

(1,1)	(5,1)	(8,1)
(1,1,1)	(1,5,1)	(1,8,1)
(5,1,1)	(5,5,1)	(5,8,1)
(8,1,1)	(8,5,1)	(8,8,1)
(1,8,8,1)	(8,8,8,1)	

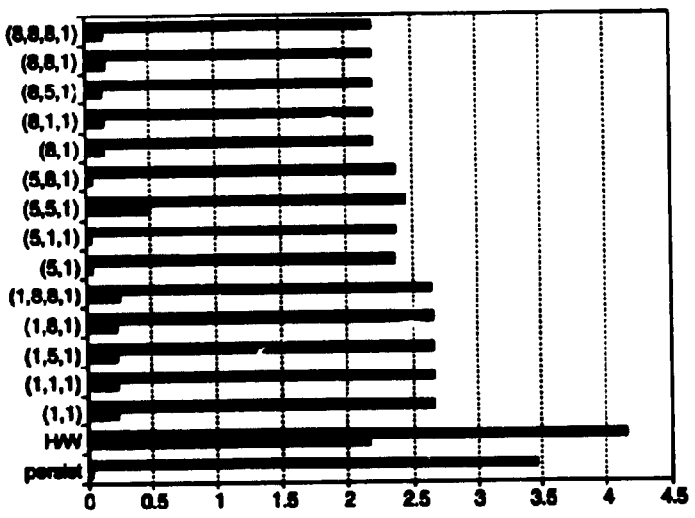

Figure 49. The performance (mean error (the lower bar of the two bars per model) and rms error, both in m/s) of the 14 tested neural networks compared to the HIRLAM/WAsP model ('H/W) and persistence ('persist') for Salamanca (station 29) for the 36 hour forecast.

Directional dependent neural network MOS

To see whether the forecasts can be improved, having knowledge of the direction, the thresholds and weights of the (1,5,1) network has been made dependent on direction. Each threshold and weight is now a function of twelve 30 degree sectors. The network has then been retrained. This procedure is equivalent to having 12 networks each trained on the appropriate subset of the observations. The problem here is that the grouping of the observations (of which only half a year is used) results in some rather small groups, most are sufficiently large, though. Looking at the results, cf Table 21 in Appendix C, it is seen that no further improvement for the 'bad' stations is found, and that the 'good' stations are only slightly better as compared to MOS using neural networks not dependent on direction, but still worse than the linear model. This is somewhat surprising, since one might expect that the knowledge of the direction would make it easier for the neural network. This not being the case, confirms the fact that the neural networks mainly see the persistence.

14.5 Conclusions MOS

As can be seen from Table 12 does the 0th order linear MOS system perform as well as, and sometimes even better, than the neural network MOS. Since the training of neural networks is much more time-consuming and complicated, it must be concluded that for MOS, only the linear model is needed.

Table 12. The result of the two MOS systems applied to the 6 stations for the 3, 18 and 36 hour look-ahead times compared to the HIRLAM/WA^{3}P model and persistence. The two MOS systems are optimised on data from the period December 1990 to May 1991 and tested on the second half year (June 1991 to November 1991). The column labeled '#' contains the station number, the 'F' column is the forecast time (in hours), the column marked '0th MOS' is the value of either the mean error (e_s) (model-observed) or the rms error ($RMSE_s$) (in m/s), the column marked 'NN MOS' is the value of either the mean error or the rms error of the (1,5,1) neural network. Columns marked 'rel. H/W' are the absolute values of the statistical quantities divided by the model output from HIRLAM/WA^{3}P, columns marked 'rel. pers.' are the absolute values of the statistical quantities divided by the result of the persistence forecast, a station is 'good' if this last number is less than 1.0 for RMSE for the +18 and +36 hour forecast.

			0th order MOS			Neural network MOS		
#	F		0th MOS	rel. H/W	rel. pers.	NN MOS	rel. H/W	rel. pers.
19	3	e	0.06	0.07	5.00	0.02	0.02	1.67
		RMSE	2.06	1.03	1.13	2.09	1.05	1.15
	18	e	0.17	0.94	8.50	−0.09	0.49	3.91
		RMSE	2.10	0.97	0.70	2.16	1.00	0.72
	36	e	0.09	0.15	15.00	0.30	0.49	50.00
		RMSE	2.42	1.03	0.71	2.21	0.93	0.65
56	3	e	−0.11	0.38	27.50	−0.10	0.34	25.00
		RMSE	1.51	0.74	0.98	2.13	1.04	1.38
	18	e	−0.09	0.64	6.92	−0.19	1.36	14.62
		RMSE	1.72	0.94	0.62	1.84	1.01	0.66
	36	e	−0.04	0.17	20.00	−0.20	0.89	100.00
		RMSE	2.38	1.10	0.77	2.17	1.00	0.70
57	3	e	0.21	7.00	210.00	−3.47	124.37	3470.00
		RMSE	1.51	0.76	1.14	2.13	1.06	1.61
	18	e	0.25	0.81	13.16	−3.36	10.69	176.84
		RMSE	1.76	0.99	0.73	2.08	1.18	0.87
	36	e	0.15	1.25	15.00	0.27	2.32	27.00
		RMSE	1.74	0.91	0.64	1.90	1.00	0.70
29	3	e	0.08	0.05	20.00	−0.02	0.01	5.00
		RMSE	2.79	0.68	1.47	2.84	0.69	1.50
	18	e	−0.24	0.13	11.43	−0.21	0.11	10.00
		RMSE	2.37	0.70	0.83	2.52	0.74	0.88
	36	e	−0.06	0.04	0.95	0.23	0.14	3.65
		RMSE	2.49	0.71	0.75	2.66	0.75	0.80
35	3	e	−0.13	0.09	2.17	−0.13	0.09	2.17
		RMSE	2.49	0.58	1.42	2.70	0.63	1.54
	18	e	0.06	0.02	0.88	−0.12	0.04	1.76
		RMSE	2.48	0.50	0.96	3.06	0.62	1.18
	36	e	0.18	0.08	7.83	0.31	0.13	13.48
		RMSE	2.04	0.52	0.68	2.19	0.55	0.73
41	3	e	−0.06	0.04	3.75	0.07	0.05	4.38
		RMSE	1.95	0.86	1.29	1.95	0.86	1.29
	18	e	−0.14	0.14	46.67	−0.12	0.12	40.00
		RMSE	1.70	0.86	0.75	1.73	0.88	0.77
	36	e	−0.09	0.06	10.00	−0.04	0.03	4.44
		RMSE	2.18	0.99	0.83	2.10	0.95	0.80

15 The stability-dependent model

In order to see whether it is possible to improve the prediction skill of the neutral HIRLAM/WA^{9}P model, a stability dependent version of it will be developed. First of all, it must be tested if the *error* of the neutral model is dependent on stability or not. To this end, the vertical buoyancy flux, B_s, will be used as an indicator of atmospheric stability, it is defined as

$$B_s = \frac{H_s}{\theta_{surf} c_p} + 0.608 \frac{H_l}{L_c} \tag{123}$$

where H_s is the sensible heat flux, θ_{surf} the potential surface temperature, c_p the specific heat of dry air at constant pressure, H_l the latent heat flux, and L_c the latent heat of condensation at 0°C. B_s in HIRLAM is, contrary to normal convention, positive when the heatflux is directed downwards, ie when the atmosphere is stable.

A plot of the error versus stability for May 1991, for all stations, for the neutral model with forecast length +3 hours is shown in Figure 50. This figure shows that as the stability of the atmosphere gets further and further away from neutral, there is a tendency for the error to increase. The conclusion of this being, that – if we can succeed in modelling the stability dependence – it can be expected that the inclusion of stability dependence will reduce the model error.

Another interesting fact appearing from the figure, is that there seems to be a majority of unstable situations, this is valid for day-time conditions, but also – more surprising – for night-time conditions. This is due to the fact that during the summer the model surface receives so much solar radiation, that it continues being warmer than the atmosphere during much of the night, Jørgensen (1991, private communication). This is obviously not a true model of the atmospheric stability. Furthermore, it has been reported that due to an error, the initial analysis makes the atmosphere more stable than it is in reality. This should force HIRLAM in the opposite direction than the one seen. The lack of daily variation, is expected to have influence – in a negative way – on the performance of the stability dependent version of the HIRLAM/WA^{9}P model.

15.1 The model

Using the theory in Part I, it is possible to construct a model that takes stability into account. It is in two places that it is necessary to change the neutral HIRLAM/WA^{9}P model: in the geostrophic drag law, where the A and B parameters are made stability dependent, and in the velocity profile, where an extra stability dependent term has to be included.

The stability dependence of the *wind profile* is quite well established, but unfortunately there is no single expression for the A and B parameters on which consensus has been reached, see Section 2.4. Therefore, all the different suggestions have been tried out. Furthermore, an average of the different curves is also tested, the averaged curves are shown in Figure 51.

The 7 different models listed in Table 13 are tested on data from the entire period on the 3 'good' and the 3 'bad' stations, see Section 14 for definitions. The results are shown in Figures 52 and 53.

As can be seen from the figures, the stability dependent models perform quite poorly compared to persistence as well as to the neutral model. So contrary to what was expected, the inclusion of stability does not improve the forecasting skills. The reason is, that it is very difficult to model the surface boundary layer generally and in a model using parameterisation of the boundary layer (as HIRLAM) especially.

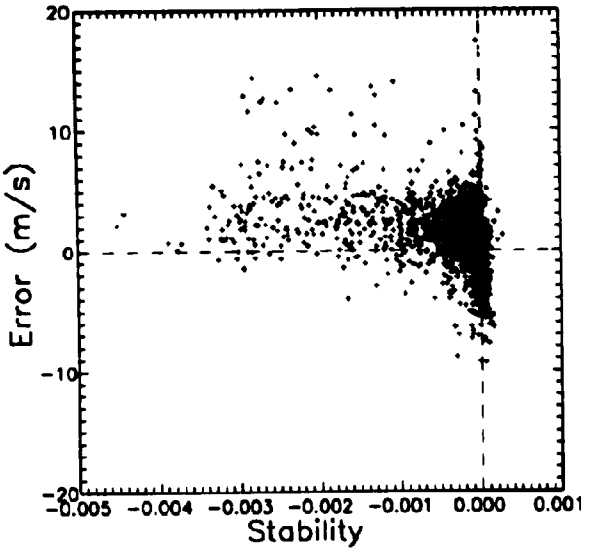

Figure 50. The error of the neutral model plotted versus stability. Data are from the 3 hour forecast for all stations in May 1991. As an indicator of stability the vertical buoyancy flux, negative for unstable conditions, defined in Eq. 123, is used.

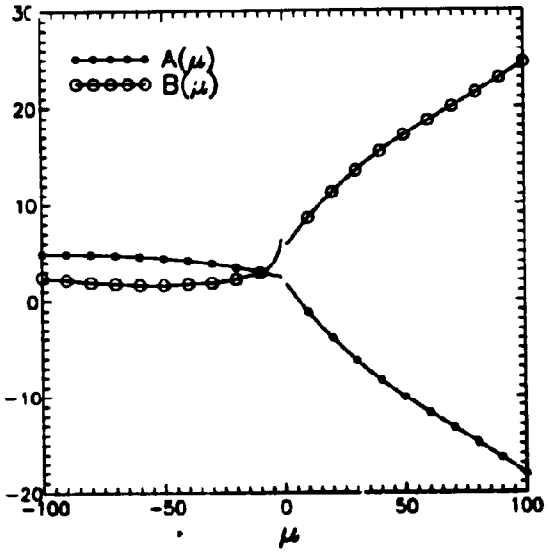

Figure 51. The average A and B curves of all the proposed curves as a function of μ.

As a consequence of the above-mentioned, another situation occurs quite frequently: with the set-up of the stability parameters, the Coriolis parameter, and the roughness length, we get a function $G(u_*)$ that has no solution for the geostrophic wind, G, output from HIRLAM, see Figure 54 for reference, meaning that it is impossible to obtain a solution, u_*, and as a consequence a prediction of the local wind. This occurs between 10 to 50 per cent of the time for all the models. An occurrence of 50 per cent rejections is totally unacceptable, if a usable forecasting system is wanted. It means that every second forecast is not available.

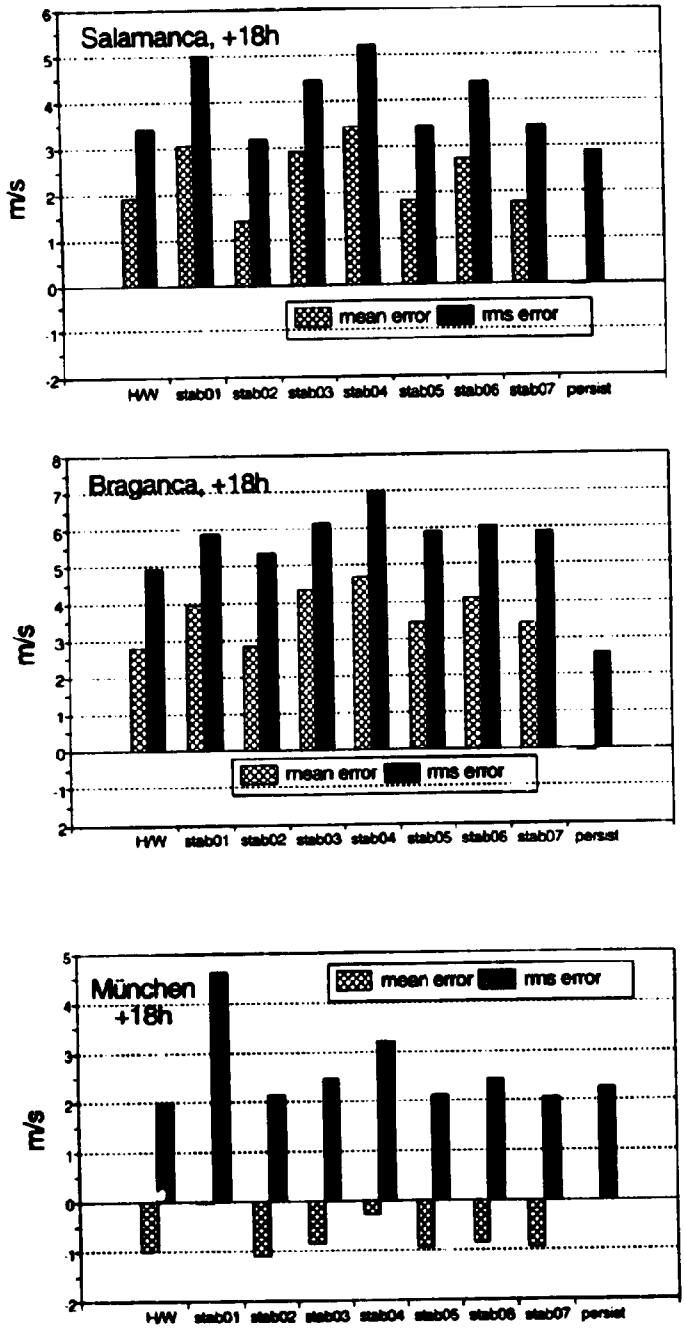

Figure 52. The mean error and the rms error of the 7 stability dependent models run for the entire period on data from the 'bad' stations (29, 35, and 41) compared to the neutral HIRLAM/WASP model ('H/W') and persistence ('persist').

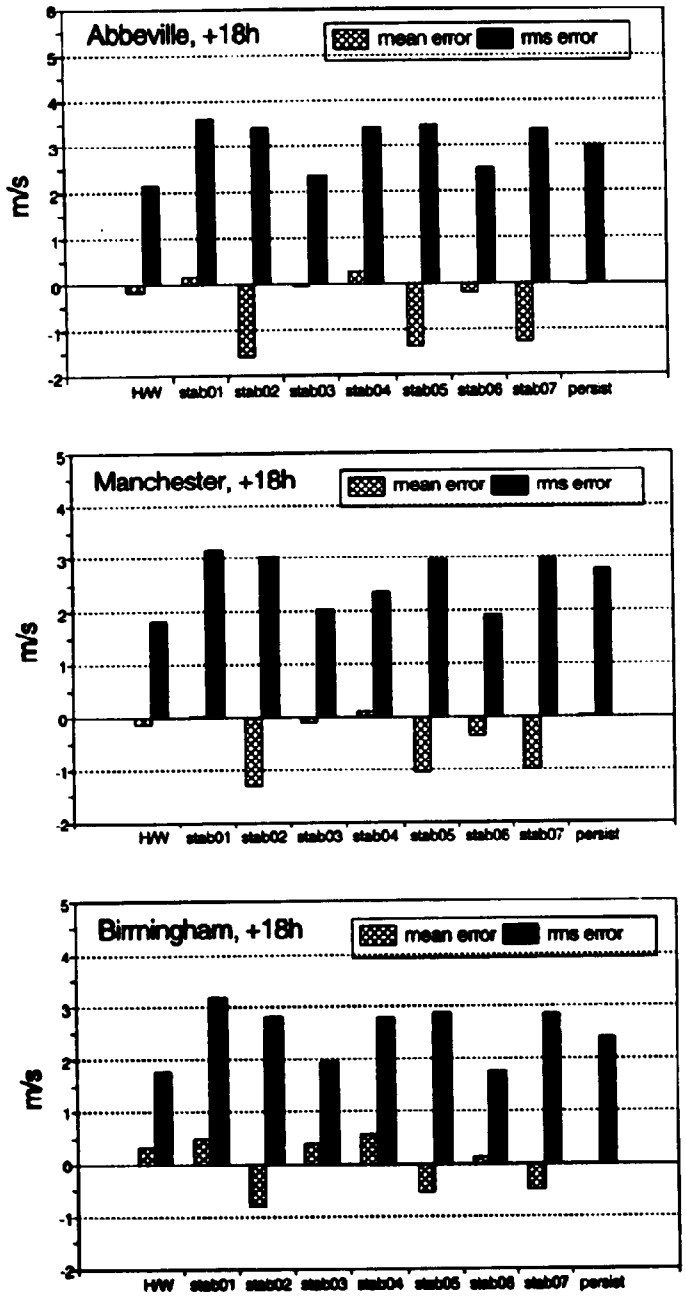

Figure 53. The mean error and the rms error of the 7 stability dependent models run for the entire period on data from the 'good' stations (19, 56, and 57) compared to the neutral HIRLAM/WA^{3}P model ('H/W') and persistence ('persist').

Table 13. The six stability dependent models plus the averaged A and B profiles.

stab01	Zilitinkevich, 1975
stab02	Arya, 1975
stab03	Arya, 1977
stab04	Long and Guffey, 1977
stab05	Billard, 1981
stab06	Jensen et al, 1984
stab07	Average of the above

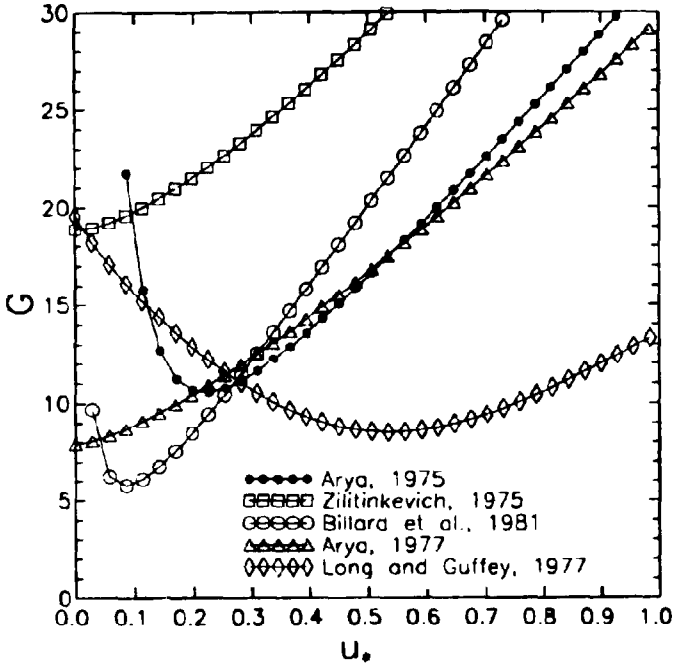

Figure 54. G plotted versus u_* using the geostrophic drag law for a certain set of parameters ($z_0 = 0.03$, $f_0 = 1.2 \cdot 10^{-4}$, $\mu u_*^2 = 1.78$) for some of the selected models. Note that winds output from HIRLAM (ie the G's) below 5 m/s will not have a matching u_*, and as a consequence that no local wind can be calculated.

Studying the two stability parameters (the latent and sensible heat flux) output from HIRLAM will cast some light on the problem, since there is a lack of the expected daily variation (cf Figure 55). This is explained by the fact that stations situated up to 2 grid-spacings (110 km) from the coast, will have values taken from gridpoints that have a prescribed constant sea surface temperature taken month by month from climatological values. This inhibits – of course – the variation. The displayed station (Abbeville) is 25 km from the coast, and falls therefore within the category mentioned above. It must be stressed that HIRLAM is a state-of-the-art forecasting model, and therefore that we cannot expect to find other models giving better results. So the aim of studying the stability dependence is as much to see whether the stability – at present – can be modeled with sufficient accuracy to be used for short-term prediction. As can be seen from the above, this is not the case, yet. It should be noted, however, that modelling the boundary layer (including the fluxes) is one of the major fields of ongoing research.

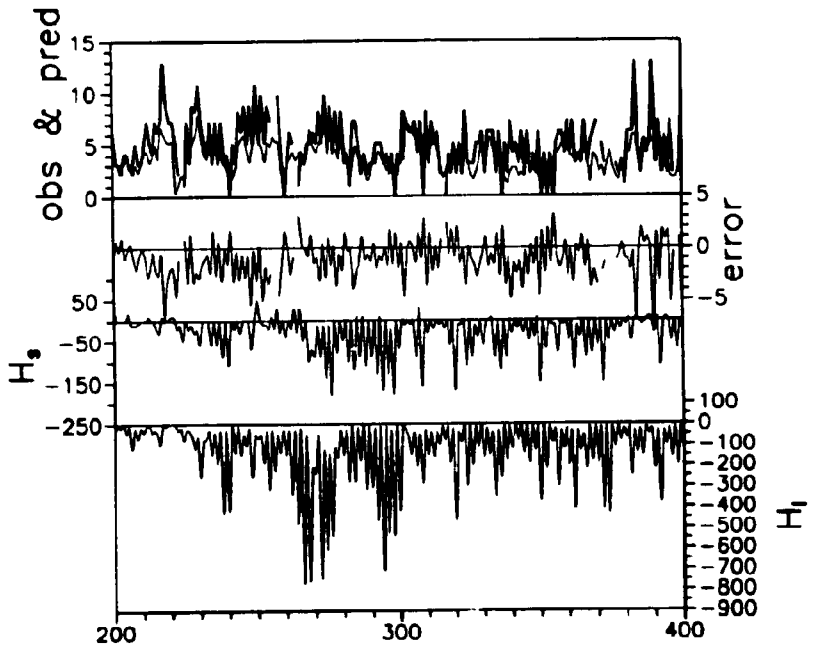

Figure 55. An example of the variation of the sensible (3rd x-axis from above) and the latent heat flux (4th x-axis from above), H_s and H_l, respectively. The data are taken from Salamanca (station 19), and are for the +3 hour forecast, which are taken at 03 and 15 UTC, in the period March 10th to June 18th 1991. The uppermost lines are the predicted (thin line) and the observed values (bold line), the line around the 2nd x-axis from above is the error (predicted − observed) in m/s.

16 Other prediction methods

16.1 Statistical methods

In this section two other methods for short-term prediction are presented. They both base themselves solely on *observed values*, ie no physical modelling at all is involved. The two methods are:

- A simple linear correlation
- Neural networks

These methods are - in compliance with the testing of the other models developed so far - optimised on data from the first half year of the one year period (December 1990 - May 1991) and evaluated on the last period (June 1991 - November 1991). Note that in this case approximately 2900 observations are available, since all of the 3 hourly observations are available. This is contrary to the HIRLAM/WA^{9}P model where only forecasts every 12 hours are at hand for each look-ahead time, because HIRLAM is only run twice a day.

Linear model

The linear model uses the same principle as the linear model in the section about MOS; however, instead of using winds output from a physical model, previous (known) observations are used. In this simple approach the linear relation between the wind 24 hours ahead (say) and the presently observed wind is established, according to the following formula

$$u(t) = a(t) + b(t)u_{\text{obs}}(0) \tag{124}$$

where $u(t)$ is the wind at look-ahead time t and $u_{\text{obs}}(0)$ is the observed wind at the beginning of the forecast period. $a(t)$ and $b(t)$ are the coefficients linking the observed wind at time $t = 0$ to the observed wind at time t. Note, that no dependence on direction is modelled.

The linear model has been tried on the 6 selected stations and the results of the forecasts are found to be very good, especially for the 'bad' stations where the rms error is slightly better than that of the HIRLAM/WA^{9}P model with linear MOS applied. The mean error is of the same magnitude for the 'bad' stations. For the 'good' stations the results are of the same magnitude. Bear in mind that these models base themselves on *observations* only. The results are listed in Appendix C, Table 19. Examples of results using the linear model are shown in Figures 60 to 65 in Section 17.

The sensitivity to the number of samples used in the optimisation of the linear model has been investigated. It can be seen from Figure 56 that if less than 600 samples (ie approx 2.4 months) are used, the forecasts will be highly unreliable in the sense that the mean error is fluctuating rapidly. After 600 samples is can be seen that some seasonal variation is still present even out to 1400 samples (ie approx. 5.7 months). Clearly, at least one whole year must be covered, to take all seasonal variation into account.

Forecasting with neural networks

Two different neural networks have been trained on the first 1448 observations (equal to the first half year): a very simple network (1,5,1) and a more complex: (5,10,10,1). Remember that one of the conclusions, when using neural networks

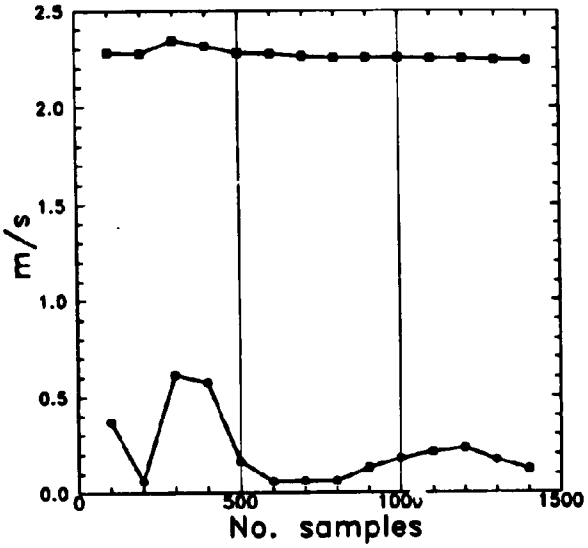

Figure 56. The mean error (in m/s, solid circles) and the rms error (in m/s, solid squares) of the linear model predicting 18 hours ahead for Manchester (station 56) plotted against the number of samples used during the optimisation of the parameters. All the models have been tested on the last half of the period.

to do MOS, was that the complexity did not play any role with respect to performance, and that, furthermore, the neural networks did not perform better than the simple linear MOS. The validity of these statements is tested for neural networks trained on observations only in this section.

It is found that the use of neural networks as the predicting tool for the 6 selected stations does not perform better than the HIRLAM/WA^{3}P model with linear MOS for the 'bad' stations and without MOS for the 'good' ones. Furthermore, is it found that – in this case of only two different models – the more complex network performs better than the simpler one. The difference is not very pronounced, however. Examples of the performance of the (5,10,10,1) network are shown in Figures 60 to 65 in Section 17.

It has been tested to see how strong the influence of the number of samples in the time series (ie the time spent carrying out on-site measurements) is on the different evaluation parameters. Referring to Figure 57, it can be seen that especially the mean error is dependent on the number of samples, but after approximately 700 samples the error seems to have found its level, with only small oscillations around this. The pattern is very much like that found for the linear model. The sensitivity to the number of iterations in each training session has also been investigated and it was found that within the range of 500 to 10000 iterations there was no dependence. All other networks in this project have been trained using 2000 iterations. Finally, the sensitivity to the magnitude of ϵ has been looked into and no dependence of the mean error or the rms error was found for a fixed number of iterations (2000) either.

16.2 Conclusion, statistical models

As stated above, the linear and the neural network models does perform equally well. They have both performances that are equal to or better than the physical model. Since the training and implementation of the linear model is much simpler

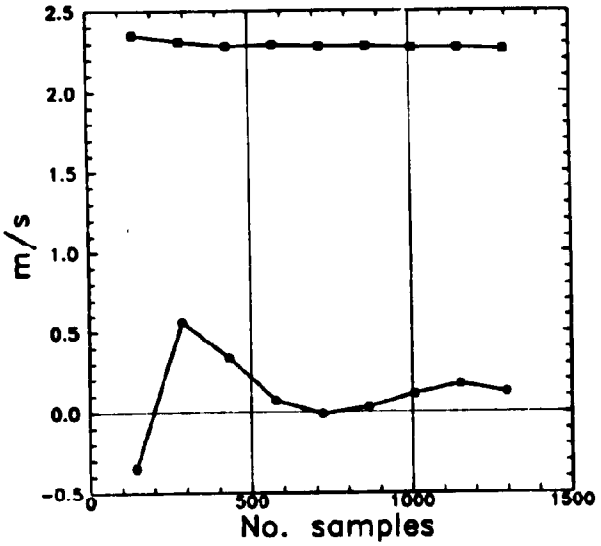

Figure 57. The mean error (in m/s, solid circles) and the rms error (in m/s, solid squares) of the (1,5,1) neural network predicting 18 hours ahead for Manchester (station 56) plotted against the number of samples used during the training of the network. All the networks have been tested on the last half of the period.

than the neural network, it must be concluded, that if on-site data exists the linear model should be used.

16.3 Using the UK Meso-scale model

To see the effect of the resolution (mainly spatial, but also temporal) of the weather prediction model on the performance of the model predicting local wind conditions, the British Meteorological Office's UK MESO (United Kingdom Meso-Scale) model is used instead of HIRLAM. The model is non-hydrostatic and has a spatial resolution of 15 km (HIRLAM: 57 km). The UK-MESO covers only the United Kingdom, Ireland, and minor parts of continental Europe and can therefore only be used for the stations situated in the United Kingdom. See Golding (1990) for further information on the UK MESO model.

The output used from the model is the 10 m wind. The model we then develop, is taking this wind and correcting it for the local effects. The assumption is that the 10 m wind output from the UK MESO model is completely unaffected by local conditions. This is of course not true, since the orography of the United Kingdom is present in the model. But because of the resolution of UK MESO, the orography is not resolved on the same scale as in WA^{S}P. Comparing the forecast using UK MESO and WA^{S}P to the HIRLAM/WA^{S}P model for all the selected stations in the UK (ie station 1, 60 and 52 to 58), we see, without any exceptions, that the rms error is reduced with typically 70 - 80 per cent. The mean error is typically of the same magnitude as when using the HIRLAM model. An example of this is shown in Figure 58. There are, however, a few stations where the mean error is quite big: station 1, 57 and 58, where the error is typically around 1 m/s. Note that no MOS was applied to either of the models, so biases like these would have been removed if it was used.

In conclusion it can be said that - as expected - the higher spatial resolution gives improved forecasts. Note that the 'price' paid for this improvement is a significant reduction of the area covered. This fact can only be changed with the use and development of more powerful computers.

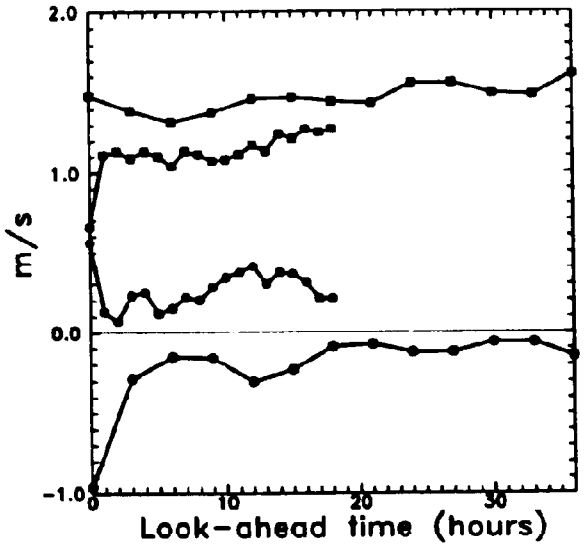

Figure 58. The mean error (in m/s, denoted by circles) and rms error (in m/s, denoted by squares) of the HIRLAM/WA^{S}P-model (open symbols) compared to the UK MESO model (solid symbols) combined with WA^{S}P for Manchester for the entire period (December 1990 to November 1991). The look-ahead time (in hours) is along the x-axis.

17 Summary and conclusions

In this section a brief overview of the study will be given, since quite a few models have been presented. Furthermore, a conclusion will be given as to which models are to be used when.

Eight different models have been used in this study, they are listed in Figure 59. They can basically be grouped in two:

1. Models that use numerical weather prediction models (NWP) (such as HIRLAM and the UK MESO model).
2. Models that base themselves solely on observations.

The first group can be subdivided into models that use physical models only (the HIRLAM/WA^{S}P in its neutral and stability dependent versions and the UK MESO/WA^{S}P models) and models that are based on some statistical knowledge of past observations (the two MOS (Model Output Statistics) models, one based on a linear relation and another based on a relation generated by a neural network). Likewise, the second group can be subdivided in two: one that does nothing to the observations (the persistence model) and one that performs some sort of transformation of the observations (the linear and the neural network models).

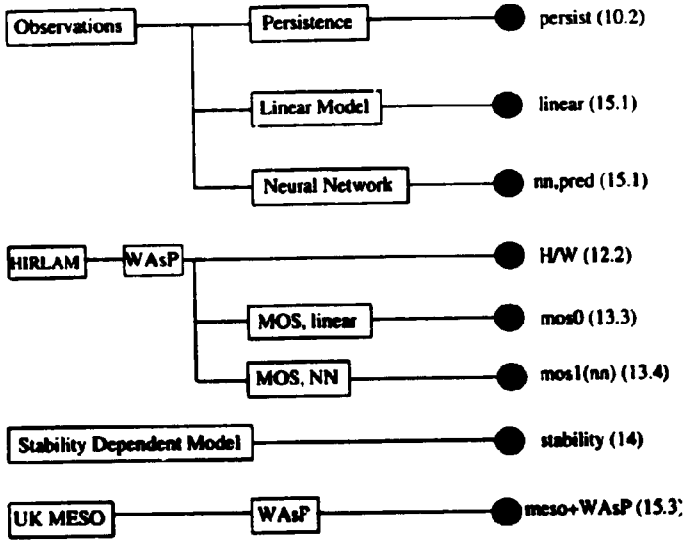

Figure 59. An overview of the different models used to predict the local wind conditions. The numbers in the parenthesis refer to the section where the model is described.

The emphasis in this study has been laid on the development of the neutral model using output from HIRLAM, transforming this to the surface layer, and correcting the resulting free-stream wind for local effects using output from the WA^{S}P model. The neutral model has also been extended to include stability dependence.

17.1 Comparing the 8 models

In Figures 60 to 65 the mean error and the rms error of the eight models are given for the 6 stations, selected for a closer examination. Three of the stations

are categorised as 'good', ie well predicted (as compared to persistence) by the neutral version of the HIRLAM/WA^{S}P model, and three as 'bad'. This ratio of 'good' to 'bad' is not representative of the 50 stations studied, since at least 80 per cent of these are labeled as 'good'. It is well known, however, that one learns, not from the successes, but f .m the failures.

To make a fair comparison of the different models, only data from the last half of the period (ie from June 1991 to November 1991) has been used in the evaluation for all the models. Of the stability dependent models only one of the 7 is presented as an example.

17.2 Conclusions

A number of conclusions can be drawn:

- The performance of existing forecast methods (mainly persistence) has been surpassed significantly by the methods developed and presented in this study.
- At sites with high mean wind speeds the neutral HIRLAM/WA^{S}P model is found to perform particularly well.
- If no data is available at the site (the typical case) the neutral version of the HIRLAM/WA^{S}P model should be used. If an NWP model exists with a higher resolution than HIRLAM, it should be used instead. If the site is dominated by strong local thermally driven circulation, the model should be used with great caution.
- For look-ahead times shorter than 3 to 6 hours, the persistence model should be used, since none of the models perform as well.
- If on-site data is available two approaches can be taken:
  - If output from NWP models is at hand the forecast using the neutral version of the HIRLAM/WA^{S}P model should be used, corrected with the linear MOS model
  - If no output from from NWP's is at hand, the linear correlation method based on observations only should be used.
- The stability-dependent version of the neutral model failed to produce any improvement over the neutral model, mainly because of the difficulty for the NWP model in predicting the heat fluxes at the surface.
- The neural networks performed quite well, often better than the neutral HIRLAM/WA^{S}P model, but since the much more simple linear models performed equally well (for the MOS version and for the prediction based on observations only), it must be concluded that neural networks – in this study – have not shown any outstanding performance. This is most likely due to the fact that, even though the problem of predicting the wind locally is a hard one, persistence is performing quite well, and there is not much for the neural network to 'learn'.

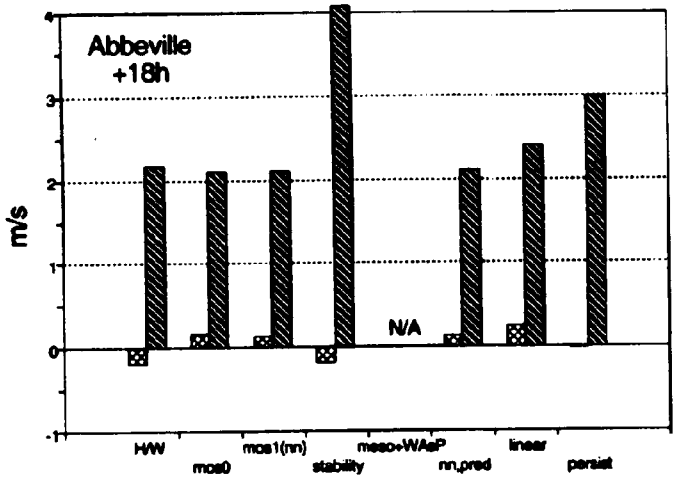

Figure 60. The comparison of the eight models for Abbeville (stat. 19). The first bar (of the two for each model) is the mean error (in m/s) and the second is the rms error (also in m/s). An explanation of the different abbreviations of the different models can be found in Figure 59. 'N/A' means that the UK MESO forecast is not available, because the station is not within the area covered by the model. Abbeville is categorised as a 'good' station meaning that the HIRLAM/WA^{3}P model predicts it well (as compared to persistence).

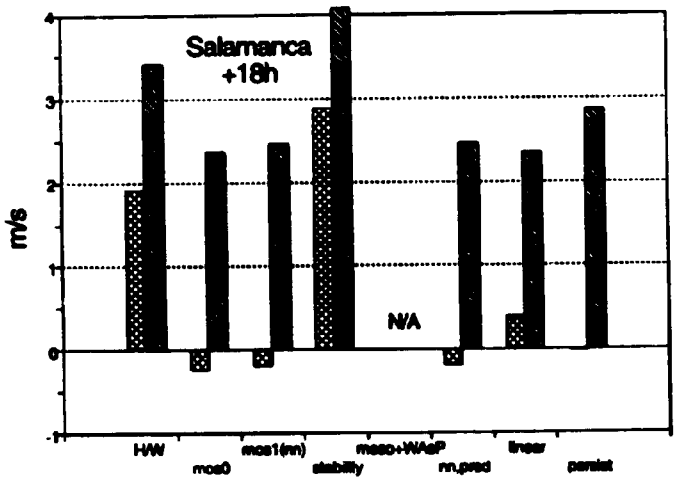

Figure 61. The comparison of the eight models for Salamanca (stat. 29). See Figure 60 for explanation. Salamanca is a 'bad' station.

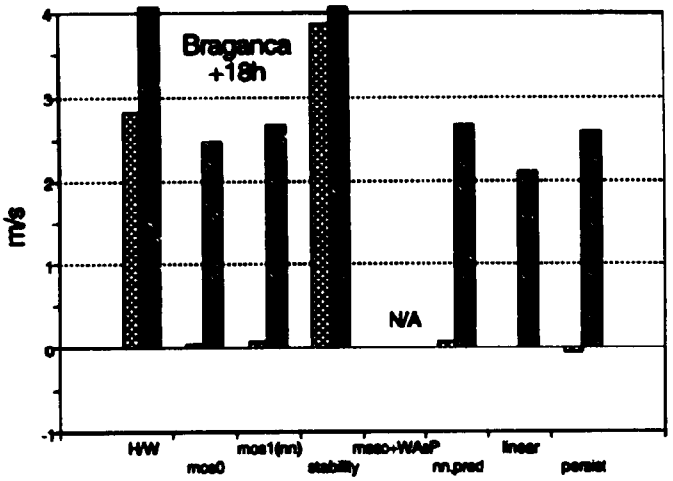

Figure 62. The comparison of the eight models for Bragança (stat. 35). See Figure 60 for explanation. Bragança is a 'bad' station.

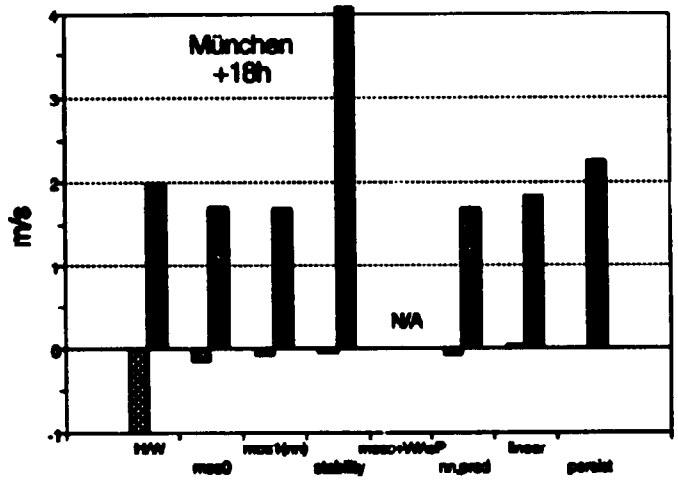

Figure 63. The comparison of the eight models for München (stat. 41). See Figure 60 for explanation. München is a 'bad' station.

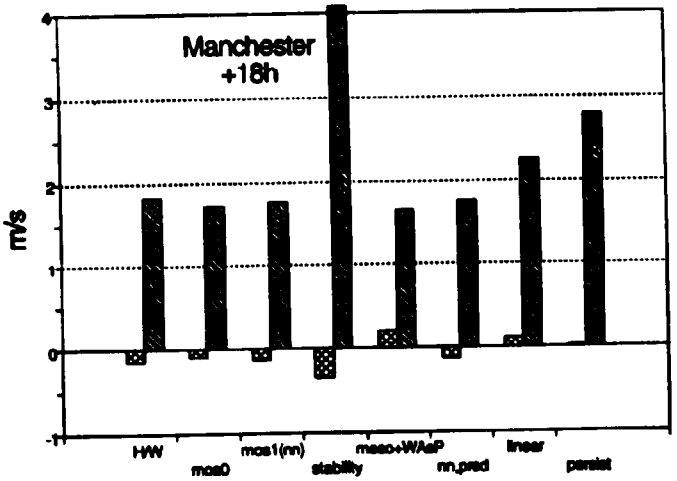

Figure 64. The comparison of the eight models for Manchester (stat. 56). See Figure 60 for explanation. Manchester is a 'good' station.

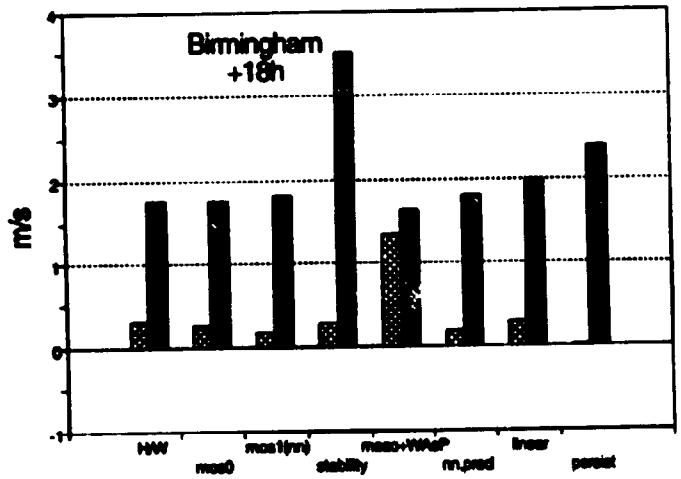

Figure 65. The comparison of the eight models for Birmingham (stat. 57). See Figure 60 for explanation. Birmingham is a 'good' station.

17.3 Using the models

In this last section a sketch of the possible use of the neutral version of the HIRLAM/WA^{S}P model will be given. The problem is that HIRLAM is only run twice a day (at 00 UTC and at 12 UTC). This means that for a given time of day there will only be forecasts available from a certain look-ahead time. As an example, consider the available forecasts for 09 UTC:

- the +9 hour forecast from the model run at 00 UTC on the same day.
- the +33 hour forecast from the model run the day before at 00 UTC, and
- the +21 hour forecast from the model run at 12 UTC the day before.

A complete overview of this is given in Figure 66.

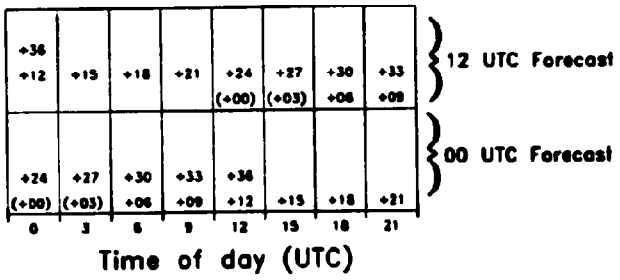

Figure 66. The available forecasts during the day from HIRLAM. Numbers in parenthesis refer to the fact that the forecasts are not available, until between 3 to 6 hours after the observations were made.

The implementation of the model is quite simple: In the case of a single wind turbine, only 24 values from the NWP model (the x and y-components of the forecast wind every third hour for 12 time steps) are needed twice a day. These values can be transferred from the meteorological institute through some electronic transferal system, by fax, or by phone. When the values are received they are entered into the PC, the program developed in this study is then run (taking less than 30 sec) and the forecasts are output from the PC. These forecasts can then be used in the planning and scheduling of the conventional power plant. This procedure is depicted in Figure 67. Before the first forecast is made, a WA^{S}P analysis of the site, similar to the one sketched in Section 12.2, has to be carried out. In the analysis the following topics need to be accessed: the distribution of the obstacles around the site, the roughness of the surrounding terrain, and the orography of the terrain. This information has then to be entered into WA^{S}P, and the program run. The resulting correction matrix for the local effects can then be output from WA^{S}P.

If a wind farm is considered, the power production must be analysed using a program that takes the fact that the turbines most likely will be in each-other's wakes into account. A program that does this is PARK, see Sanderhoff (1993).

If - for scheduling purposes - forecasts with a higher temporal resolution are needed, these can be obtained either by linear interpolation between the existing forecasts or by obtaining more detailed output from the NWP. Generally NWP models have time-steps of the order of a few minutes.

Figure 67. The implementation of the neutral model.

Acknowledgements

This study has been funded by the Danish Research Academy and the EEC JOULE-programme under contract JOUR-0091-C(MB). The HIRLAM data and the observations have been provided by the Danish Meteorological Institute. The British Meteorological Office has through Rutherford Appleton Laboratory provided the data from the UK MESO model.

I would like to thank Dr Aksel Walløe Hansen, University of Copenhagen, Geophysical Institute, Dr Erik Lundtang Petersen, Dr Søren E. Larsen and Jakob Mann, all from Department of Meteorology and Wind Energy, Risø National Laboratory for helpful discussions and Frances for correcting 'bad language' and for letting me share my life with her.

I would like to thank Niels G. Mortensen for being a good colleague and for scrutinising the draft, resulting in many good corrections I would also like to thank Dr Simon J. Watson, Rutherford Appleton Laboratory, for good coorporation and for being the 'yard-stick' at RAF Dunkeswell. At the met. station at RAF Dunkeswell I would like to thank Mr John Pawley for being very helpful. Finally, I would like to thank Rasmus Poulsen for digitising the maps of Dunkeswell.

Dansk sammendrag

En model til at lave kortfristede forudsigelser (dvs op til 36 timer) af lokale vindforhold (dvs den vind, der måles af anemometret på en meteorologisk mast) er blevet udviklet og evalueret. Modellen bygger på forudsagte vinde fra Danmarks Meteorologiske Instituts HIRLAM model. Disse vinde, der blæser i et niveau udenfor grænselaget, bliver transformeret ned til overfladen ved hjælp af den neutrale version af den geostrofiske 'drag'-lov. Ved overfladen bruges den neutrale vindprofil og vinden korrigeres for lokale forhold ved hjælp af Forskningscenter Risøs WA^{S}P model. De lokale forhold er: lævirkning af nærtstående forhindringer, indflydelsen af aerodynamisk ruhed og af orografi. Denne model vil i det følgende blive kaldt 'den neutrale model'.

Under udviklingen af modellen viste det sig, at den faktiske modelvind i 137 m's højde fra HIRLAM gav de bedste resultater. Dette i modstrid med hvad man ville forvente, nemlig at det var den *geostrofiske* vind, der ville give de bedste resultater. Forklaringen på dette er formentligt, at det er forbundet med vanskeligheder at beregne geostrofvinden nøjagtigt i en model, der benytter sig af et σ-koordinatsystem. Et σ-koordinatsystem er et system hvor vertikalkoordinaten er det atmosfæriske tryk normaliseret med trykket ved overfladen.

Modellen er blevet evalueret ved at bruge observationer af vindhastighed og -retning fra 50 meteorologiske stationer fordelt over hele Europa. Der er blevet brugt observationer fra et helt år (december 1990 til og med november 1991).

Resultatet af evalueringen er, at modellen er bedre end en persistensmodel - efter 4-6 timer. En persistensmodel er en model, der anvender den seneste observation som forudsigelsen feks 18 timer frem. Årsagen til, at den her udviklede model først er bedre efter en vis tid, er, at de fejl, der uundgåeligt optræder i en numerisk vejrforudsigelsesmodel, er så store at den simple persistensmodel forudsiger mere nøjagtigt i begyndelsen. Som et eksempel kan det nævnes, at for 18 timers forudsigelsen var 80% af stationerne forudsagte bedre ved hjælp af den neutrale model end af persistensmodellen. Det viste sig, at observationer fra stationer med høje middelvindhastigheder (set i forhold til standard-afvigelsen) var bedre forudsagte end stationer med lave middelhastigheder.

Endvidere blev en stabilitetsafhængig (dvs afhængig af den *atmosfæriske* stabilitet) version af den føromtalte neutrale model udviklet og afprøvet. Det viste sig, på grund af vanskeligheder (for dagens matematiske modeller af atmosfæren) ved at forudsige varmefluksene ved jordoverfladen, at denne stabilitetsafhængige model ikke forbedrede den neutrale models forudsigelser.

Et andet tiltag for at forbedre den neutrale models forudsigelsesevne var at anvende MOS (Model Output Statistics). Denne metode bygger på, at man forsøger at finde en feks lineær sammenhæng mellem det en fysisk model forudsiger og det faktiskt observerede. Denne metode gav meget gode resultater, især for de 20% af stationerne hvis observationer ikke var forudsagte særligt godt af den neutrale model; så stor, at forudsigelsen blev bedre end persistensmodellens. Hvis det er muligt, dvs hvis der eksisterer tidligere observationer og forudsigelser, bør den neutrale model derfor kombineres med MOS.

For at bedømme den neutrale models forudsigelsesevne blev et antal simple (mht deres indhold af fysik) modeller udviklet og afprøvet. Nogle af disse modeller bygger på lineær regression og andre på neurale netværk. Det viste sig, at begge disse typer modeller forudsagde observationerne forbavsende godt; dette kan feks ses af Figurerne 60 til 65. Da optimeringen af modeller byggende på neurale netværk er betydeligt mere beregningskrævende end modeller byggende på lineær regression og da begge typer modeller lavede gode forudsigelser, må det anbefales at bruge den model, der bygger på lineær regression.

References

Abramowitz and Stegun, 1964: *Handbook of Mathematical Functions*. Washington: National Bureau of Standards, 504.

Arya, S.P.S., 1975: *Geostrophic drag and heat transfer relations for the atmospheric boundary layer*. Q. J. R. Meteorol. Soc., **101**, 147-161.

Arya, S.P.S., 1977: *Suggested Revisions to Certain Boundary Layer Parameterization Schemes Used in Atmospheric Circulation Models*. Mon. Weather Rev., **105**, 215-227.

Arya, S.P.S., 1985: *The Schematics of Balance of Forces in the Planetary Boundary Layer*. J. Clim. Appl. Meteorol., **24**, 1001-1002.

Autzen, C., 1991: *Evaluation of the Danish HIRLAM*. (In Danish). Danish Meteorological Institute, Copenhagen, Denmark.

de Baas, A., 1990: *The K-ε model in separating flows*. In: Proceedings of Ninth Symposium on Turbulence and Diffusion, Roskilde. American Meteorological Society, 359-362.

Billard C., J-C. André, and R. du Vachat, 1981: *On the Similarity Functions A and B as determined from the the 'VOVES' experiment*. Boundary-Layer Meteorol., **21**, 495-507.

Blackadar, A.K., 1965: *A Single Layer Theory of the Vertical Distribution of Wind in a Baroclinic Neutral Atmospheric Boundary Layer*. In: Flux of Heat and Momentum in the Planetary Boundary Layer of the Atmosphere, Final report, Penn. State Univ., Meteorology Dept., Contract AFCRL-65-531, 1-22.

Blackadar, A.K. and H. Tennekes, 1968: *Asymptotic Similarity in Neutral Barotropic Planetary Boundary Layers*. J. Atmos. Sci., **25**, 1015-1020.

Bradley, E.F. and P.J. Mulhearn, 1983: *Development of velocity and shear stress distributions in the wake of a porous shelter fence*. J. Wind Eng. Ind. Aerodyn., **15**, 145-156.

Bradshaw, P., 1971: *Variations on a theme of Prandtl*. AGARD Conf. on turbulent Shear Flows, London.

Byun, D.W., 1991: *Determination of similarity functions of the resistance laws for the planetary boundary layer using surface-layer similarity functions*. Boundary-Layer Meteorol., **57**, 17-48.

Castro, I.P., 1979: *Relaxing wakes behind surface-mounted obstacles in rough wall boundary layers*. J. Fluid Mech., **93**, 631-659.

Clarke, R.H., 1970: *Observational Studies in the Atmospheric Boundary Layer*. Q. J. R. Meteorol. Soc., **96**, 91-114.

Clarke, R.H., A.J. Dyer, R.R. Brooke, D.G. Reid, and A.J. Troup, 1971: *The WANGARA experiment. Boundary-Layer Data*. Paper No. 19, Division of Meteorological Physics, CSIRO, Australia.

Clarke, R.H. and G.D. Hess, 1974: *Geostrophic Departure and the Functions A and B of Rossby-Number Similarity Theory*. Boundary-Layer Meteorol., **7**, 267-287.

Counihan, J., J.C.R. Hunt, and P.S. Jackson, 1974: *Wakes behind two-dimensional surface obstacles in turbulent boundary layers*. J. Fluid Mech., **64**, 529-563.

Counihan, J., 1969: *An improved method of simulating an atmospheric boundary layer in a wind tunnel*. Atmos. Environ., **3**, 197.

Csanady, G.T., 1972: *Geostrophic drag, heat and mass transfer coefficients for the diabatic Ekman layer*. J. Atmos. Sci., **29**, 488-496.

Deacon, E.L., 1973: *Geostrophic Drag Coefficients*. Boundary-Layer Meteorol., **5**, 321-340.

Deardorff, J.W., 1972: *Parameterization of the planetary boundary layer in general circulation models*. Mon. Weather Rev., **100**, 93-106.

Dyer, A.J., 1974: *A review of flux-profile relationships*. Boundary-Layer Meteorol.,

7, 363-372.

Fiedler, F., 1972: *The Effect of Baroclinicity on the Resistance Law in a Diabatic Ekman Layer.* Beitr. Phys. Atmos., **45**, 164-173.

Finnigan, J.J., 1988: *Air flow over complex terrain.* In: Flow and transport in the Natural Environment: Advances and Applications. Eds W.L. Steffen and O.T. Denmead, Springer-Verlag, 183-229.

Glahn, H.R. and D.A. Lowry, 1972: *The Use of Model Output Statistics (MOS) in Objective Weather Forecasting.* J. Appl. Meteorol., **11**, 1203-1211.

Golding, B.W., 1990: *The Meteorological Office Mesoscale Model: An Overview.* Meteorol. Mag., **119**, 81-96.

Hall, C.D., 1987: *A common verification Scheme for Limited Area Models.* LAM Newsletter, December, EWGLAM, U.K. Met. Office.

Holton, J.R., 1979: *An Introduction to Dynamic Meteorology.* International Geophysics Series Volume 23. Academic Press, New York, U.S.A.

Hunt, J.C.R., 1971: *The effect of single buildings and structures.* Philos. Trans. R. Soc. London A, **269**, 457-467.

Hunt, J.C.R., C.J. Abell, J.A. Peterka, and H.G.C. Woo, 1978: *Kinematical studies of the flows around free or surface-mounted obstacles; applying topology to flow visualization.* J. Fluid Mech., **86**, 179-200.

Högström, U., 1988: *Non-dimensional wind and temperature profiles in the atmospheric surface layer: A re-evaluation.* Boundary-Layer Meteorol., **42**, 55-78.

Jackson, P. S. and J. C. R. Hunt, 1975: *Turbulent flow over a low hill.* Q. J. R. Meteorol. Soc., **101**, 929-955.

Jensen, N.O., E.L. Petersen, and I. Troen, 1984: *Extrapolation of mean statistics with special regard to wind energy applications.* World Meteorological Organization, World Climate Applications Programme, WCP-86, WMO/TD-No. 15. 85 pp.

Joelsen R., 1990: *Subjective evaluation of the quality of sea level pressure forecast from HIRLAM (FMI), LAM(SMHI) and Fine-mesh(UKMO) for the period 2 October 1990 - 2 January 1991 (77 cases).* SMHI, Norrköping, Sweden.

Kazanski, A.B. and A.S. Monin, 1960: *A Turbulent Regime above the Atmospheric Surface Layer.* Izv. Atmos. Ocean. Phys., **1**, 165-168.

Landberg, L., 1992: *Neurale netværk anvendt til forudsigelse af en geofysisk tidsserie. En sammenligning* (Neural networks utilized for the prediction of a geophysical time series, A comparison). In Danish. Risø-R-656(DA). Risø National Laboratory, Roskilde, Denmark, 76 pp.

Landberg, L. and P. Ingham, 1992: *Two wind energy related prediction methods, Part I.* In Proceedings of the European Wind Energy Association Special Topic Conference '92, Denmark (eds. P.H. Madsen and P. Lundsager). C12-1 - C12-4.

Landberg, L., S.J. Watson, J.A. Halliday, and J.U. Jørgensen, 1993: *Short-term prediction of local wind conditions.* Report to the CEC, project JOULE JOUR-0091-MB(C).

Lapedes, A. and R. Farber, 1987: *Nonlinear Signal Processing Using Neural Networks: Prediction and System Modelling.* Preprint LA-UR-87-2662.

Larsen, S.E., K. Hedegaard, and I. Troen, 1982: *The Change of Terrain Roughness Problem Extended to Mesoscale Fetches.* In *Proceedings of the First International Conference on Meteorology and Air/Sea Interaction* (Amer. Meteorol. Soc., Boston, USA and KNMI, the Netherlands), 8-13.

Lindholm, G., E. Kristenson, and K. Nilsson, 1988: *Växter som vindskydd.* (Vegetation for shelter), Stad & Land, No. 62, Alnarp (in Swedish).

Long, R.R. and L.J. Guffey, 1977: *Drag and heat transfer relations for the planetary boundary layer.* Boundary-Layer Meteorol., **11**, 363-373.

Lettau, H.H. and B. Davidson, 1957: *Exploring the atmosphere's first mile.* Vol 1 and 2, Pergamon Press, New York.

Machenhauer, B. (ed), 1988: *HIRLAM Final Report.* HIRLAM Technical Report 5, Copenhagen, December.

Machenhauer, B., U.B. Nielsen, and A. Rasmussen, 1991: *Evaluation of the quality especially of the wind-forecasts by the operational meteorological High Resolution Limited Area Model.* In: Proceedings of Advanced Modelling and Computer Codes for Calculating Local Scale and Meso-Scale Atmospheric Dispersion of Radionuclides and their Applications, 6-8 March, Paris (F), 152-163.

Mason, P. J. and J. C. King, 1985: *Measurements and Predictions of Flow and Turbulence Over an Isolated Hill of Moderate Slope.* Q. J. R. Meteorol. Soc., 111, 617-640.

Mason, P. J. and R. I. Sykes, 1979: *Flow over an isolated hill of moderate slope.* Q. J. R. Meteorol. Soc., 105, 383-395.

Miyake, M., 1965: *Transformation of the Atmospheric Boundary Layer over Inhomogeneous Surfaces.* Scientific report, University of Washington, Seattle.

Mortensen, N.G., L. Landberg, I. Troen, and E.L. Petersen, 1993: *Wind Atlas Analysis and Application Program (WA^{s}P) - User's Guide.* Risø-I-666(EN)(v.2). Risø National Laboratory, Roskilde, Denmark, 133 pp.

Nord, M., 1991: *Shelter effects of vegetation belts - results of field measurements.* Boundary-Layer Meteorol., 54, 363-385.

Obukhov, A.M., 1946: *Turbulence in thermally inhomogeneous atmosphere.* Trudy In-ta Teoret. Geofiz. AN SSSR, 1, 95-115.

Palutikof, J.P., J.H. Bass, J.A. Halliday, T.D. Davies, and C.P. Watkins, 1988: *A methodology for the prediction of windspeeds at a candidate wind turbine site.* In proceedings of: 10th British Wind Energy Association Conference, London.

Panofsky, H. A., 1973: *Tower Micrometeorology.* In *Workshop on Micrometeorology* (Ed. D. A. Haugen), Amer. Meteorol. Soc., Boston, 151-176.

Perera, M.D.A.E.S., 1981: *Shelter behind two-dimensional solid and porous fences.* J. Wind Eng. Ind. Aerodyn., 8, 93-104.

Peterka, J.A., R.N. Meroney, and K.M. Kothari, 1985: *Wind flow patterns about buildings.* J. Wind Eng. Ind. Aerodyn., 21, 21-38.

Prandtl, L., 1932: *Meteorologische Andwendungen der Strömungslehre.* Beitr. Phys. Atmos., 19, 188-202.

Press, W.H., B.P. Flannery, S.A. Teukolsky, and W.T. Vetterling, 1986: *Numerical Recipes. The Art of Scientific Computing.* Cambridge University Press, Cambridge.

Priestly, C.H.B., 1959: *Turbulent transfer in the lower atmosphere.* Univ. of Chicago Press, Chicago, Ill.

Rao, K. S., J. C. Wyngard, and D. R. Coté, 1974: *The Structure of the Two-Dimensional Internal Boundary Layer over a Sudden Change of Surface Roughness.* J. Atmos. Sci., 26, 432-440.

Rossby, C.G. and R.B. Montgomery, 1935: *The layer of frictional influence in wind and ocean currents.* Papers Phys. Oceanogr. Meteor., MIT and Woods Hole Oceanogr Inst., 3, No. 3, 101 pp.

Rumelhart, D. E., J. E. McClelland and the PDP Research Group, 1986: *Parallel Distributed Processing. Explorations in the Microstructure of Cognition.* Volume 1: Foundations. MIT Press.

Sanderhoff, P., 1993: *PARK - User's Guide, A PC-program for calculation of wind turbine park performance.* Risø-I-668(EN), Risø National Laboratory, Denmark. 8 pp.

Sass, B.H. and L.S. Sørensen, 1992: *The DMI Operational HIRLAM Forecasting System, A Short Summary.* Danish Meteorological Institute Technical Report, 92-12, Copenhagen.

Sempreviva, A.M., S.E. Larsen, N.G. Mortensen, and I. Troen, 1990: *Response of Neutral Boundary Layers to Changes of Roughness.* Boundary-Layer Meteorol.,

50, 205-225.

Söder, L, 1988: *Benefit assessment of wind power in hydro-thermal power systems.* The Royal Institute of Technology, Stockholm. ISBN 91-7170-931-2.

Taylor, P. A., J. L. Walmsley, and J. R. Salmon, 1983: *A Simple Model of Neutrally Stratified Boundary-Layer Flow Over Real Terrain Incorporating Wavenumber-Dependent Scaling.* Boundary-Layer Meteorol., **26**, 169-189.

Taylor, P. A., 1988: *Turbulent wakes in the atmospheric boundary layer.* In: *Flow and transport in the natural environment*, ed. W.L. Steffen and O.T. Denmead. Springer, 270-292.

Tennekes, H. and J. L. Lumley, 1983: *A First Course in Turbulence.* The MIT Press.

Townsend, A.A., 1956: *The structure of turbulent shear flow.* Cambridge University Press.

Townsend, A.A., 1972: *Flow in a deep turbulent boundary layer over a surface distorted by water waves.* J. Fluid Mech., **55**, 719.

Tritton, D.J., 1977: *Physical Fluid Dynamics.* Van Nostrand Reinhold (UK) Co. Ltd., United Kingdom.

Troen, I., 1990: *On Diagnostic Wind Field Models.* From College on Atmospheric Boundary Layer Physics, Trieste, Italy.

Troen, I. and E.L. Petersen, 1989: *European Wind Atlas.* Published for CEC DGXII by Risø National Laboratory, Denmark.

Van Dyke, M.D., 1964: *Perturbation Methods in Fluid Mechanics.* New York, Academic Press, 229 pp.

Walmsley, J.L., P.A. Taylor, and T. Keith, 1986: *A Simple Model of Neutrally Stratified Boundary-Layer Flow Over Complex Terrain with Surface Roughness Modulations (MS3DJH/3R).* Boundary-Layer Meteorol., **36**, 157-186.

Walmsley, J.L., I. Troen, D.P. Lalas, and P.J. Mason, 1990: *Surface-layer flow in complex terrain: comparison of models and full-scale observations.* Boundary-Layer Meteorol., **52**, 259-281.

Weibull, W., 1951: *A statistical distribution function of wide applicability.* J. Appl. Mech., **18**, 293-297.

Yordanov, D. and F. Wipperman, 1972: *The parameterization of the turbulent fluxes of momentum, heat and moisture at the ground in a baroclinic planetary boundary-layer.* Beitr. Phys. Atmos., **45**, 58-65.

Zilitinkevich, S.S and D.V. Chalikov, 1968: *The laws of resistance and of heat and moisture exchange in the interaction between the atmosphere and an underlying surface.* Izv. Atmos. Ocean Phys., **4**, 438-441 (English ed.).

Zilitinkevich, S.S., 1975: *Resistance laws and the prediction equations for the depth of the planetary boundary layer.* J. Atmos. Sci., **32**, 741-752.

Zilitinkevich, S.S., 1989: *Velocity Profiles, the Resistance Law and the Dissipation Rate of Mean Flow Kinetic Energy in a Neutrally and Stably Stratified Planetary Boundary Layer.* Boundary-Layer Meteorol., **46**, 367-387.

A Detailed listing of the stations

In this appendix the selected stations will be described in some detail. For an even more detailed description, see Troen and Petersen (1989). Station 59 (Exeter) was discontinued on May 31st, 1991, which is in the middle of the period, the nearby station RAF Dunkeswell (WMO code: 3840) was used instead from June 1st, 1991. The results shown here for Exeter are only from the period where the station was operational. For a detailed description of RAF Dunkeswell, see Section 11.2.

The letters in the column 'WA^{S}P code' refer to the country of the station, see Table 14.

Table 14. The country codes used in the WA^{S}P codes.

B	Belgium	D	Germany
DK	Denmark	E	Spain
EI	Ireland	F	France
GB	Great Britain	GR	Greece
I	Italy	NL	The Netherlands
P	Portugal		

In the following a list of the selected stations will be given. 'Number' is the number of the station used in this study, 'WMO code' the World Meteorological Organization code number for the station, 'WA^{S}P code' is the code used in the European Wind Atlas, 'Name' the name of the station, 'Height station' the height of the station above sea-level in m, 'Height anem.' is the height of the anemometer in m above ground level (WMO standard is 10 m), 'Lat.' the latitude in degrees North, and 'Long.' the longitude in degrees East. * means that the station was originally selected but later rejected because of lack of data, and † that the station only reports to the GTS-network every 6th hour.

Number	WMO code	WA^{S}P code	Name	Height station	Height anem.	Lat.	Long.
01	3075	GB01	Wick	35.0	10.0	58.5	−3.1
02	*N/A	GB22	Lowther Hill	727.0	27.0	55.4	3.8
03	*N/A	GB14	Snaefell	615.0	13.0	54.3	−4.5
04	*3952	EI05	Roches Point	40.0	12.0	51.8	−8.3
05	3953	EI06	Valentia	18.0	12.0	51.9	−10.3
06	3962	EI01	Shannon	8.0	12.0	52.7	−8.9
07	3976	EI04	Belmullet	9.0	12.0	54.2	−10.0
08	3980	EI09	Malin Head	24.0	21.0	55.4	−7.3
09	6030	DK01	Ålborg	3.0	10.0	57.1	9.9
10	6120	DK08	Beldringe	17.0	8.0	55.5	10.3
11	6180	DK02	Kastrup	5.0	10.0	55.6	12.7
12	6190	DK09	Rønne	16.0	10.0	55.1	14.8
13	6240	NL01	Schiphol	-4.0	10.0	52.3	4.8
14	*6250	NL05	Terschelling	1.0	10.0	53.4	5.2
15	6280	NL06	Eelde	5.0	10.0	53.1	6.6
16	6370	NL02	Eindhoven	20.0	10.0	51.5	5.4
17	6407	B01	Middelkerke	4.0	12.7	51.2	2.9
18	6456	B04	Florennes	280.0	6.4	50.2	4.7
19	7005	F11	Abbeville	77.0	11.0	50.1	1.8
20	*7024	F15	Cherbourg	138.0	10.5	49.7	−1.5

Number	WMO code	WASP code	Name	Height station	Height anem.	Lat.	Long.
21	7110	F01	Brest	103.0	10.5	48.5	−4.4
22	†7480	F22	Lyon	201.0	12.0	45.7	5.0
23	7510	F03	Bordeaux	51.0	11.0	44.8	−0.7
24	*7560	F24	Mont Aigoual	1565.0	11.5	44.1	3.6
25	†7635	F14	Carcassonne	130.0	11.2	43.2	2.3
26	†7647	F05	Istres	24.0	10.0	43.5	4.9
27	*8042	E05	Santiago de Compostela	364.0	6.0	42.9	−8.4
28	8160	E13	Zaragoza	247.0	23.0	41.7	−1.0
29	8202	E19	Salamanca	790.0	10.3	40.9	−5.5
30	8280	E17	Albacete	700.0	5.7	38.9	−1.9
31	8487	E14	Almeria	20.0	6.7	36.9	−2.4
32	8538	P07	Sagres	40.0	6.0	37.0	−9.0
33	*8541	P08	Sines	15.0	8.0	38.0	−8.9
34	8543	P09	Viana do Castelo	16.0	11.0	41.7	−8.8
35	8575	P14	Bragança	691.0	9.1	41.8	−6.7
36	8579	P06	Lisboa	103.0	7.0	38.8	−9.1
37	10020	D07	List/Sylt	26.0	12.1	55.0	8.4
38	10224	D01	Bremen	3.0	10.0	53.1	8.8
39	10338	D03	Hannover	51.0	10.0	52.5	9.7
40	10384	D09	Berlin	48.0	10.0	52.5	13.4
41	10866	D04	München	527.0	10.0	48.1	11.7
42	16158	I13	Pisa	2.0	6.0	43.7	10.4
43	*16312	I15	Gioia del Colle	350.0	6.0	40.7	16.9
44	16320	I16	Brindisi	15.0	6.0	40.7	18.0
45	*16332	I17	Lecca Galatina	48.0	6.0	40.2	18.2
46	16520	I21	Alghero	40.0	10.0	40.6	8.3
47	16560	I12	Cagliari	18.0	6.5	39.3	9.1
48	16641	GR03	Kerkyra	2.0	4.0	39.6	19.9
49	16716	GR12	Athina	28.0	10.0	37.9	23.7
50	16732	GR15	Naxos	9.0	10.0	37.0	25.4
51	16749	GR20	Rodos	4.0	7.0	36.4	28.1
52	3022	GB09	Benbecula	6.0	10.0	57.5	−7.4
53	3162	GB15	Eskdalemuir	249.0	10.0	55.3	−3.2
54	3302	GB02	Valley	10.0	16.0	53.3	−4.5
55	3318	GB10	Blackpool	10.0	12.0	53.8	−3.0
56	3334	GB03	Manchester	70.0	10.0	53.4	−2.3
57	3534	GB08	Birmingham	94.0	10.0	52.5	−1.7
58	3772	GB07	London	24.0	10.0	51.5	−0.5
59	3839	GB12	Exeter	31.0	12.0	50.7	−3.4
60	3862	GB11	Bournemouth	10.0	13.0	50.8	−1.8

B The WASP-matrices for each station

In this appendix the matrices containing the local corrections generated by WASP (using dump option $P_{63} = 3$ and the ':'-dump command) are listed by station number. The first column (labeled 'DIR') is the direction from which the undisturbed wind comes. The second and third column (labeled 'INPUT') are user specified corrections of speed and direction, respectively. The fourth and fifth are the change in speed and direction, respectively, due to obstacles (labeled 'OBSTACLES'). The sixth and seventh are the change in speed and direction, respectively, due to roughness (labeled 'ROUGHNESS'). The eight and ninth column are the change in speed and direction, respectively, due to orography (labeled 'OROGRAPHY'). '-9.608' means that the free-stream wind has to be multiplied by (100-9.608)/100=0.90392. Finally is the 'meso-scale' roughness (ie the roughness calculated using Formula 100) listed, the column is labeled 'Z0'.

Station 1, Wick, Great Britain

DIR		INPUT		OBSTACLES		ROUGHNESS		OROGRAPHY		Z0
0	0.000	0.000	0.000	0.000	-9.608	0.000	0.000	0.000	0.000406
30	0.000	0.000	0.000	0.000	-9.696	0.000	0.000	0.000	0.000551
60	0.000	0.000	0.000	0.000	-9.696	0.000	0.000	0.000	0.000551
90	0.000	0.000	0.000	0.000	-9.706	0.000	0.000	0.000	0.000475
120	0.000	0.000	0.000	0.000	-15.263	0.000	0.000	0.000	0.000630
150	0.000	0.000	0.000	0.000	-18.539	0.000	0.000	0.000	0.001095
180	0.000	0.000	0.000	0.000	-8.237	0.000	0.000	0.000	0.027754
210	0.000	0.000	0.000	0.000	4.287	0.000	0.000	0.000	0.046942
240	0.000	0.000	0.000	0.000	5.312	0.000	0.000	0.000	0.046225
270	0.000	0.000	0.000	0.000	5.312	0.000	0.000	0.000	0.046225
300	0.000	0.000	0.000	0.000	0.000	0.000	0.000	0.000	0.010000
330	0.000	0.000	0.000	0.000	0.000	0.000	0.000	0.000	0.010000

Station 4, Roches Point, Ireland

DIR		INPUT		OBSTACLES		ROUGHNESS		OROGRAPHY		Z0
0	0.000	0.000	-0.007	0.000	0.000	0.000	16.283	-7.215	0.050000
30	0.000	0.000	-0.017	0.000	17.473	0.000	0.963	-7.697	0.359560
60	0.000	0.000	0.000	0.000	0.000	0.000	-5.179	1.953	0.100000
90	0.000	0.000	0.000	0.000	0.000	0.000	6.968	8.525	0.100000
120	0.000	0.000	0.000	0.000	-18.454	0.000	20.185	4.911	0.000361
150	0.000	0.000	0.000	0.000	-15.874	0.000	23.741	-1.579	0.000319
180	0.000	0.000	0.000	0.000	-11.937	0.000	13.734	-6.178	0.000271
210	0.000	0.000	0.000	0.000	-8.386	0.000	0.995	-5.111	0.000262
240	0.000	0.000	0.000	0.000	16.189	0.000	-4.259	1.442	0.038162
270	0.000	0.000	0.000	0.000	24.678	0.000	3.999	8.696	0.085239
300	0.000	0.000	0.000	0.000	18.746	0.000	15.959	4.713	0.038161
330	0.000	0.000	0.000	0.000	0.000	0.000	18.987	-1.093	0.000223

Station 5, Valentia, Ireland

DIR		INPUT		OBSTACLES		ROUGHNESS		OROGRAPHY		Z0
0	0.000	0.000	0.000	0.000	-15.563	0.000	-0.550	4.403	0.001756
30	0.000	0.000	0.000	0.000	-12.841	0.000	1.845	-1.341	0.006297
60	0.000	0.000	0.000	0.000	-9.442	0.000	-5.438	-6.747	0.061375
90	0.000	0.000	-5.521	0.000	0.000	0.000	-15.565	-5.319	0.060000
120	0.000	0.000	-4.123	0.000	0.000	0.000	-18.850	1.635	0.048432
150	0.000	0.000	-2.071	0.000	-12.748	0.000	-11.310	7.104	0.058207
180	0.000	0.000	-1.553	0.000	0.000	0.000	-0.882	5.030	0.096630
210	0.000	0.000	0.000	0.000	0.000	0.000	1.777	-1.323	0.049206
240	0.000	0.000	0.000	0.000	-6.699	0.000	-4.636	-5.251	0.012275
270	0.000	0.000	0.000	0.000	-21.346	0.000	-10.471	-3.124	0.000315
300	0.000	0.000	0.000	0.000	-15.318	0.000	-16.596	1.548	0.001520
330	0.000	0.000	0.000	0.000	12.798	0.000	-10.571	5.919	0.000415

Station 6, Shannon, Ireland

DIR		INPUT		OBSTACLES		ROUGHNESS		OROGRAPHY		Z0
0	0.000	0.000	-6.759	0.000	6.887	0.000	0.000	0.000	0.000	0.171580
30	0.000	0.000	-11.154	0.000	0.863	0.000	0.000	0.000	0.000	0.140090
60	0.000	0.000	-0.676	0.000	16.887	0.000	0.000	0.000	0.000	0.283984
90	0.000	0.000	-2.874	0.000	-6.856	0.000	0.000	0.000	0.000	0.013388
120	0.000	0.000	-0.370	0.000	-7.491	0.000	0.000	0.000	0.000	0.012891
150	0.000	0.000	0.000	0.000	-6.354	0.000	0.000	0.000	0.000	0.011655
180	0.000	0.000	0.000	0.000	-6.354	0.000	0.000	0.000	0.000	0.011655
210	0.000	0.000	0.000	0.000	-6.354	0.000	0.000	0.000	0.000	0.011655
240	0.000	0.000	0.000	0.000	0.000	0.000	0.000	0.000	0.000	0.050000
270	0.000	0.000	0.000	0.000	9.585	0.000	0.000	0.000	0.000	0.170982
300	0.000	0.000	0.000	0.000	9.460	0.000	0.000	0.000	0.000	0.175282
330	0.000	0.000	0.000	0.000	9.357	0.000	0.000	0.000	0.000	0.177505

Station 7, Belmullet, Ireland

DIR		INPUT		OBSTACLES		ROUGHNESS		OROGRAPHY		Z0
0	0.000	0.000	0.000	0.000	0.000	0.000	7.983	2.342	0.000	0.030000
30	0.000	0.000	0.000	0.000	0.000	0.000	10.091	-0.316	0.000	0.030000
60	0.000	0.000	0.000	0.000	0.000	0.000	6.959	-2.690	0.000	0.030000
90	0.000	0.000	-2.585	0.000	4.379	0.000	1.502	-2.468	0.000	0.043974
120	0.000	0.000	-11.560	0.000	8.041	0.000	-0.717	0.329	0.000	0.037749
150	0.000	0.000	-11.485	0.000	0.000	0.000	2.377	2.531	0.000	0.000221
180	0.000	0.000	-2.313	0.000	11.595	0.000	6.887	2.039	0.000	0.037129
210	0.000	0.000	-0.046	0.000	10.083	0.000	8.774	-0.267	0.000	0.039111
240	0.000	0.000	0.000	0.000	7.955	0.000	6.104	-2.361	0.000	0.041220
270	0.000	0.000	0.000	0.000	2.913	0.000	1.392	-2.361	0.000	0.046942
300	0.000	0.000	-1.668	0.000	0.000	0.000	-0.800	0.351	0.000	0.030000
330	0.000	0.000	-0.018	0.000	0.000	0.000	2.570	2.805	0.000	0.030000

Station 8, Malin Head, Ireland

DIR		INPUT		OBSTACLES		ROUGHNESS		OROGRAPHY		Z0
0	0.000	0.000	0.000	0.000	0.000	0.000	9.121	2.884	0.000	0.000238
30	0.000	0.000	-0.109	0.000	0.000	0.000	12.887	0.766	0.000	0.000229
60	0.000	0.000	-4.331	0.000	0.000	0.000	11.547	-2.019	0.000	0.000229
90	0.000	0.000	-3.039	0.000	0.000	0.000	5.936	-2.883	0.000	0.000217
120	0.000	0.000	-1.113	0.000	0.000	0.000	0.778	-0.615	0.000	0.050000
150	0.000	0.000	-0.244	0.000	0.000	0.000	3.554	3.026	0.000	0.051035
180	0.000	0.000	0.000	0.000	0.000	0.000	10.344	3.376	0.000	0.050000
210	0.000	0.000	0.000	0.000	-12.181	0.000	13.824	0.571	0.000	0.000620
240	0.000	0.000	0.000	0.000	-12.643	0.000	11.685	-2.441	0.000	0.000678
270	0.000	0.000	0.000	0.000	-12.811	0.000	5.518	-3.101	0.000	0.000907
300	0.000	0.000	-0.022	0.000	-9.138	0.000	2.577	-0.819	0.000	0.000373
330	0.000	0.000	-0.082	0.000	0.00[illegible]	0.000	3.719	2.185	0.000	0.000248

Station 9, Ålborg, Denmark

DIR		INPUT		OBSTACLES		ROUGHNESS		OROGRAPHY		Z0
0	0.000	0.000	0.000	0.000	12.751	0.000	0.000	0.000	0.000	0.082777
30	0.000	0.000	0.000	0.000	12.947	0.000	0.000	0.000	0.000	0.077543
60	0.000	0.000	0.000	0.000	12.116	0.000	0.000	0.000	0.000	0.072562
90	0.000	0.000	0.000	0.000	12.116	0.000	0.000	0.000	0.000	0.072562
120	0.000	0.000	0.000	0.000	14.136	0.000	0.000	0.000	0.000	0.081132
150	0.000	0.000	0.000	0.000	22.013	0.000	0.000	0.000	0.000	0.171901
180	0.000	0.000	0.000	0.000	11.430	0.000	0.000	0.000	0.000	0.061682
210	0.000	0.000	0.000	0.000	0.000	0.000	0.000	0.000	0.000	0.019000
240	0.000	0.000	0.000	0.000	-9.470	0.000	0.000	0.000	0.000	0.000360
270	0.000	0.000	0.000	0.000	3.986	0.000	0.000	0.000	0.000	0.014390
300	0.000	0.000	0.000	0.000	11.569	0.000	0.000	0.000	0.000	0.060090
330	0.000	0.000	0.000	0.000	15.391	0.000	0.000	0.000	0.000	0.098226

Station 10, Beldringe, Denmark

DIR		INPUT		OBSTACLES		ROUGHNESS		OROGRAPHY		Z0
0	0.000	0.000	0.000	0.000	-0.302	0.000	0.000	0.000	0.000	0.032323
30	0.000	0.000	0.000	0.000	-2.398	0.000	0.000	0.000	0.000	0.020657
60	0.000	0.000	0.000	0.000	-1.464	0.000	0.000	0.000	0.000	0.023806
90	0.000	0.000	0.000	0.000	0.369	0.000	0.000	0.000	0.000	0.032268
120	0.000	0.000	0.000	0.000	8.793	0.000	0.000	0.000	0.000	0.076444
150	0.000	0.000	-2.953	0.000	19.939	0.000	0.000	0.000	0.000	0.195068
180	0.000	0.000	-28.659	0.000	19.939	0.000	0.000	0.000	0.000	0.195068
210	0.000	0.000	-30.594	0.000	8.583	0.000	0.000	0.000	0.000	0.135096
240	0.000	0.000	-14.791	0.000	11.267	0.000	0.000	0.000	0.000	0.111875
270	0.000	0.000	0.000	0.000	15.288	0.000	0.000	0.000	0.000	0.107976
300	0.000	0.000	0.000	0.000	4.024	0.000	0.000	0.000	0.000	0.043068
330	0.000	0.000	0.000	0.000	1.329	0.000	0.000	0.000	0.000	0.029725

Station 11, Kastrup, Denmark

DIR		INPUT		OBSTACLES		ROUGHNESS		OROGRAPHY		Z0
0	0.000	0.000	-3.370	0.000	-9.013	0.000	0.000	0.000	0.000	0.000311
30	0.000	0.000	0.000	0.000	-8.640	0.000	0.000	0.000	0.000	0.000290
60	0.000	0.000	0.000	0.000	-7.586	0.000	0.000	0.000	0.000	0.000270
90	0.000	0.000	0.000	0.000	-7.888	0.000	0.000	0.000	0.000	0.000275
120	0.000	0.000	0.000	0.000	-8.640	0.000	0.000	0.000	0.000	0.000290
150	0.000	0.000	0.000	0.000	-8.640	0.000	0.000	0.000	0.000	0.000290
180	0.000	0.000	0.000	0.000	-11.647	0.000	0.000	0.000	0.000	0.001371
210	0.000	0.000	0.000	0.000	-8.178	0.000	0.000	0.000	0.000	0.003012
240	0.000	0.000	0.000	0.000	11.850	0.000	0.000	0.000	0.000	0.053216
270	0.000	0.000	0.000	0.000	11.889	0.000	0.000	0.000	0.000	0.067183
300	0.000	0.000	-2.292	0.000	22.426	0.000	0.000	0.000	0.000	0.173772
330	0.000	0.000	-8.144	0.000	18.266	0.000	0.000	0.000	0.000	0.150391

Station 12, Rønne, Denmark

DIR		INPUT		OBSTACLES		ROUGHNESS		OROGRAPHY		Z0
0	0.000	0.000	0.000	0.000	1.764	0.000	0.000	0.000	0.000	0.075360
30	0.000	0.000	0.000	0.000	0.020	0.000	0.000	0.000	0.000	0.066610
60	0.000	0.000	0.000	0.000	2.560	0.000	0.000	0.000	0.000	0.076321
90	0.000	0.000	0.000	0.000	3.432	0.000	0.000	0.000	0.000	0.082719
120	0.000	0.000	0.000	0.000	-10.126	0.000	0.000	0.000	0.000	0.002186
150	0.000	0.000	0.000	0.000	-11.304	0.000	0.000	0.000	0.000	0.000292
180	0.000	0.000	0.000	0.000	-6.866	0.000	0.000	0.000	0.000	0.000242
210	0.000	0.000	0.000	0.000	-2.341	0.000	0.000	0.000	0.000	0.000229
240	0.000	0.000	0.000	0.000	-1.120	0.000	0.000	0.000	0.000	0.000225
270	0.000	0.000	0.000	0.000	-6.882	0.000	0.000	0.000	0.000	0.000261
300	0.000	0.000	0.000	0.000	-8.012	0.000	0.000	0.000	0.000	0.002042
330	0.000	0.000	0.000	0.000	-10.826	0.000	0.000	0.000	0.000	0.009163

Station 13, Schiphol, The Netherlands

DIR		INPUT		OBSTACLES		ROUGHNESS		OROGRAPHY		Z0
0	0.000	0.000	0.000	0.000	20.109	0.000	0.000	0.000	0.000	0.118548
30	0.000	0.000	0.000	0.000	22.738	0.000	0.000	0.000	0.000	0.153757
60	0.000	0.000	-0.585	0.000	24.109	0.000	0.000	0.000	0.000	0.176883
90	0.000	0.000	-4.008	0.000	27.006	0.000	0.000	0.000	0.000	0.263672
120	0.000	0.000	-5.274	0.000	18.378	0.000	0.000	0.000	0.000	0.163204
150	0.000	0.000	-1.216	0.000	18.261	0.000	0.000	0.000	0.000	0.131767
180	0.000	0.000	-0.929	0.000	12.582	0.000	0.000	0.000	0.000	0.106184
210	0.000	0.000	-1.328	0.000	15.000	0.000	0.000	0.000	0.000	0.089456
240	0.000	0.000	-1.284	0.000	14.887	0.000	0.000	0.000	0.000	0.078292
270	0.000	0.000	-4.519	0.000	-0.091	0.000	0.000	0.000	0.000	0.015912
300	0.000	0.000	-8.836	0.000	1.548	0.000	0.000	0.000	0.000	0.026615
330	0.000	0.000	-6.062	0.000	8.301	0.000	0.000	0.000	0.000	0.063903

Station 14, Terschelling, The Netherlands

DIR		INPUT		OBSTACLES		ROUGHNESS		OROGRAPHY		Z0
0	0.000	0.000	0.000	0.000	0.078	0.000	0.000	0.000	0.000	0.000357
30	0.000	0.000	0.000	0.000	-0.203	0.000	0.000	0.000	0.000	0.002027
60	0.000	0.000	0.000	0.000	20.719	0.000	0.000	0.000	0.000	0.042078
90	0.000	0.000	0.000	0.000	0.000	0.000	0.000	0.000	0.000	0.000200
120	0.000	0.000	0.000	0.000	0.000	0.000	0.000	0.000	0.000	0.000200
150	0.000	0.000	0.000	0.000	0.000	0.000	0.000	0.000	0.000	0.000200
180	0.000	0.000	0.000	0.000	0.000	0.000	0.000	0.000	0.000	0.000200
210	0.000	0.000	0.000	0.000	0.000	0.000	0.000	0.000	0.000	0.000200
240	0.000	0.000	0.000	0.000	0.000	0.000	0.000	0.000	0.000	0.000200
270	0.000	0.000	0.000	0.000	0.000	0.000	0.000	0.000	0.000	0.000200
300	0.000	0.000	0.000	0.000	0.000	0.000	0.000	0.000	0.000	0.000200
330	0.000	0.000	0.000	0.000	0.000	0.000	0.000	0.000	0.000	0.000200

Station 15, Eelde, The Netherlands

DIR		INPUT		OBSTACLES		ROUGHNESS		OROGRAPHY		Z0
0	0.000	0.000	0.000	0.000	14.819	0.000	0.000	0.000	0.000	0.135144
30	0.000	0.000	0.000	0.000	17.679	0.000	0.000	0.000	0.000	0.163332
60	0.000	0.000	-3.462	0.000	0.000	0.000	0.000	0.000	0.000	0.200000
90	0.000	0.000	-9.092	0.000	0.000	0.000	0.000	0.000	0.000	0.150000
120	0.000	0.000	-9.790	0.000	6.537	0.000	0.000	0.000	0.000	0.142175
150	0.000	0.000	-9.788	0.000	8.702	0.000	0.000	0.000	0.000	0.143208
180	0.000	0.000	-9.474	0.000	8.880	0.000	0.000	0.000	0.000	0.138676
210	0.000	0.000	-6.626	0.000	8.880	0.000	0.000	0.000	0.000	0.138676
240	0.000	0.000	-0.227	0.000	15.497	0.000	0.000	0.000	0.000	0.102866
270	0.000	0.000	0.000	0.000	15.269	0.000	0.000	0.000	0.000	0.118814
300	0.000	0.000	0.000	0.000	15.269	0.000	0.000	0.000	0.000	0.118814
330	0.000	0.000	0.000	0.000	23.058	0.000	0.000	0.000	0.000	0.204216

Station 16, Eindhoven, The Netherlands

DIR		INPUT		OBSTACLES		ROUGHNESS		OROGRAPHY		Z0
0	0.000	0.000	0.000	0.000	18.266	0.000	0.000	0.000	0.000	0.150391
30	0.000	0.000	0.000	0.000	21.926	0.000	0.000	0.000	0.000	0.246094
60	0.000	0.000	0.000	0.000	20.615	0.000	0.000	0.000	0.000	0.254145
90	0.000	0.000	0.000	0.000	26.363	0.000	0.000	0.000	0.000	0.296600
120	0.000	0.000	0.000	0.000	18.992	0.000	0.000	0.000	0.000	0.319402
150	0.000	0.000	0.000	0.000	10.583	0.000	0.000	0.000	0.000	0.165308
180	0.000	0.000	0.000	0.000	16.116	0.000	0.000	0.000	0.000	0.162049
210	0.000	0.000	0.000	0.000	21.721	0.000	0.000	0.000	0.000	0.173173
240	0.000	0.000	0.000	0.000	17.149	0.000	0.000	0.000	0.000	0.161890
270	0.000	0.000	0.000	0.000	15.306	0.000	0.000	0.000	0.000	0.115923
300	0.000	0.000	0.000	0.000	15.532	0.000	0.000	0.000	0.000	0.109118
330	0.000	0.000	0.000	0.000	15.532	0.000	0.000	0.000	0.000	0.109118

Station 17, Middelherke, Belgium

DIR		INPUT		OBSTACLES		ROUGHNESS		OROGRAPHY		Z0
0	0.000	0.000	-0.974	0.000	-11.210	0.000	0.000	0.000	0.000	0.000441
30	0.000	0.000	-5.173	0.000	-10.533	0.000	0.000	0.000	0.000	0.000065
60	0.000	0.000	0.000	0.000	17.770	0.000	0.000	0.000	0.000	0.225540
90	0.000	0.000	0.000	0.000	13.169	0.000	0.000	0.000	0.000	0.000822
120	0.000	0.000	0.000	0.000	12.482	0.000	0.000	0.000	0.000	0.078043
150	0.000	0.000	-2.647	0.000	10.612	0.000	0.000	0.000	0.000	0.000007
180	0.000	0.000	-2.647	0.000	10.537	0.000	0.000	0.000	0.000	0.000077
210	0.000	0.000	0.000	0.000	9.194	0.000	0.000	0.000	0.000	0.000673
240	0.000	0.000	0.000	0.000	10.111	0.000	0.000	0.000	0.000	0.007487
270	0.000	0.000	-0.079	0.000	-10.384	0.000	0.000	0.000	0.000	0.000004
300	0.000	0.000	-0.191	0.000	-10.818	0.000	0.000	0.000	0.000	0.000002
330	0.000	0.000	-0.083	0.000	-11.112	0.000	0.000	0.000	0.000	0.000369

Station 18, Florennes, Belgium

DIR		INPUT		OBSTACLES		ROUGHNESS		OROGRAPHY		ZO
0	0.000	0.000	0.000	0.000	23.484	0.000	0.000	0.000	0.168643
30	0.000	0.000	0.000	0.000	23.386	0.000	0.000	0.000	0.156579
60	0.000	0.000	0.000	0.000	23.335	0.000	0.000	0.000	0.131767
90	0.000	0.000	0.000	0.000	23.335	0.000	0.000	0.000	0.131767
120	0.000	0.000	0.000	0.000	28.272	0.000	0.000	0.000	0.228351
150	0.000	0.000	0.000	0.000	28.107	0.000	0.000	0.000	0.200959
180	0.000	0.000	0.000	0.000	30.215	0.000	0.000	0.000	0.234633
210	0.000	0.000	0.000	0.000	30.316	0.000	0.000	0.000	0.223865
240	0.000	0.000	0.000	0.000	30.138	0.000	0.000	0.000	0.208906
270	0.000	0.000	0.000	0.000	22.407	0.000	0.000	0.000	0.116197
300	0.000	0.000	0.000	0.000	23.740	0.000	0.000	0.000	0.155607
330	0.000	0.000	0.000	0.000	29.559	0.000	0.000	0.000	0.226590

Station 19, Abbeville, France

DIR		INPUT		OBSTACLES		ROUGHNESS		OROGRAPHY		ZO
0	0.000	0.000	0.000	0.000	11.356	0.000	4.268	-0.788	0.065877
30	0.000	0.000	0.000	0.000	20.603	0.000	3.548	-0.150	0.181258
60	0.000	0.000	0.000	0.000	23.837	0.000	4.281	0.699	0.205801
90	0.000	0.000	0.000	0.000	24.668	0.000	5.877	0.834	0.221238
120	0.000	0.000	0.000	0.000	24.400	0.000	7.142	0.221	0.255350
150	0.000	0.000	0.000	0.000	24.555	0.000	6.656	-0.674	0.264562
180	0.000	0.000	0.000	0.000	27.935	0.000	5.040	-0.909	0.305209
210	0.000	0.000	0.000	0.000	24.649	0.000	3.785	-0.213	0.243657
240	0.000	0.000	0.000	0.000	20.745	0.000	4.216	0.709	0.170620
270	0.000	0.000	0.000	0.000	18.289	0.000	5.972	0.873	0.190341
300	0.000	0.000	0.000	0.000	9.756	0.000	7.033	0.269	0.109054
330	0.000	0.000	0.000	0.000	17.132	0.000	5.152	-0.670	0.123640

Station 20, Cherbourg, France

10.5

DIR		INPUT		OBSTACLES		ROUGHNESS		OROGRAPHY		ZO
0	0.000	0.000	0.000	0.000	-19.038	0.000	3.974	-5.387	0.001550
30	0.000	0.000	0.000	0.000	16.503	0.000	-3.610	-2.858	0.262353
60	0.000	0.000	0.000	0.000	21.933	0.000	-2.689	2.946	0.234633
90	0.000	0.000	0.000	0.000	22.347	0.000	6.000	5.094	0.198177
120	0.000	0.000	0.000	0.000	0.391	0.000	15.236	2.388	0.285187
150	0.000	0.000	0.000	0.000	0.000	0.000	14.656	-3.175	0.290017
180	0.000	0.000	0.000	0.000	9.296	0.000	5.083	-5.984	0.264527
210	0.000	0.000	0.000	0.000	9.296	0.000	-4.471	-2.886	0.264527
240	0.000	0.000	0.000	0.000	6.389	0.000	-3.823	3.819	0.290416
270	0.000	0.000	0.000	0.000	11.628	0.000	6.588	5.821	0.279647
300	0.000	0.000	0.000	0.000	-26.633	0.000	13.044	1.963	0.001272
330	0.000	0.000	0.000	0.000	-17.518	0.000	10.564	-2.765	0.000863

Station 21, Brest, France

DIR		INPUT		OBSTACLES		ROUGHNESS		OROGRAPHY		ZO
0	0.000	0.000	0.000	0.000	22.356	0.000	0.000	0.000	0.217047
30	0.000	0.000	0.000	0.000	22.309	0.000	0.000	0.000	0.210602
60	0.000	0.000	0.000	0.000	15.471	0.000	0.000	0.000	0.240496
90	0.000	0.000	0.000	0.000	15.431	0.000	0.000	0.000	0.268123
120	0.000	0.000	0.000	0.000	10.476	0.000	0.000	0.000	0.329401
150	0.000	0.000	0.000	0.000	10.476	0.000	0.000	0.000	0.329401
180	0.000	0.000	0.000	0.000	8.831	0.000	0.000	0.000	0.283420
210	0.000	0.000	0.000	0.000	8.831	0.000	0.000	0.000	0.283420
240	0.000	0.000	0.000	0.000	8.831	0.000	0.000	0.000	0.283420
270	0.000	0.000	0.000	0.000	12.270	0.000	0.000	0.000	0.255046
300	0.000	0.000	0.000	0.000	21.006	0.000	0.000	0.000	0.248094
330	0.000	0.000	0.000	0.000	19.621	0.000	0.000	0.000	0.264145

Station 22, Lyon, France

DIR		INPUT	OBSTACLES		ROUGHNESS		OROGRAPHY		Z0
0	0.000	0.000	-1.147	0.000	17.772	0.000	0.000	0.000	0.130701
30	0.000	0.000	-11.509	0.000	18.089	0.000	0.000	0.000	0.161563
60	0.000	0.000	-8.160	0.000	19.383	0.000	0.000	0.000	0.212924
90	0.000	0.000	0.000	0.000	19.389	0.000	0.000	0.000	0.215521
120	0.000	0.000	0.000	0.000	20.041	0.000	0.000	0.000	0.267611
150	0.000	0.000	0.000	0.000	14.265	0.000	0.000	0.000	0.147628
180	0.000	0.000	-11.731	0.000	14.904	0.000	0.000	0.000	0.301917
210	0.000	0.000	-24.080	0.000	16.468	0.000	0.000	0.000	0.265777
240	0.000	0.000	-22.675	0.000	15.588	0.000	0.000	0.000	0.242018
270	0.000	0.000	-7.858	0.000	12.890	0.000	0.000	0.000	0.463342
300	0.000	0.000	-6.937	0.000	16.367	0.000	0.000	0.000	0.456598
330	0.000	0.000	-4.264	0.000	19.580	0.000	0.000	0.000	0.393507

Station 23, Bordeaux, France

DIR		INPUT	OBSTACLES		ROUGHNESS		OROGRAPHY		Z0
0	0.000	0.000	0.000	0.000	18.910	0.000	0.000	0.000	0.433783
30	0.000	0.000	0.000	0.000	9.060	0.000	0.000	0.000	0.381316
60	0.000	0.000	0.000	0.000	9.944	0.000	0.000	0.000	0.372633
90	0.000	0.000	-6.648	0.000	13.133	0.000	0.000	0.000	0.361874
120	0.000	0.000	-11.061	0.000	14.182	0.000	0.000	0.000	0.367403
150	0.000	0.000	-6.116	0.000	16.476	0.000	0.000	0.000	0.496762
180	0.000	0.000	-9.533	0.000	19.232	0.000	0.000	0.000	0.450558
210	0.000	0.000	0.000	0.000	21.078	0.000	0.000	0.000	0.355695
240	0.000	0.000	0.000	0.000	28.376	0.000	0.000	0.000	0.260546
270	0.000	0.000	0.000	0.000	31.146	0.000	0.000	0.000	0.370439
300	0.000	0.000	0.000	0.000	30.911	0.000	0.000	0.000	0.387491
330	0.000	0.000	0.000	0.000	22.720	0.000	0.000	0.000	0.334139

Station 24, Mont Aigoual, France

DIR		INPUT	OBSTACLES		ROUGHNESS		OROGRAPHY		Z0
0	0.000	0.000	0.000	0.000	0.923	0.000	209.368	5.002	0.097185
30	0.000	0.000	0.000	0.000	0.000	0.000	193.861	-13.344	0.097644
60	0.000	0.000	0.000	0.000	0.923	0.000	113.457	-26.237	0.097185
90	0.000	0.000	0.000	0.000	0.759	0.000	24.530	-12.679	0.098303
120	0.000	0.000	0.000	0.000	0.000	0.000	60.722	25.294	0.098637
150	0.000	0.000	0.000	0.000	0.000	0.000	160.386	21.874	0.099313
180	0.000	0.000	0.000	0.000	0.000	0.000	214.857	5.046	0.099313
210	0.000	0.000	0.000	0.000	0.000	0.000	193.861	-13.344	0.097644
240	0.000	0.000	0.000	0.000	2.362	0.000	112.512	-26.116	0.098504
270	0.000	0.000	0.000	0.000	6.655	0.000	23.186	-11.558	0.089175
300	0.000	0.000	0.000	0.000	6.655	0.000	56.443	23.899	0.089175
330	0.000	0.000	0.000	0.000	4.851	0.000	151.554	21.292	0.094297

Station 25, Carcassonne, France

DIR		INPUT	OBSTACLES		ROUGHNESS		OROGRAPHY		Z0
0	0.000	0.000	0.000	0.000	8.506	0.000	0.000	0.000	0.183084
30	0.000	0.000	0.000	0.000	11.845	0.000	0.000	0.000	0.177834
60	0.000	0.000	0.000	0.000	15.097	0.000	0.000	0.000	0.165635
90	0.000	0.000	0.000	0.000	12.686	0.000	0.000	0.000	0.387833
120	0.000	0.000	0.000	0.000	0.188	0.000	0.000	0.000	0.203936
150	0.000	0.000	0.000	0.000	0.000	0.000	0.000	0.000	0.196260
180	0.000	0.000	0.000	0.000	0.000	0.000	0.000	0.000	0.196260
210	0.000	0.000	0.000	0.000	0.000	0.000	0.000	0.000	0.196260
240	0.000	0.000	0.000	0.000	0.000	0.000	0.000	0.000	0.196260
270	0.000	0.000	0.000	0.000	0.000	0.000	0.000	0.000	0.196260
300	0.000	0.000	0.000	0.000	13.867	0.000	0.000	0.000	0.172814
330	0.000	0.000	0.000	0.000	11.845	0.000	0.000	0.000	0.177834

Station 26, Istres, France

DIR		INPUT	OBSTACLES		ROUGHNESS		OROGRAPHY		Z0
0	0.000	0.000	0.000	0.000	7.573	0.000	0.000	0.000	0.052419
30	0.000	0.000	0.000	0.000	17.217	0.000	0.000	0.000	0.118081
60	0.000	0.000	0.000	0.000	23.077	0.000	0.000	0.000	0.210502
90	0.000	0.000	0.000	0.000	24.330	0.000	0.000	0.000	0.299444
120	0.000	0.000	0.000	0.000	22.660	0.000	0.000	0.000	0.181434
150	0.000	0.000	0.000	0.000	15.391	0.000	0.000	0.000	0.098226
180	0.000	0.000	0.000	0.000	22.514	0.000	0.000	0.000	0.165271
210	0.000	0.000	0.000	0.000	0.000	0.000	0.000	0.000	0.010000
240	0.000	0.000	0.000	0.000	0.000	0.000	0.000	0.000	0.010000
270	0.000	0.000	0.000	0.000	0.000	0.000	0.000	0.000	0.010000
300	0.000	0.000	0.000	0.000	0.000	0.000	0.000	0.000	0.010000
330	0.000	0.000	0.000	0.000	0.000	0.000	0.000	0.000	0.010000

Station 27, Santiago de Compostela, Spain

DIR		INPUT	OBSTACLES		ROUGHNESS		OROGRAPHY		Z0
0	0.000	0.000	0.000	0.000	31.481	0.000	6.512	-3.248	0.234633
30	0.000	0.000	0.000	0.000	30.580	0.000	-2.020	-5.542	0.254145
60	0.000	0.000	0.000	0.000	30.580	0.000	-9.769	-2.076	0.254145
90	0.000	0.000	0.000	0.000	31.481	0.000	-7.557	3.743	0.234633
120	0.000	0.000	0.000	0.000	31.481	0.000	1.406	5.160	0.234633
150	0.000	0.000	0.000	0.000	28.927	0.000	7.430	1.719	0.161944
180	0.000	0.000	-1.274	0.000	29.331	0.000	6.158	-3.097	0.173263
210	0.000	0.000	-5.289	0.000	26.718	0.000	-2.038	-5.366	0.192459
240	0.000	0.000	-8.420	0.000	29.201	0.000	-9.842	-2.091	0.255872
270	0.000	0.000	-3.737	0.000	26.380	0.000	-8.446	4.090	0.275836
300	0.000	0.000	0.000	0.000	29.775	0.000	1.318	5.472	0.262544
330	0.000	0.000	0.000	0.000	31.118	0.000	8.203	1.686	0.246094

Station 28, Zaragoza, Spain

DIR		INPUT	OBSTACLES		ROUGHNESS		OROGRAPHY		Z0
0	0.000	0.000	-0.883	0.000	0.000	0.000	-32.381	-14.672	0.300000
30	0.000	0.000	-0.650	0.000	0.000	0.000	-35.550	11.746	0.300000
60	0.000	0.000	-0.919	0.000	0.000	0.000	-6.816	18.941	0.300000
90	0.000	0.000	-1.437	0.000	2.755	0.000	15.832	8.477	0.285345
120	0.000	0.000	-2.097	0.000	8.513	0.000	15.797	-4.934	0.176736
150	0.000	0.000	0.000	0.000	9.670	0.000	-1.700	-14.273	0.147936
180	0.000	0.000	0.000	0.000	9.670	0.000	-25.887	-11.751	0.147936
210	0.000	0.000	0.000	0.000	10.264	0.000	-30.767	7.668	0.167855
240	0.000	0.000	0.000	0.000	11.810	0.000	-8.671	15.947	0.186016
270	0.000	0.000	0.000	0.000	12.384	0.000	11.624	7.505	0.124131
300	0.000	0.000	-8.425	0.000	10.250	0.000	16.004	-4.860	0.196919
330	0.000	0.000	-1.103	0.000	0.000	0.000	-2.428	-18.059	0.300000

Station 29, Salamanca, Spain

DIR		INPUT	OBSTACLES		ROUGHNESS		OROGRAPHY		Z0
0	0.000	0.000	0.000	0.000	11.908	0.000	0.000	0.000	0.071145
30	0.000	0.000	0.000	0.000	11.746	0.000	0.000	0.000	0.065877
60	0.000	0.000	0.000	0.000	11.924	0.000	0.000	0.000	0.072662
90	0.000	0.000	0.000	0.000	11.896	0.000	0.000	0.000	0.076295
120	0.000	0.000	-2.982	0.000	7.074	0.000	0.000	0.000	0.147166
150	0.000	0.000	-2.775	0.000	12.567	0.000	0.000	0.000	0.136737
180	0.000	0.000	0.000	0.000	14.706	0.000	0.000	0.000	0.129208
210	0.000	0.000	0.000	0.000	11.924	0.000	0.000	0.000	0.072662
240	0.000	0.000	0.000	0.000	17.891	0.000	0.000	0.000	0.176319
270	0.000	0.000	0.000	0.000	22.412	0.000	0.000	0.000	0.186797
300	0.000	0.000	0.000	0.000	22.664	0.000	0.000	0.000	0.210502
330	0.000	0.000	0.000	0.000	12.186	0.000	0.000	0.000	0.096182

Station 30, Albacete, Spain

DIR		INPUT		OBSTACLES		ROUGHNESS		OROGRAPHY		Z0
0	0.000	0.000	0.000	0.000	25.513	0.000	0.000	0.000	0.000	0.204896
30	0.000	0.000	0.000	0.000	24.221	0.000	0.000	0.000	0.000	0.157649
60	0.000	0.000	0.000	0.000	15.396	0.000	0.000	0.000	0.000	0.089378
90	0.000	0.000	0.000	0.000	15.396	0.000	0.000	0.000	0.000	0.089378
120	0.000	0.000	0.000	0.000	16.259	0.000	0.000	0.000	0.000	0.072562
150	0.000	0.000	0.000	0.000	15.774	0.000	0.000	0.000	0.000	0.065877
180	0.000	0.000	0.000	0.000	15.774	0.000	0.000	0.000	0.000	0.065877
210	0.000	0.000	0.000	0.000	23.790	0.000	0.000	0.000	0.000	0.116197
240	0.000	0.000	0.000	0.000	21.344	0.000	0.000	0.000	0.000	0.092008
270	0.000	0.000	0.000	0.000	20.180	0.000	0.000	0.000	0.000	0.091813
300	0.000	0.000	-1.566	0.000	24.450	0.000	0.000	0.000	0.000	0.176095
330	0.000	0.000	-0.055	0.000	20.770	0.000	0.000	0.000	0.000	0.166637

Station 31, Almería, Spain

DIR		INPUT		OBSTACLES		ROUGHNESS		OROGRAPHY		Z0
0	0.000	0.000	-2.246	0.000	28.352	0.000	0.000	0.000	0.000	0.254145
30	0.000	0.000	-0.327	0.000	28.352	0.000	0.000	0.000	0.000	0.254145
60	0.000	0.000	0.000	0.000	23.378	0.000	0.000	0.000	0.000	0.275836
90	0.000	0.000	0.000	0.000	11.801	0.000	0.000	0.000	0.000	0.287589
120	0.000	0.000	0.000	0.000	-36.304	0.000	0.000	0.000	0.000	0.000753
150	0.000	0.000	0.000	0.000	-33.342	0.000	0.000	0.000	0.000	0.000328
180	0.000	0.000	0.000	0.000	-31.807	0.000	0.000	0.000	0.000	0.000286
210	0.000	0.000	0.000	0.000	-32.644	0.000	0.000	0.000	0.000	0.000306
240	0.000	0.000	0.000	0.000	-8.679	0.000	0.000	0.000	0.000	0.033642
270	0.000	0.000	-0.059	0.000	28.627	0.000	0.000	0.000	0.000	0.214190
300	0.000	0.000	-1.436	0.000	27.516	0.000	0.000	0.000	0.000	0.262544
330	0.000	0.000	-2.391	0.000	25.314	0.000	0.000	0.000	0.000	0.271310

Station 32, Sagres. Portugal

DIR		INPUT		OBSTACLES		ROUGHNESS		OROGRAPHY		Z0
0	0.000	0.000	0.000	0.000	20.158	0.000	23.603	1.271	0.193943
30	0.000	0.000	0.000	0.000	26.783	0.000	18.909	2.225	0.158362
60	0.000	0.000	0.000	0.000	-11.484	0.000	22.296	1.088	0.000461
90	0.000	0.000	0.000	0.000	-8.734	0.000	22.106	-0.755	0.000223
120	0.000	0.000	0.000	0.000	-8.734	0.000	18.588	-2.234	0.000223
150	0.000	0.000	0.000	0.000	-4.771	0.000	15.039	-2.082	0.000217
180	0.000	0.000	0.000	0.000	-4.771	0.000	13.442	0.771	0.000217
210	0.000	0.000	0.000	0.000	-4.771	0.000	17.745	2.777	0.000217
240	0.000	0.000	0.000	0.000	-4.771	0.000	23.384	1.941	0.000217
270	0.000	0.000	0.000	0.000	-8.734	0.000	22.106	-0.755	0.000223
300	0.000	0.000	0.000	0.000	-8.734	0.000	18.588	-2.234	0.000223
330	0.000	0.000	0.000	0.000	-16.483	0.000	22.369	-1.514	0.000591

Station 33, Sines, Portugal

DIR		INPUT		OBSTACLES		ROUGHNESS		OROGRAPHY		Z0
0	0.000	0.000	0.000	0.000	0.000	0.000	7.848	1.581	0.000204
30	0.000	0.000	0.000	0.000	-9.411	0.000	9.102	-1.898	0.000320
60	0.000	0.000	0.000	0.000	-0.550	0.000	4.456	-6.008	0.198799
90	0.000	0.000	0.000	0.000	-0.550	0.000	-5.103	-2.938	0.198312
120	0.000	0.000	0.000	0.000	-29.067	0.000	-4.253	2.419	0.000434
150	0.000	0.000	0.000	0.000	-27.687	0.000	3.342	4.540	0.000338
180	0.000	0.000	0.000	0.000	-13.686	0.000	8.650	1.987	0.000241
210	0.000	0.000	0.000	0.000	0.000	0.000	7.726	-1.726	0.000205
240	0.000	0.000	0.000	0.000	0.000	0.000	2.377	-3.483	0.000204
270	0.000	0.000	0.000	0.000	0.000	0.000	-3.074	-1.758	0.000204
300	0.000	0.000	0.000	0.000	0.000	0.000	-2.911	1.915	0.000204
330	0.000	0.000	0.000	0.000	0.000	0.000	2.687	3.472	0.000204

Station 34, Viana do Castelo, Portugal

DIR		INPUT	OBSTACLES		ROUGHNESS		OROGRAPHY		ZO
0	0.000	0.000	0.000	0.000	0.000	0.000	-18.363	5.297	0.400000
30	0.000	0.000	0.000	0.000	0.000	0.000	-6.644	7.397	0.400000
60	0.000	0.000	0.000	0.000	0.000	0.000	2.342	2.531	0.300000
90	0.000	0.000	0.000	0.000	0.000	0.000	0.962	-4.077	0.300000
120	0.000	0.000	0.000	0.000	-1.104	0.000	-12.201	-6.241	0.120848
150	0.000	0.000	0.000	0.000	6.432	0.000	-18.433	-1.726	0.127863
180	0.000	0.000	0.000	0.000	-0.242	0.000	-16.140	4.917	0.152702
210	0.000	0.000	0.000	0.000	-28.102	0.000	-5.878	5.710	0.001407
240	0.000	0.000	0.000	0.000	-33.084	0.000	1.973	2.546	0.002154
270	0.000	0.000	0.000	0.000	-32.852	0.000	1.057	-3.686	0.002417
300	0.000	0.000	0.000	0.000	-30.379	0.000	-9.869	-7.441	0.009054
330	0.000	0.000	0.000	0.000	0.000	0.000	-19.428	-3.216	0.300000

Station 35, Bragança, Portugal

DIR		INPUT	OBSTACLES		ROUGHNESS		OROGRAPHY		ZO
0	0.000	0.000	0.000	0.000	0.000	0.000	146.297	-7.087	0.300000
30	0.000	0.000	0.000	0.000	0.000	0.000	99.756	-19.604	0.300000
60	0.000	0.000	0.000	0.000	0.000	0.000	33.456	-15.934	0.300000
90	0.000	0.000	0.000	0.000	0.000	0.000	28.368	13.692	0.300000
120	0.000	0.000	0.000	0.000	0.000	0.000	92.972	20.323	0.300000
150	0.000	0.000	0.000	0.000	0.000	0.000	143.577	8.651	0.300000
180	0.000	0.000	0.000	0.000	0.000	0.000	146.297	-7.087	0.300000
210	0.000	0.000	0.000	0.000	0.000	0.000	99.756	-19.604	0.300000
240	0.000	0.000	0.000	0.000	0.000	0.000	33.456	-15.934	0.300000
270	0.000	0.000	0.000	0.000	0.000	0.000	30.341	14.038	0.400000
300	0.000	0.000	0.000	0.000	0.000	0.000	100.260	21.261	0.400000
330	0.000	0.000	0.000	0.000	0.000	0.000	143.577	8.651	0.300000

Station 36, Lisboa, Portugal

DIR		INPUT	OBSTACLES		ROUGHNESS		OROGRAPHY		ZO
0	0.000	0.000	0.000	0.000	28.602	0.000	-3.594	0.179	0.210502
30	0.000	0.000	0.000	0.000	14.167	0.000	-1.282	2.722	0.285187
60	0.000	0.000	0.000	0.000	-22.805	0.000	3.633	2.303	0.002278
90	0.000	0.000	0.000	0.000	-33.544	0.000	5.804	-0.107	0.001819
120	0.000	0.000	0.000	0.000	-31.688	0.000	3.192	-2.474	0.001813
150	0.000	0.000	0.000	0.000	-22.344	0.000	-1.810	-2.492	0.003596
180	0.000	0.000	0.000	0.000	28.602	0.000	-3.594	0.179	0.210502
210	0.000	0.000	0.000	0.000	28.675	0.000	-0.691	2.664	0.217047
240	0.000	0.000	0.000	0.000	27.735	0.000	4.426	2.333	0.205944
270	0.000	0.000	0.000	0.000	27.509	0.000	6.396	-0.129	0.254145
300	0.000	0.000	0.000	0.000	27.135	0.000	3.699	-2.522	0.258300
330	0.000	0.000	0.000	0.000	28.685	0.000	-1.200	-2.518	0.223965

Station 37, List/Sylt, Germany

DIR		INPUT	OBSTACLES		ROUGHNESS		OROGRAPHY		ZO
0	0.000	0.000	0.000	0.000	-19.405	0.000	33.031	0.834	0.001764
30	0.000	0.000	0.000	0.000	-20.292	0.000	32.689	-1.016	0.000700
60	0.000	0.000	0.000	0.000	-20.137	0.000	28.949	-1.907	0.000617
90	0.000	0.000	-1.740	0.000	-16.228	0.000	23.664	-1.024	0.000313
120	0.000	0.000	-27.426	0.000	-8.088	0.000	21.189	1.494	0.000251
150	0.000	0.000	-5.923	0.000	-8.088	0.000	26.396	2.587	0.000251
180	0.000	0.000	0.000	0.000	-11.821	0.000	31.485	1.065	0.000271
210	0.000	0.000	0.000	0.000	-16.228	0.000	31.922	-1.110	0.000313
240	0.000	0.000	0.000	0.000	-19.389	0.000	28.968	-1.904	0.001694
270	0.000	0.000	0.000	0.000	-20.446	0.000	25.404	-0.883	0.001801
300	0.000	0.000	0.000	0.000	-20.436	0.000	25.609	1.066	0.000891
330	0.000	0.000	0.000	0.000	-20.376	0.000	29.525	1.980	0.001253

Station 38, Bremen, Germany

DIR		INPUT		OBSTACLES		ROUGHNESS		OROGRAPHY		Z0
0	0.000	0.000	-10.683	0.000	26.154	0.000	0.000	0.000	0.000	0.322673
30	0.000	0.000	-6.091	0.000	23.058	0.000	0.000	0.000	0.000	0.204216
60	0.000	0.000	-0.099	0.000	23.058	0.000	0.000	0.000	0.000	0.204216
90	0.000	0.000	0.000	0.000	23.058	0.000	0.000	0.000	0.000	0.204216
120	0.000	0.000	0.000	0.000	23.058	0.000	0.000	0.000	0.000	0.204216
150	0.000	0.000	0.000	0.000	23.058	0.000	0.000	0.000	0.000	0.204216
180	0.000	0.000	0.000	0.000	11.932	0.000	0.000	0.000	0.000	0.080323
210	0.000	0.000	0.000	0.000	11.932	0.000	0.000	0.000	0.000	0.080323
240	0.000	0.000	0.000	0.000	12.075	0.000	0.000	0.000	0.000	0.077076
270	0.000	0.000	0.000	0.000	21.240	0.000	0.000	0.000	0.000	0.157373
300	0.000	0.000	-0.440	0.000	17.835	0.000	0.000	0.000	0.000	0.124744
330	0.000	0.000	-8.072	0.000	12.464	0.000	0.000	0.000	0.000	0.098611

Station 39, Hannover, Germany

DIR		INPUT		OBSTACLES		ROUGHNESS		OROGRAPHY		Z0
0	0.000	0.000	0.000	0.000	17.957	0.000	0.000	0.000	0.000	0.158855
30	0.000	0.000	0.000	0.000	10.145	0.000	0.000	0.000	0.000	0.154544
60	0.000	0.000	0.000	0.000	17.666	0.000	0.000	0.000	0.000	0.121260
90	0.000	0.000	-21.766	0.000	16.393	0.000	0.000	0.000	0.000	0.155801
120	0.000	0.000	-28.895	0.000	13.916	0.000	0.000	0.000	0.000	0.177704
150	0.000	0.000	-6.054	0.000	20.667	0.000	0.000	0.000	0.000	0.144470
180	0.000	0.000	-4.900	0.000	20.696	0.000	0.000	0.000	0.000	0.147313
210	0.000	0.000	0.000	0.000	22.208	0.000	0.000	0.000	0.000	0.182165
240	0.000	0.000	0.000	0.000	17.795	0.000	0.000	0.000	0.000	0.147767
270	0.000	0.000	0.000	0.000	17.731	0.000	0.000	0.000	0.000	0.151954
300	0.000	0.000	0.000	0.000	17.753	0.000	0.000	0.000	0.000	0.116197
330	0.000	0.000	0.000	0.000	18.145	0.000	0.000	0.000	0.000	0.154544

Station 40, Berlin, Germany

DIR		INPUT		OBSTACLES		ROUGHNESS		OROGRAPHY		Z0
0	0.000	0.000	0.000	0.000	21.925	0.000	0.000	0.000	0.000	0.246094
30	0.000	0.000	0.000	0.000	21.925	0.000	0.000	0.000	0.000	0.246094
60	0.000	0.000	0.000	0.000	19.561	0.000	0.000	0.000	0.000	0.259142
90	0.000	0.000	0.000	0.000	18.668	0.000	0.000	0.000	0.000	0.262544
120	0.000	0.000	0.000	0.000	20.615	0.000	0.000	0.000	0.000	0.254145
150	0.000	0.000	0.000	0.000	20.615	0.000	0.000	0.000	0.000	0.254145
180	0.000	0.000	0.000	0.000	22.777	0.000	0.000	0.000	0.000	0.230970
210	0.000	0.000	0.000	0.000	23.046	0.000	0.000	0.000	0.000	0.217047
240	0.000	0.000	0.000	0.000	23.058	0.000	0.000	0.000	0.000	0.204216
270	0.000	0.000	0.000	0.000	21.974	0.000	0.000	0.000	0.000	0.161944
300	0.000	0.000	0.000	0.000	21.974	0.000	0.000	0.000	0.000	0.161944
330	0.000	0.000	0.000	0.000	23.058	0.000	0.000	0.000	0.000	0.204216

Station 41, München, Germany

DIR		INPUT		OBSTACLES		ROUGHNESS		OROGRAPHY		Z0
0	0.000	0.000	-9.958	0.000	0.000	0.000	0.000	0.000	0.000	0.010165
30	0.000	0.000	-7.210	0.000	0.000	0.000	0.000	0.000	0.000	0.010165
60	0.000	0.000	-2.117	0.000	4.477	0.000	0.000	0.000	0.000	0.033206
90	0.000	0.000	0.000	0.000	0.000	0.000	0.000	0.000	0.000	0.010000
120	0.000	0.000	0.000	0.000	18.760	0.000	0.000	0.000	0.000	0.109878
150	0.000	0.000	0.000	0.000	18.760	0.000	0.000	0.000	0.000	0.109878
180	0.000	0.000	0.000	0.000	21.778	0.000	0.000	0.000	0.000	0.157518
210	0.000	0.000	0.000	0.000	22.660	0.000	0.000	0.000	0.000	0.181436
240	0.000	0.000	-6.513	0.000	20.944	0.000	0.000	0.000	0.000	0.141378
270	0.000	0.000	-27.706	0.000	22.796	0.000	0.000	0.000	0.000	0.186797
300	0.000	0.000	-25.727	0.000	22.150	0.000	0.000	0.000	0.000	0.165505
330	0.000	0.000	-29.934	0.000	0.000	0.000	0.000	0.000	0.000	0.010220

Station 42, Pisa, Italy

DIR		INPUT		OBSTACLES		ROUGHNESS		OROGRAPHY		Z0
0	0.000	0.000	0.000	0.000	32.744	0.000	0.000	0.000	0.300252
30	0.000	0.000	0.000	0.000	28.305	0.000	0.000	0.000	0.250117
60	0.000	0.000	0.000	0.000	28.305	0.000	0.000	0.000	0.250117
90	0.000	0.000	0.000	0.000	28.305	0.000	0.000	0.000	0.250117
120	0.000	0.000	0.000	0.000	29.772	0.000	0.000	0.000	0.285204
150	0.000	0.000	0.000	0.000	23.999	0.000	0.000	0.000	0.268133
180	0.000	0.000	0.000	0.000	23.999	0.000	0.000	0.000	0.268133
210	0.000	0.000	0.000	0.000	23.741	0.000	0.000	0.000	0.205301
240	0.000	0.000	0.000	0.000	28.305	0.000	0.000	0.000	0.250117
270	0.000	0.000	0.000	0.000	23.311	0.000	0.000	0.000	0.197630
300	0.000	0.000	0.000	0.000	23.311	0.000	0.000	0.000	0.197630
330	0.000	0.000	0.000	0.000	25.199	0.000	0.000	0.000	0.248352

Station 43, Gioia del Colle, Italy

DIR		INPUT		OBSTACLES		ROUGHNESS		OROGRAPHY		Z0
0	0.000	0.000	0.000	0.000	18.222	0.000	0.000	0.000	0.166965
30	0.000	0.000	0.000	0.000	18.222	0.000	0.000	0.000	0.166965
60	0.000	0.000	0.000	0.000	18.222	0.000	0.000	0.000	0.166965
90	0.000	0.000	0.000	0.000	18.222	0.000	0.000	0.000	0.166965
120	0.000	0.000	0.000	0.000	18.222	0.000	0.000	0.000	0.166965
150	0.000	0.000	0.000	0.000	18.222	0.000	0.000	0.000	0.166965
180	0.000	0.000	0.000	0.000	18.222	0.000	0.000	0.000	0.166965
210	0.000	0.000	0.000	0.000	18.222	0.000	0.000	0.000	0.166965
240	0.000	0.000	0.000	0.000	18.222	0.000	0.000	0.000	0.166965
270	0.000	0.000	0.000	0.000	18.222	0.000	0.000	0.000	0.166965
300	0.000	0.000	0.000	0.000	18.222	0.000	0.000	0.000	0.166965
330	0.000	0.000	0.000	0.000	18.222	0.000	0.000	0.000	0.166965

Station 44, Brindisi, Italy

DIR		INPUT		OBSTACLES		ROUGHNESS		OROGRAPHY		Z0
0	0.000	0.000	0.000	0.000	-17.163	0.000	0.000	0.000	0.000451
30	0.000	0.000	0.000	0.000	-10.925	0.000	0.000	0.000	0.000280
60	0.000	0.000	0.000	0.000	-10.582	0.000	0.000	0.000	0.000232
90	0.000	0.000	0.000	0.000	-20.706	0.000	0.000	0.000	0.000449
120	0.000	0.000	0.000	0.000	-20.588	0.000	0.000	0.000	0.000392
150	0.000	0.000	0.000	0.000	4.173	0.000	0.000	0.000	0.063545
180	0.000	0.000	0.000	0.000	6.776	0.000	0.000	0.000	0.097748
210	0.000	0.000	0.000	0.000	6.202	0.000	0.000	0.000	0.090307
240	0.000	0.000	0.000	0.000	0.000	0.000	0.000	0.000	0.100000
270	0.000	0.000	0.000	0.000	0.000	0.000	0.000	0.000	0.100000
300	0.000	0.000	0.000	0.000	0.000	0.000	0.000	0.000	0.050000
330	0.000	0.000	0.000	0.000	-21.216	0.000	0.000	0.000	0.000678

Station 45, Lecca Galatina, Italy

DIR		INPUT		OBSTACLES		ROUGHNESS		OROGRAPHY		Z0
0	0.000	0.000	0.000	0.000	17.336	0.000	0.000	0.000	0.182326
30	0.000	0.000	0.000	0.000	17.336	0.000	0.000	0.000	0.182326
60	0.000	0.000	0.000	0.000	17.336	0.000	0.000	0.000	0.182326
90	0.000	0.000	0.000	0.000	17.336	0.000	0.000	0.000	0.182326
120	0.000	0.000	0.000	0.000	17.336	0.000	0.000	0.000	0.182326
150	0.000	0.000	0.000	0.000	17.336	0.000	0.000	0.000	0.182326
180	0.000	0.000	0.000	0.000	17.336	0.000	0.000	0.000	0.182326
210	0.000	0.000	0.000	0.000	17.336	0.000	0.000	0.000	0.182326
240	0.000	0.000	0.000	0.000	17.336	0.000	0.000	0.000	0.182326
270	0.000	0.000	0.000	0.000	17.336	0.000	0.000	0.000	0.182326
300	0.000	0.000	0.000	0.000	17.336	0.000	0.000	0.000	0.182326
330	0.000	0.000	0.000	0.000	17.336	0.000	0.000	0.000	0.182326

Station 46, Alghero, Italy

DIR		INPUT	OBSTACLES		ROUGHNESS		OROGRAPHY		Z0
0	0.000	0.000	0.000	0.000	11.637	0.000	0.000	0.000	0.071691
30	0.000	0.000	0.000	0.000	11.637	0.000	0.000	0.000	0.071691
60	0.000	0.000	0.000	0.000	11.637	0.000	0.000	0.000	0.071691
90	0.000	0.000	0.000	0.000	11.637	0.000	0.000	0.000	0.071691
120	0.000	0.000	0.000	0.000	11.637	0.000	0.000	0.000	0.071691
150	0.000	0.000	0.000	0.000	11.637	0.000	0.000	0.000	0.071691
180	0.000	0.000	0.000	0.000	-10.833	0.000	0.000	0.000	0.000718
210	0.000	0.000	0.000	0.000	-16.091	0.000	0.000	0.000	0.002912
240	0.000	0.000	0.000	0.000	-16.091	0.000	0.000	0.000	0.002912
270	0.000	0.000	0.000	0.000	-6.853	0.000	0.000	0.000	0.004037
300	0.000	0.000	0.000	0.000	-6.853	0.000	0.000	0.000	0.004037
330	0.000	0.000	0.000	0.000	-5.505	0.000	0.000	0.000	0.007287

Station 47, Cagliari, Italy

DIR		INPUT	OBSTACLES		ROUGHNESS		OROGRAPHY		Z0
0	0.000	0.000	0.000	0.000	13.711	0.000	0.000	0.000	0.175282
30	0.000	0.000	0.000	0.000	13.711	0.000	0.000	0.000	0.175282
60	0.000	0.000	0.000	0.000	13.711	0.000	0.000	0.000	0.175282
90	0.000	0.000	0.000	0.000	23.829	0.000	0.000	0.000	0.292917
120	0.000	0.000	0.000	0.000	11.882	0.000	0.000	0.000	0.094338
150	0.000	0.000	0.000	0.000	-20.019	0.000	0.000	0.000	0.000548
180	0.000	0.000	0.000	0.000	-18.196	0.000	0.000	0.000	0.000773
210	0.000	0.000	0.000	0.000	-12.877	0.000	0.000	0.000	0.002926
240	0.000	0.000	0.000	0.000	-4.920	0.000	0.000	0.000	0.012249
270	0.000	0.000	0.000	0.000	1.936	0.000	0.000	0.000	0.034688
300	0.000	0.000	0.000	0.000	8.660	0.000	0.000	0.000	0.056804
330	0.000	0.000	0.000	0.000	13.711	0.000	0 000	0.000	0.175282

Station 48, Kerkyra, Greece

DIR		INPUT	OBSTACLES		ROUGHNESS		OROGRAPHY		Z0
0	0.000	0.000	0.000	0.000	-23.353	0.000	-0.914	0.740	0.000781
30	0.000	0.000	0.000	0.000	-25.235	0.000	-0.623	-0.448	0.000814
60	0.000	0.000	0.000	0.000	-26.176	0.000	-2.545	-1.174	0.000464
90	0.000	0.000	0.000	0.000	-26.136	0.000	-4.256	-0.498	0.000437
120	0.000	0.000	0.000	0.000	-17.752	0.000	-3.831	0.592	0.000425
150	0.000	0.000	0.000	0.000	-7.561	0.000	-2.161	0.814	0.000309
180	0.000	0.000	0.000	0.000	27.065	0.000	-1.285	0.475	0.061765
210	0.000	0.000	0.000	0.000	17.676	0.000	-1.253	-0.640	0.046141
240	0.000	0.000	0.000	0.000	27.311	0.000	-2.922	-1.113	0.082452
270	0.000	0.000	0.000	0.000	14.607	0.000	-4.567	-0.682	0.071913
300	0.000	0.000	0.000	0.000	11.961	0.000	-4.715	0.591	0.096879
330	0.000	0.000	0.000	0.000	-21.230	0.000	-2.971	1.214	0.001412

Station 49, Athens, Greece

DIR		INPUT	OBSTACLES		ROUGHNESS		OROGRAPHY		Z0
0	0.000	0.000	0.000	0.000	23.046	0.000	1.542	-3.396	0.217047
30	0.000	0.000	0.000	0.000	23.058	0.000	-6.633	-5.213	0.206216
60	0.000	0.000	0.000	0.000	6.534	0.000	-13.126	-1.643	0.040006
90	0.000	0.000	0.000	0.000	8.876	0.000	-11.075	3.853	0.073212
120	0.000	0.000	0.000	0.000	7.763	0.000	-2.312	4.713	0.044822
150	0.000	0.000	0.000	0.000	11.500	0.000	3.309	1.306	0.004673
180	0.000	0.000	0.000	0.000	-13.619	0.000	1.588	-2.998	0.000408
210	0.000	0.000	0.000	0.000	-13.732	0.000	-5.382	-4.173	0.000259
240	0.000	0.000	0.000	0.000	-11.043	0.000	-10.579	-1.177	0.000244
270	0.000	0.000	0.000	0.000	-15.711	0.000	-8.000	3.201	0.000274
300	0.000	0.000	0.000	0.000	-17.946	0.000	-1.583	4.000	0.000290
330	0.000	0.000	0.000	0.000	9.855	0.000	3.823	1.418	0.151431

Station 50, Naxos, Greece

DIR		INPUT		OBSTACLES		ROUGHNESS		OROGRAPHY		Z0
0	0.000	0.000	0.000	0.000	0.000	0.000	1.739	1.222	0.000200
30	0.000	0.000	0.000	0.000	-4.224	0.000	0.688	-2.388	0.000248
60	0.000	0.000	0.000	0.000	-4.228	0.000	-7.879	-5.417	0.207868
90	0.000	0.000	0.000	0.000	-4.228	0.000	-14.756	-1.727	0.207868
120	0.000	0.000	0.000	0.000	1.653	0.000	-12.169	3.856	0.197274
150	0.000	0.000	0.000	0.000	22.131	0.000	-3.762	4.693	0.151812
180	0.000	0.000	0.000	0.000	26.649	0.000	1.852	1.275	0.100521
210	0.000	0.000	0.000	0.000	-0.935	0.000	0.486	-2.541	0.000515
240	0.000	0.000	0.000	0.000	-0.041	0.000	-5.561	-3.936	0.000350
270	0.000	0.000	0.000	0.000	0.000	0.000	-10.177	-1.384	0.000200
300	0.000	0.000	0.000	0.000	0.000	0.000	-9.012	2.568	0.000200
330	0.000	0.000	0.000	0.000	0.000	0.000	-2.942	3.690	0.000200

Station 51, Rodos, Greece

DIR		INPUT		OBSTACLES		ROUGHNESS		OROGRAPHY		Z0
0	0.000	0.000	0.000	0.000	-4.543	0.000	-8.835	0.355	0.000225
30	0.000	0.000	0.000	0.000	-7.927	0.000	-5.252	3.324	0.000242
60	0.000	0.000	0.000	0.000	-3.316	0.000	0.790	3.063	0.004364
90	0.000	0.000	0.000	0.000	24.484	0.000	3.711	-0.283	0.252443
120	0.000	0.000	0.000	0.000	19.102	0.000	-0.237	-3.894	0.280461
150	0.000	0.000	0.000	0.000	14.167	0.000	-7.676	-3.884	0.285187
180	0.000	0.000	0.000	0.000	13.378	0.000	-10.716	0.340	0.188481
210	0.000	0.000	0.000	0.000	22.186	0.000	-6.632	4.122	0.275836
240	0.000	0.000	0.000	0.000	25.657	0.000	0.773	3.407	0.266880
270	0.000	0.000	0.000	0.000	-8.853	0.000	3.228	-0.378	0.001194
300	0.000	0.000	0.000	0.000	-7.927	0.000	-0.179	-3.155	0.000242
330	0.000	0.000	0.000	0.000	-4.543	0.000	-6.209	-2.991	0.000225

Station 52, Benbecula, Great Britain

DIR		INPUT		OBSTACLES		ROUGHNESS		OROGRAPHY		Z0
0	0.000	0.000	0.000	0.000	-9.364	0.000	0.000	0.000	0.001279
30	0.000	0.000	0.000	0.000	2.096	0.000	0.000	0.000	0.030256
60	0.000	0.000	0.000	0.000	2.095	0.000	0.000	0.000	0.022575
90	0.000	0.000	0.000	0.000	-9.494	0.000	0.000	0.000	0.003529
120	0.000	0.000	0.000	0.000	-13.294	0.000	0.000	0.000	0.006590
150	0.000	0.000	0.000	0.000	-0.430	0.000	0.000	0.000	0.050240
180	0.000	0.000	0.000	0.000	-1.423	0.000	0.000	0.000	0.050108
210	0.000	0.000	0.000	0.000	-18.357	0.000	0.000	0.000	0.001237
240	0.000	0.000	0.000	0.000	-23.127	0.000	0.000	0.000	0.000713
270	0.000	0.000	0.000	0.000	-18.359	0.000	0.000	0.000	0.000693
300	0.000	0.000	0.000	0.000	-11.797	0.000	0.000	0.000	0.000287
330	0.000	0.000	0.000	0.000	-11.797	0.000	0.000	0.000	0.000287

Station 53, Eskdalemuir, Great Britain

DIR		INPUT		OBSTACLES		ROUGHNESS		OROGRAPHY		Z0
0	0.000	0.000	0.000	0.000	17.787	0.000	-0.418	-2.983	0.254018
30	0.000	0.000	0.000	0.000	17.219	0.000	-5.844	-2.856	0.262363
60	0.000	0.000	0.000	0.000	18.111	0.000	-9.000	-0.631	0.217686
90	0.000	0.000	0.000	0.000	18.161	0.000	-6.087	3.000	0.240000
120	0.000	0.000	0.000	0.000	18.161	0.000	-0.330	2.824	0.240000
150	0.000	0.000	0.000	0.000	17.787	0.000	2.646	-0.198	0.254018
180	0.000	0.000	0.000	0.000	17.219	0.000	-0.123	-2.977	0.262363
210	0.000	0.000	0.000	0.000	17.787	0.000	-6.206	-2.940	0.254018
240	0.000	0.000	0.000	0.000	17.787	0.000	-8.910	0.224	0.254018
270	0.000	0.000	0.000	0.000	16.206	0.000	-6.200	3.120	0.268133
300	0.000	0.000	0.000	0.000	16.206	0.000	1.283	2.563	0.268133
330	0.000	0.000	0.000	0.000	16.206	0.000	3.406	-0.377	0.268133

Station 54, Valley, Great Britain

DIR		INPUT		OBSTACLES		ROUGHNESS		OROGRAPHY		Z0
0	14.000	0.000	-21.837	0.000	0.000	0.000	0.000	0.000	0.100000	
30	14.000	0.000	-15.514	0.000	-3.365	0.000	0.000	0.000	0.088915	
60	14.000	0.000	0.000	0.000	-3.365	0.000	0.000	0.000	0.088915	
90	14.000	0.000	0.000	0.000	0.000	0.000	0.000	0.000	0.096501	
120	14.000	0.000	0.000	0.000	8.320	0.000	0.000	0.000	0.080323	
150	14.000	0.000	0.000	0.000	9.311	0.000	0.000	0.000	0.065877	
180	14.000	0.000	0.000	0.000	-7.063	0.000	0.000	0.000	0.000345	
210	14.000	0.000	0.000	0.000	-5.207	0.000	0.000	0.000	0.000290	
240	14.000	0.000	0.000	0.000	-5.207	0.000	0.000	0.000	0.000290	
270	14.000	0.000	0.000	0.000	-9.173	0.000	0.000	0.000	0.001520	
300	14.000	0.000	-3.233	0.000	1.033	0.000	0.000	0.000	0.015560	
330	14.000	0.000	-7.527	0.000	-2.174	0.000	0.000	0.000	0.020951	

Station 55, Blackpool, Great Britain

DIR		INPUT		OBSTACLES		ROUGHNESS		OROGRAPHY		Z0
0	0.000	0.000	0.000	0.000	16.041	0.000	0.000	0.000	0.356911	
30	0.000	0.000	0.000	0.000	15.123	0.000	0.000	0.000	0.343992	
60	0.000	0.000	0.000	0.000	15.123	0.000	0.000	0.000	0.343992	
90	0.000	0.000	0.000	0.000	19.744	0.000	0.000	0.000	0.285165	
120	0.000	0.000	0.000	0.000	19.744	0.000	0.000	0.000	0.285165	
150	0.000	0.000	0.000	0.000	19.801	0.000	0.000	0.000	0.298437	
180	0.000	0.000	0.000	0.000	-5.246	0.000	0.000	0.000	0.016491	
210	0.000	0.000	0.000	0.000	-12.829	0.000	0.000	0.000	0.000385	
240	0.000	0.000	0.000	0.000	-12.405	0.000	0.000	0.000	0.000345	
270	0.000	0.000	0.000	0.000	-14.418	0.000	0.000	0.000	0.000415	
300	0.000	0.000	0.000	0.000	-19.758	0.000	0.000	0.000	0.000521	
330	0.000	0.000	0.000	0.000	-20.960	0.000	0.000	0.000	0.000971	

Station 56, Manchester, Great Britain

DIR		INPUT		OBSTACLES		ROUGHNESS		OROGRAPHY		Z0
0	0.000	0.000	0.000	0.000	25.976	0.000	0.000	0.000	0.263432	
30	0.000	0.000	0.000	0.000	24.958	0.000	0.000	0.000	0.334139	
60	0.000	0.000	0.000	0.000	24.808	0.000	0.000	0.000	0.202640	
90	0.000	0.000	0.000	0.000	21.397	0.000	0.000	0.000	0.174204	
120	0.000	0.000	0.000	0.000	17.957	0.000	0.000	0.000	0.158855	
150	0.000	0.000	0.000	0.000	16.940	0.000	0.000	0.000	0.167982	
180	0.000	0.000	0.000	0.000	11.508	0.000	0.000	0.000	0.084673	
210	0.000	0.000	0.000	0.000	12.116	0.000	0.000	0.000	0.072562	
240	0.000	0.000	0.000	0.000	13.888	0.000	0.000	0.000	0.177836	
270	0.000	0.000	0.000	0.000	18.668	0.000	0.000	0.000	0.262644	
300	0.000	0.000	0.000	0.000	-2.052	0.000	0.000	0.000	0.196777	
330	0.000	0.000	0.000	0.000	21.831	0.000	0.000	0.000	0.226361	

Station 57, Birmingham, Great Britain

DIR		INPUT		OBSTACLES		ROUGHNESS		OROGRAPHY		Z0
0	0.000	0.000	0.000	0.000	26.154	0.000	0.000	0.000	0.322673	
30	0.000	0.000	0.000	0.000	26.771	0.000	0.000	0.000	0.306408	
60	0.000	0.000	0.000	0.000	24.958	0.000	0.000	0.000	0.334139	
90	0.000	0.000	0.000	0.000	27.080	0.000	0.000	0.000	0.281581	
120	0.000	0.000	0.000	0.000	23.020	0.000	0.000	0.000	0.269691	
150	0.000	0.000	0.000	0.000	24.923	0.000	0.000	0.000	0.236462	
180	0.000	0.000	0.000	0.000	15.738	0.000	0.000	0.000	0.172814	
210	0.000	0.000	0.000	0.000	24.958	0.000	0.000	0.000	0.334139	
240	0.000	0.000	0.000	0.000	22.178	0.000	0.000	0.000	0.312614	
270	0.000	0.000	0.000	0.000	26.571	0.000	0.000	0.000	0.239280	
300	0.000	0.000	0.000	0.000	26.571	0.000	0.000	0.000	0.239280	
330	0.000	0.000	0.000	0.000	26.771	0.000	0.000	0.000	0.306408	

Station 58, London, Great Britain

DIR		INPUT	OBSTACLES		ROUGHNESS		OROGRAPHY		Z0
0	0.000	0.000	0.000	0.000	9.539	0.000	0.000	0.000	0.069378
30	0.000	0.000	0.000	0.000	15.738	0.000	0.000	0.000	0.172814
60	0.000	0.000	0.000	0.000	25.268	0.000	0.000	0.000	0.212734
90	0.000	0.000	0.000	0.000	11.932	0.000	0.000	0.000	0.080323
120	0.000	0.000	0.000	0.000	13.358	0.000	0.000	0.000	0.375219
150	0.000	0.000	0.000	0.000	20.348	0.000	0.000	0.000	0.352530
180	0.000	0.000	0.000	0.000	19.889	0.000	0.000	0.000	0.246307
210	0.000	0.000	0.000	0.000	16.298	0.000	0.000	0.000	0.185091
240	0.000	0.000	0.000	0.000	20.926	0.000	0.000	0.000	0.186312
270	0.000	0.000	0.000	0.000	12.723	0.000	0.000	0.000	0.188055
300	0.000	0.000	0.000	0.000	24.090	0.000	0.000	0.000	0.278070
330	0.000	0.000	0.000	0.000	24.090	0.000	0.000	0.000	0.278070

Station 59, Exeter, Great Britain. Covering only the period from December 1990 to May 1991.

DIR		INPUT	OBSTACLES		ROUGHNESS		OROGRAPHY		Z0
0	0.000	0.000	0.000	0.000	9.741	0.000	0.000	0.000	0.084673
30	0.000	0.000	0.000	0.000	9.741	0.000	0.000	0.000	0.084673
60	0.000	0.000	0.000	0.000	9.741	0.000	0.000	0.000	0.084673
90	0.000	0.000	0.000	0.000	-6.103	0.000	0.000	0.000	0.104402
120	0.000	0.000	0.000	0.000	-6.103	0.000	0.000	0.000	0.104402
150	0.000	0.000	0.000	0.000	-4.415	0.000	0.000	0.000	0.103300
180	0.000	0.000	0.000	0.000	-4.415	0.000	0.000	0.000	0.103300
210	0.000	0.000	0.000	0.000	-4.415	0.000	0.000	0.000	0.103300
240	0.000	0.000	0.000	0.000	8.026	0.000	0.000	0.000	0.208845
270	0.000	0.000	0.000	0.000	15.767	0.000	0.000	0.000	0.186661
300	0.000	0.000	0.000	0.000	10.016	0.000	0.000	0.000	0.083775
330	0.000	0.000	0.000	0.000	10.702	0.000	0.000	0.000	0.080323

Station 60, Bournemouth, Great Britain

DIR		INPUT	OBSTACLES		ROUGHNESS		OROGRAPHY		Z0
0	0.000	0.000	0.000	0.000	18.696	0.000	0.000	0.000	0.305751
30	0.000	0.000	0.000	0.000	21.647	0.000	0.000	0.000	0.311710
60	0.000	0.000	0.000	0.000	11.801	0.000	0.000	0.000	0.359560
90	0.000	0.000	0.000	0.000	16.029	0.000	0.000	0.000	0.348397
120	0.000	0.000	0.000	0.000	15.220	0.000	0.000	0.000	0.350274
150	0.000	0.000	0.000	0.000	-16.831	0.000	0.000	0.000	0.005758
180	0.000	0.000	0.000	0.000	-9.312	0.000	0.000	0.000	0.004220
210	0.000	0.000	0.000	0.000	21.068	0.000	0.000	0.000	0.254796
240	0.000	0.000	-0.618	0.000	19.484	0.000	0.000	0.000	0.191261
270	0.000	0.000	-7.320	0.000	16.666	0.000	0.000	0.000	0.131649
300	0.000	0.000	-12.638	0.000	22.886	0.000	0.000	0.000	0.281581
330	0.000	0.000	0.000	0.000	15.421	0.000	0.000	0.000	0.137337

C Results station by station

The results of the different model runs will be displayed in the following.

C.1 The neutral HIRLAM/WA^{S}P model

Results marked 'N/A' means that the values are not available because of either missing data (stations reporting only every 6 hours) or division by zero.

Table 15. Results HIRLAM/WA^{S}P model. The column marked 'H/W' is the column with the results of the runs for the entire period (December 1990 to November 1991) for the selected stations. 'pers' is the results from the persistence model, and 'rel' is the ratio of the neutral HIRLAM/WA^{S}P model to persistence (numbers smaller than 1.0 indicates that the HIRLAM/WA^{S}P model preformed better than persistence). Results for the 3, 18, and 36 hour forecasts are displayed. e is the mean error, | e | the mean absolute error, and RMSE the rms error (all in m/s).

		+3			+18			+36		
		H/W	pers	rel	H/W	pers	rel	H/W	pers	rel
1	e	-0.52	0.00	-516.00	-0.07	-0.01	5.67	-0.12	-0.02	6.39
	$\|e\|$	1.57	1.54	1.02	1.67	2.77	0.60	1.93	3.22	0.60
	RMSE	2.00	2.07	0.97	2.25	3.61	0.62	2.54	4.17	0.61
5	e	-0.78	0.00	-196.25	-0.46	-0.02	25.72	-0.57	-0.02	25.77
	$\|e\|$	2.01	1.61	1.25	1.97	3.16	0.62	2.25	3.50	0.64
	RMSE	2.61	2.21	1.18	2.64	4.07	0.65	2.90	4.42	0.65
6	e	-0.47	-0.01	93.60	-0.07	-0.00	18.25	-0.21	-0.04	5.78
	$\|e\|$	1.69	1.50	1.12	1.73	2.72	0.64	1.86	3.01	0.62
	RMSE	2.18	1.97	1.10	2.26	3.55	0.64	2.51	3.84	0.65
7	e	-0.76	-0.02	44.41	-0.23	0.00	-57.75	-0.57	-0.01	47.25
	$\|e\|$	1.87	1.61	1.16	1.99	3.27	0.61	2.18	3.66	0.59
	RMSE	2.58	2.21	1.17	2.62	4.26	0.62	2.93	4.65	0.63
8	e	-0.97	-0.00	973.00	-0.72	-0.01	89.88	-0.63	-0.03	19.12
	$\|e\|$	2.04	1.95	1.04	2.29	3.69	0.62	2.49	4.12	0.60
	RMSE	2.63	2.62	1.01	3.08	4.73	0.65	3.21	5.30	0.61
9	e	-0.32	-0.01	24.69	0.12	-0.01	-8.43	-0.17	-0.02	8.74
	$\|e\|$	1.54	1.29	1.20	1.53	2.40	0.64	1.91	2.88	0.66
	RMSE	2.01	1.73	1.16	2.12	3.09	0.69	2.49	3.64	0.68
10	e	-1.06	-0.00	265.50	-0.72	0.03	-25.71	-1.03	0.01	-171.00
	$\|e\|$	1.75	1.19	1.47	1.56	2.15	0.73	1.94	2.60	0.75
	RMSE	2.47	1.56	1.58	2.11	2.76	0.76	2.50	3.28	0.76
11	e	-0.61	-0.01	121.20	-0.46	-0.00	457.00	-0.50	0.00	-165.33
	$\|e\|$	1.53	1.22	1.26	1.51	2.19	0.69	1.85	2.45	0.76
	RMSE	2.07	1.60	1.29	2.07	2.80	0.74	2.48	3.11	0.80
12	e	-0.41	-0.00	204.00	-0.37	0.02	-17.71	-0.45	0.01	-56.63
	$\|e\|$	1.70	1.16	1.47	1.72	2.31	0.74	1.92	2.73	0.70
	RMSE	2.41	1.55	1.56	2.35	2.98	0.79	2.51	3.48	0.72

Table 16. Results HIRLAM/WAP model.

		+3			+18			+36		
		H/W	pers	rel	H/W	pers	rel	H/W	pers	rel
13	e	-0.37	0.00	-122.00	-0.11	-0.01	21.40	-0.33	0.02	-21.80
	$\|e\|$	1.57	1.31	1.20	1.53	2.49	0.61	1.89	3.04	0.62
	RMSE	2.20	1.73	1.27	2.04	3.25	0.63	2.48	3.88	0.64
15	e	-0.11	0.00	N/A	0.21	0.00	207.00	-0.05	0.01	-5.30
	$\|e\|$	1.42	1.11	1.28	1.38	2.07	0.66	1.63	2.52	0.65
	RMSE	1.96	1.55	1.26	1.83	2.72	0.67	2.16	3.24	0.67
16	e	0.27	0.00	67.50	0.68	0.00	N/A	0.23	-0.00	-230.00
	$\|e\|$	1.27	1.11	1.15	1.34	1.95	0.69	1.59	2.35	0.68
	RMSE	1.80	1.51	1.19	1.78	2.53	0.70	2.08	2.98	0.70
17	e	-0.84	0.00	-280.33	-0.36	-0.02	19.11	-0.63	0.01	-105.50
	$\|e\|$	1.77	1.38	1.28	1.75	2.74	0.64	1.89	3.13	0.60
	RMSE	2.37	2.06	1.15	2.43	3.62	0.67	2.49	4.07	0.61
18	e	-1.02	0.01	-102.00	-0.55	-0.01	68.75	-0.86	-0.01	61.71
	$\|e\|$	1.62	1.08	1.50	1.37	1.97	0.69	1.70	2.35	0.72
	RMSE	2.23	1.45	1.53	1.84	2.58	0.71	2.22	2.96	0.75
19	e	-0.82	0.00	N/A	-0.27	-0.03	8.58	-0.70	-0.02	46.80
	$\|e\|$	1.62	1.39	1.17	1.53	2.38	0.64	1.86	2.80	0.66
	RMSE	2.06	1.88	1.10	2.03	3.09	0.66	2.40	3.51	0.68
21	e	-0.65	0.00	-322.50	-0.20	-0.01	39.40	-0.55	-0.04	15.[illegible]
	$\|e\|$	1.56	1.20	1.30	1.44	2.23	0.65	1.74	2.56	0.68
	RMSE	2.14	1.64	1.30	1.88	2.90	0.65	2.24	3.25	0.69
22	e	0.88	N/A	N/A	-1.91	0.03	-70.59	-2.01	0.04	-45.64
	$\|e\|$	0.88	N/A	N/A	2.65	2.37	1.11	2.69	2.90	0.93
	RMSE	1.33	N/A	N/A	3.44	3.17	1.09	3.62	3.75	0.97
23	e	-0.73	0.01	-146.80	-0.20	0.00	-204.00	-0.31	0.01	-34.89
	$\|e\|$	1.64	1.23	1.33	1.44	1.89	0.76	1.70	2.22	0.77
	RMSE	2.20	1.67	1.32	1.96	2.46	0.80	2.26	2.81	0.80
25	e	1.39	N/A	N/A	-2.86	0.01	-238.25	-3.32	-0.00	1107.67
	$\|e\|$	1.39	N/A	N/A	3.25	2.95	1.10	3.74	3.53	1.06
	σ_e	1.97	N/A	N/A	4.03	3.72	1.08	4.63	4.37	1.06
26	e	3.28	N/A	N/A	-1.11	0.04	-25.74	-1.73	0.02	-78.77
	$\|e\|$	3.28	N/A	N/A	2.15	2.78	0.77	2.63	3.33	0.79
	RMSE	4.64	N/A	N/A	2.86	3.75	0.76	3.64	4.40	0.83
28	e	-1.93	0.01	-193.10	-1.22	0.04	-30.60	-1.92	0.05	-37.63
	$\|e\|$	3.19	1.72	1.85	3.03	2.84	1.07	3.14	3.38	0.93
	RMSE	4.16	2.33	1.79	3.91	3.67	1.07	4.11	4.31	0.95
29	e	1.88	0.01	313.50	2.57	-0.01	-428.50	2.16	0.04	50.28
	$\|e\|$	3.41	1.37	2.49	3.49	2.22	1.57	3.30	2.68	1.23
	RMSE	4.26	1.90	2.26	4.30	2.93	1.47	4.16	3.46	1.20
30	e	-1.26	-0.00	1256.00	-0.39	0.01	-35.45	-1.01	0.02	-63.31
	$\|e\|$	3.06	1.67	1.84	2.76	2.60	1.06	2.85	3.05	0.94
	RMSE	3.96	2.41	1.64	3.51	3.55	0.99	3.74	4.05	0.92
31	e	-2.32	-0.02	154.60	-1.58	0.02	-88.06	-1.90	0.01	-380.40
	$\|e\|$	3.18	1.83	1.73	2.75	2.75	1.00	3.01	3.21	0.94
	RMSE	4.23	2.58	1.64	3.76	3.71	1.02	3.99	4.22	0.95

Table 17. Results HIRLAM/WAsP model.

		+3			+18			+36		
		H/W	pers	rel	H/W	pers	rel	H/W	pers	rel
32	e	1.17	-0.04	-32.56	2.29	-0.01	-190.67	2.22	0.05	47.23
	|e|	2.44	1.38	1.76	2.90	2.17	1.34	2.84	2.43	1.17
	RMSE	3.07	2.14	1.44	3.80	2.97	1.28	3.74	3.25	1.15
34	e	-1.68	-0.01	167.80	-0.48	0.00	-159.00	-0.76	-0.02	42.44
	|e|	2.09	1.33	1.56	1.47	1.99	0.74	1.51	2.01	0.75
	RMSE	2.59	1.81	1.43	1.97	2.55	0.77	2.03	2.65	0.77
35	e	1.47	0.05	31.87	2.54	-0.04	-65.23	2.22	0.02	123.06
	|e|	3.20	1.29	2.47	3.78	1.94	1.95	3.22	2.36	1.36
	RMSE	4.04	1.81	2.23	4.85	2.61	1.85	4.21	3.08	1.36
36	e	-0.50	0.01	-35.86	-0.19	0.03	-7.11	0.15	0.04	3.69
	|e|	1.83	1.53	1.19	1.84	2.47	0.74	1.75	2.97	0.59
	RMSE	2.35	2.06	1.14	2.26	3.15	0.72	2.23	3.67	0.61
37	e	-0.88	-0.01	73.42	-0.74	-0.01	92.00	-0.75	-0.02	39.63
	|e|	1.95	1.34	1.45	2.12	2.79	0.76	2.35	3.39	0.69
	RMSE	2.69	1.78	1.52	2.99	3.61	0.83	3.17	4.29	0.74
38	e	0.11	0.01	14.13	0.38	-0.00	-126.00	0.05	-0.01	-6.86
	|e|	1.43	1.13	1.27	1.42	1.96	0.73	1.53	2.35	0.65
	RMSE	2.06	1.49	1.38	1.87	2.54	0.74	1.97	2.99	0.66
39	e	-0.09	-0.01	12.86	0.25	-0.01	-41.33	-0.06	-0.00	18.33
	|e|	1.29	1.08	1.19	1.19	1.85	0.64	1.50	2.28	0.66
	RMSE	1.77	1.46	1.22	1.64	2.39	0.68	1.95	2.86	0.68
40	e	-0.34	-0.00	114.67	-0.18	0.01	-19.67	-0.37	0.03	-14.80
	|e|	1.28	1.04	1.23	1.18	1.82	0.65	1.44	2.18	0.66
	RMSE	1.90	1.39	1.37	1.60	2.39	0.67	1.96	2.79	0.70
41	e	-1.32	0.01	-147.00	-0.76	-0.00	762.00	-1.21	0.01	-100.92
	|e|	2.19	1.14	1.92	1.71	1.78	0.96	2.08	2.09	1.00
	RMSE	2.77	1.54	1.80	2.28	2.36	0.96	2.69	2.72	0.99
42	e	-1.69	0.01	-211.25	-1.27	0.02	-84.60	-1.45	-0.00	1451.00
	|e|	2.19	1.48	1.48	1.78	2.06	0.87	2.05	2.28	0.90
	RMSE	2.99	1.98	1.51	2.46	2.69	0.91	2.80	2.97	0.94
44	e	-0.65	0.00	-163.25	-0.28	-0.01	28.00	-0.81	0.00	N/A
	|e|	1.98	1.32	1.50	1.92	2.41	0.80	2.09	2.85	0.73
	RMSE	2.68	1.93	1.39	2.64	3.17	0.83	2.72	3.68	0.74
46	e	0.30	0.01	24.83	1.12	-0.01	-79.79	0.49	0.01	69.57
	|e|	1.78	1.47	1.21	1.79	2.39	0.75	1.95	2.81	0.70
	RMSE	2.48	2.13	1.17	2.37	3.17	0.75	2.57	3.57	0.72
47	e	-2.12	0.02	-88.37	-1.52	-0.01	116.92	-1.85	0.02	-123.40
	|e|	2.61	1.58	1.66	2.10	2.39	0.88	2.36	2.78	0.85
	RMSE	3.34	2.26	1.48	2.90	3.24	0.90	3.09	3.60	0.86
48	e	-0.69	0.01	-57.08	0.11	-0.01	-11.89	-0.74	-0.00	247.00
	|e|	2.23	1.34	1.67	2.10	2.37	0.88	2.27	2.98	0.76
	RMSE	3.02	2.24	1.35	2.70	3.44	0.79	2.94	4.02	0.73
49	e	-0.68	0.00	N/A	-0.36	-0.01	39.78	-0.61	-0.01	55.27
	|e|	2.20	1.63	1.35	2.01	2.61	0.77	2.13	3.20	0.67
	RMSE	2.95	2.31	1.28	2.58	3.42	0.75	2.65	4.03	0.66

Table 18. Results HIRLAM/WASP model.

		+3			+18			+36		
		H/W	pers	rel	H/W	pers	rel	H/W	pers	rel
50	e	-2.22	0.00	-2216.00	-1.29	-0.12	10.78	-2.80	-0.10	27.19
	$\|e\|$	3.22	1.93	1.66	3.29	3.66	0.90	3.79	4.86	0.78
	RMSE	4.21	2.64	1.59	4.31	4.77	0.90	4.85	6.24	0.78
51	e	-2.10	0.01	-190.73	-1.53	-0.03	47.78	-2.36	-0.03	81.24
	$\|e\|$	2.87	1.46	1.96	2.48	2.39	1.04	3.11	2.99	1.04
	RMSE	3.66	2.00	1.83	3.09	3.10	1.00	3.85	3.79	1.01
52	e	-1.42	-0.00	353.75	-0.99	0.00	-331.00	-1.03	-0.02	60.88
	$\|e\|$	2.06	1.54	1.34	2.11	3.29	0.64	2.32	3.59	0.65
	RMSE	2.96	2.11	1.40	3.04	4.24	0.72	3.34	4.67	0.72
53	e	-0.84	-0.00	417.50	-0.45	-0.02	28.00	-0.64	-0.01	49.08
	$\|e\|$	1.87	1.38	1.35	1.80	2.49	0.72	2.04	2.93	0.70
	RMSE	2.56	1.89	1.35	2.42	3.27	0.74	2.65	3.74	0.71
54	e	-0.52	0.00	-515.00	0.06	-0.03	-2.07	-0.14	-0.06	2.47
	$\|e\|$	1.85	1.46	1.27	1.97	3.22	0.61	2.34	3.61	0.65
	RMSE	2.65	2.02	1.32	2.86	4.21	0.68	3.16	4.63	0.68
55	e	-0.88	-0.00	293.67	-0.60	-0.05	12.93	-0.54	-0.03	19.43
	$\|e\|$	1.77	1.32	1.34	1.80	2.46	0.73	1.95	2.90	0.67
	RMSE	2.23	1.81	1.23	2.34	3.26	0.72	2.66	3.71	0.72
56	e	-0.28	0.00	-95.00	-0.09	0.00	N/A	-0.15	-0.01	11.46
	$\|e\|$	1.39	1.21	1.15	1.45	2.21	0.66	1.61	2.58	0.62
	RMSE	1.97	1.64	1.20	1.89	2.88	0.66	2.11	3.29	0.64
57	e	-0.11	0.00	-105.00	0.26	0.01	51.40	0.07	-0.00	-66.00
	$\|e\|$	1.27	1.08	1.18	1.27	1.95	0.65	1.45	2.23	0.65
	RMSE	1.87	1.46	1.28	1.76	2.53	0.70	1.95	2.86	0.68
58	e	0.12	0.00	58.50	0.43	0.00	426.00	0.31	-0.00	-102.67
	$\|e\|$	1.32	1.06	1.25	1.41	1.95	0.72	1.52	2.30	0.66
	RMSE	1.90	1.42	1.33	1.89	2.55	0.74	1.98	2.92	0.68
59	e	0.15	0.01	24.50	0.74	-0.01	-52.57	0.41	-0.03	-14.75
	$\|e\|$	1.66	1.47	1.12	1.79	2.59	0.69	1.80	2.83	0.64
	RMSE	2.10	2.01	1.05	2.23	3.42	0.65	2.28	3.61	0.63
60	e	-0.05	0.01	-6.00	0.48	-0.01	-96.40	0.10	-0.01	-10.89
	$\|e\|$	1.62	1.30	1.25	1.51	2.37	0.64	1.77	2.73	0.65
	RMSE	2.17	1.80	1.21	1.91	3.10	0.62	2.32	3.49	0.66

C.2 The linear prediction model

Table 19. Results from running the linear prediction model described in Section15.1 for the 3, 18 and 36 hour forecast for the 6 selected stations. The model is evaluated using data from the last half of the period (June to November 1991).

#	F	e	|e|	RMSE
19	+3	0.103	0.503	0.623
	+18	0.242	1.897	2.395
	+36	0.387	1.996	2.475
29	+3	0.157	0.541	0.659
	+18	0.389	1.912	2.345
	+36	0.627	1.953	2.368
35	+3	−0.002	0.563	0.703
	+18	0.006	1.692	2.109
	+36	0.052	1.669	2.072
41	+3	0.020	0.439	0.570
	+18	0.042	1.409	1.823
	+36	0.075	1.434	1.866
56	+3	0.035	0.373	0.455
	+18	0.116	1.823	2.241
	+36	0.167	1.898	2.326
57	+3	0.103	0.390	0.475
	+18	0.295	1.595	1.972
	+36	0.382	1.672	2.040

C.3 Sensitivity to the local corrections

Table 20. The neutral model run without corrections for local effects, using the WA^{s}P matrix ('÷ W') for the 6 selected stations compared to persistence for the +3, +18 and +36 hour forecast for the last half of the period (June 1991 to November 1991) compared to persistence ('persist') and the neutral HIRLAM/WA^{s}P model (H/W), see Section 13.1 for further details.

		+3			+18			+36		
		÷W	pers	H/W	÷W	pers	H/W	÷W	pers	H/W
19	e	-1.63	0.00	-0.82	-1.11	-0.03	-0.18	-1.55	-0.02	-0.62
	$\|e\|$	2.08	1.39	1.69	1.78	2.38	1.59	2.24	2.80	1.82
	RMSE	2.70	1.88	2.00	2.28	3.09	2.16	2.87	3.51	2.36
29	e	1.23	0.01	1.46	1.90	-0.01	1.90	1.52	0.04	1.67
	$\|e\|$	3.04	1.37	3.47	2.99	2.22	3.13	2.88	2.68	3.02
	RMSE	3.78	1.90	4.09	3.66	2.93	3.41	3.65	3.46	3.53
35	e	-0.54	0.05	1.39	0.13	-0.04	2.81	0.03	0.02	2.38
	$\|e\|$	2.26	1.29	3.61	2.24	1.94	4.54	1.95	2.36	3.45
	RMSE	2.90	1.81	4.31	2.77	2.61	4.95	2.52	3.08	3.95
41	e	-1.28	0.01	-1.55	-0.79	-0.00	-1.00	-1.22	0.01	-1.48
	$\|e\|$	2.21	1.14	2.17	1.74	1.78	1.66	2.13	2.09	2.05
	RMSE	2.91	1.54	2.26	2.30	2.36	1.97	2.88	2.72	2.21
56	e	-0.84	0.00	-0.29	-0.63	0.00	-0.14	-0.66	-0.01	-0.23
	$\|e\|$	1.57	1.21	1.29	1.53	2.21	1.33	1.72	2.58	1.61
	RMSE	2.15	1.64	2.05	2.03	2.88	1.83	2.31	3.29	2.17
57	e	-0.85	0.00	0.03	-0.51	0.01	0.31	-0.69	-0.00	0.11
	$\|e\|$	1.46	1.08	1.25	1.30	1.95	1.28	1.56	2.23	1.35
	RMSE	2.00	1.46	2.00	1.74	2.53	1.77	2.13	2.86	1.91

C.4 Directional dependent neural network for MOS

Table 21. Results for the directional dependent neural network MOS model (1,5,1), see Section 13.4. S is the station number, F the look-ahead time (in hours), e the mean error, | e | the mean absolute error, and RMSE the rms error.

S	*F*	*e*	| *e* |	RMSE
19	+3	0.17	1.68	2.09
	+18	0.13	1.56	2.11
	+36	0.20	1.87	2.50
29	+3	0.04	2.32	2.82
	+18	-0.18	1.94	2.46
	+36	-0.13	2.05	2.72
35	+3	-0.27	2.15	2.75
	+18	0.08	2.08	2.67
	+36	0.28	1.74	2.30
41	+3	0.07	1.56	1.99
	+18	-0.08	1.29	1.69
	+36	-0.06	1.59	2.05
56	+3	-0.15	1.36	2.27
	+18	-0.12	1.35	1.76
	+36	-0.13	1.67	2.37
57	+3	0.23	1.34	2.19
	+18	0.18	1.32	1.81
	+36	0.10	1.31	1.75

D The effect of data resolution

In this section a brief (and general) derivation of the effect of resolving a timeseries with a resolution ρ. It is assumed that distribution of the measurements is stepwise constant, ie constant in steps centred around integer multiples of ρ, and having the width ρ. In the following e is the mean error, u_m the wind speed from the model, u_o the observed wind speed, and N the number of observations.

The mean error

Since the distribution is assumed homogeneous there will be no effect on the mean error of the resolution.

The mean absolute error

The effect on the mean absolute error is calculated in the following:

$$|e_a| \sim |u_m - u_o| \tag{D.1}$$

$$= \int_{u_m-\frac{1}{2}\rho}^{u_m+\frac{1}{2}\rho} |u - u_o| \, du \tag{D.2}$$

$$= \int_{u_m-\frac{1}{2}\rho}^{u_m} -(u - u_o)du + \int_{u_m}^{u_m+\frac{1}{2}\rho} (u - u_o)du \tag{D.3}$$

$$= \frac{1}{4}\rho^2 \tag{D.4}$$

If this is divided by the width of the interval we get that the effect of the resolution on the mean absolute error for each observation is

$$\frac{\frac{1}{4}\rho^2}{(u_m + \frac{1}{2}\rho) - (u_m - \frac{1}{2}\rho)} = \frac{1}{4}\rho$$

The rms error

The effect on the rms error is

$$\sigma_a \sim \sqrt{\frac{1}{2 \cdot \frac{1}{2}\rho} \int_{u_m-\frac{1}{2}\rho}^{u_m+\frac{1}{2}\rho} (u - u_o)^2 du} \tag{D.5}$$

$$= \sqrt{\frac{1}{2 \cdot \frac{1}{2}\rho} \int_{u_m-\frac{1}{2}\rho}^{u_m+\frac{1}{2}\rho} (u^2 + u_o^2 - 2uu_o)du} \tag{D.6}$$

$$= \frac{1}{\sqrt{3}}\frac{1}{2}\rho \tag{D.7}$$

Bibliographic Data Sheet **Risø-R-702(EN)**

Title and author(s)

Short-term prediction of local wind conditions

Lars Landberg

ISBN	ISSN
87-550-1916-1	0106-2840

Dept. or group	Date
Meteorology and Wind Energy	March 1994

Groups own reg. number(s)	Project/contract No(s)
MET 02631-00	JOUR-0091-C(MB)

Pages	Tables	Illustrations	References
143	21	67	81

Abstract (Max. 2000 char.)

This report describes the development and evaluation of different methods for predicting the wind locally. The look-ahead time of the forecasts ranges from 3 to 36 hours. The main model developed here is based on forecasts from a numerical weather prediction model. In this study HIRLAM (HIgh Resolution Limited Area Model) has been used. These forecasts are transformed to the surface using the geostrophic drag law and the logarithmic wind profile in their neutral versions. To take local effects into account, corrections output form WA^{s}P (Wind Atlas Analysis and Application Program) are used. The conclusion is that the model developed here performs significantly better than persistence. The model performs best when applied to sites in Northern Europe (having high wind speeds). When using MOS (Model Output Statistics) it is possible to improve the forecasts, mainly those that do not perform well.

Descriptors INIS/EDB

complex terrain; flow models; forecasting; H codes; meteorology; neural networks; numerical data; roughness; time-series analysis; W codes; weather; wind

Available on request from:
Risø Library, Risø National Laboratory (Risø Bibliotek, Forskningscenter Risø)
P.O. Box 49, DK-4000 Roskilde, Denmark
Phone (+45) 46 77 46 77, ext. 4004/4005 · Telex 43 116 · Telefax (+45) 46 75 56 27